Universitat Autònoma de Barcelona

Carboranylphosphinic acids: A New Class of Purely Inorganic Ligands to Generate Polynuclear Compounds and Multifunctional Nanohybrid Materials for Biomedical Applications

Elena Oleshkevich

TESI DOCTORAL

Programma de Doctorat de Química

Directora: Prof. Clara Viñas i Teixidor

Tutor: Dr. Lluis Escriche Martinez

Departament de Química

Facultat de Ciències

2017

ADDENDUM I

Articles publicats i presentats a la Comissió de Doctorat de la Universitat Autònoma de Barcelona al 26 de abril de 2017.

CHEMISTRY
A European Journal

www.chemeurj.org

A Journal of ChemPubSoc Europe

2016-22/11

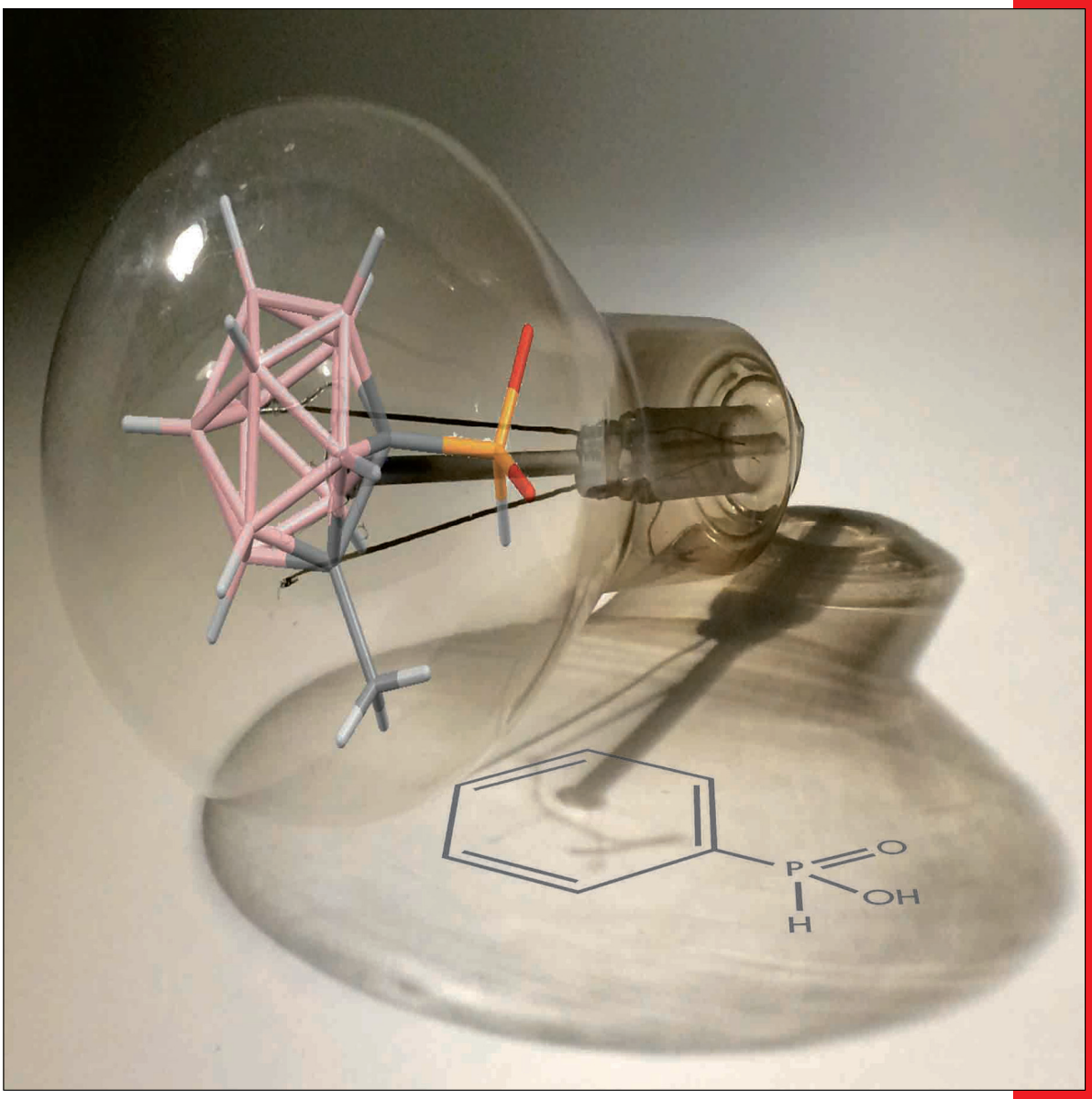

Special Issue:
Women in Chemistry

Cover Picture:
C. Viñas et al.
Carboranylphosphinic Acids: A New Class of Purely Inorganic Ligands

Supported by ACES Asian Chemical Editorial Society

WILEY-VCH

ChemPubSoc Europe

DOI: 10.1002/chem.201504408

CHEMISTRY A European Journal Communication

Carboranes |*Hot Paper*|

Carboranylphosphinic Acids: A New Class of Purely Inorganic Ligands

Elena Oleshkevich,[a] Francesc Teixidor,[a] Duane Choquesillo-Lazarte,[b] Reijo Sillanpää,[c] and Clara Viñas*[a]

Dedicated to Professor Magdolna Hargittai—a true pioneer in the field of molecular symmetry who has contributed substantially to the understanding and determination of structures of fleeting, metastable molecules—on the occasion of her 70th birthday

Abstract: Purely inorganic carboranyl phosphinates were prepared, and the influence of the cluster on the reactivity of the phosphinate group was studied. Electron-withdrawal by the carboranyl carbon atoms, combined with space-filling efficiency and enhanced aromaticity of the cluster cage, renders the phosphorus more difficult to oxidize. This enables carboranyl phosphinates to survive harsh oxidizing conditions, a property which is uncommon in organic phosphinates.

Organophosphorus compounds are organic compounds containing carbon–phosphorus bonds. Phosphines (PR_3) contain no oxygen atoms linked to P, phosphine oxides (OPR_3) contain a nonsubstituted oxygen linked to P, phosphinates ($R_2OP(OR')$) conatin two oxygen atoms, and phosphonates ($ROP(OR')_2$) contain three oxygen atoms. Organophosphorous compounds are of remarkable technological interest,[1] for example, organophosphines are important ligands in catalysis and asymmetric synthesis,[2] phosphonates have found applications as, among other things, herbicides[3] and medicines,[4] and phosphinates have also been applied as herbicides.[5] Both phosphonates and phosphinates are good chelating agents of interest as metal extractants.[6] In organophosphorus compounds, the carbon atom linked to the phosphorus is part of an organic functional group. In the work presented in this paper, the carbon is a member of a boron cluster: a carborane.

The most studied carborane is the icosahedral 1,2-dicarba-*closo*-dodecaborane, 1,2-closo-$C_2B_{10}H_{12}$, and its isomers (1,7- and 1,12-) that can be viewed as "superaromatic" systems the volumes of which approximate that displayed by a benzene molecule rotating on one of its twofold axes.[7] These carboranes exhibit an unusual combination of properties, such as low nucleophilicity, chemical inertness, thermal stability,[8] electron-withdrawal by bonding at the carboranyl carbon atoms,[9] stability, and low toxicity in biological systems.[10] These properties have stimulated the development of a wide range of potential applications based on a molecular approach for the preparation of materials. Moreover, the rigid geometry and the relative easiness of derivatization at the carbon vertexes of the carborane cluster[11] allow the preparation of a wide number of compounds potentially useful as precursors of more complex materials.[7a,12] Moreover, the use of carboranes in supramolecular chemistry is a topic that raises great interest for their particular properties[8a,13] that may induce an unexpected behavior in the supramolecular structures in which they are inserted. Our vision of the carboranyl substituent, however, is that it provides good space-filling, hydrophobicity and electron-withdrawing properties through the carbon cluster, C_c, which suggests the possibility of inducing distinct geometrical behavior in polynuclear complexes.

Taking into account the commercial relevance of organophosphorus compounds, and given that hydrocarbons and boron hydrides are so related and *closo* boron hydrides are very stable, then, why is there limited data about carboranyl phosphonates and carboranyl phosphinates? Carboranyl phosphines and carboranyl phosphine oxides have been studied in some detail.[14] A representative drawing of the carboranyl phosphines, carboranyl phosphine oxides, carboranyl phosphinates, and carboranyl phosphonates is shown in Figure 1.

Although carboranylphosphinic and carboranylphosphonic acids were reported years ago,[15] neither their characterization nor reproducible procedures of their synthesis are available. As a consequence, their reactivity towards metals has not been studied. The aim of this work is the design and development of purely inorganic ligands, carboranylphosphinic, and carboranylphosphonic acids, with no organic functional groups in the

[a] *E. Oleshkevich, Prof. Dr. F. Teixidor, Prof. Dr. C. Viñas*
Institut de Ciència de Materials de Barcelona (ICMAB-CSIC)
Campus UAB, 08193 Bellaterra (Spain)
E-mail: clara@icmab.es

[b] *Dr. D. Choquesillo-Lazarte*
Laboratorio de Estudios Cristalográficos, IACT-CSIC
Armilla, Granada (Spain)

[c] *Prof. Dr. R. Sillanpää*
Department of Chemistry, University of Jyväskylä
40014, Jyväskylä (Finland)

Supporting information for this article is available on the WWW under http://dx.doi.org/10.1002/chem.201504408. It contains the synthesis and spectroscopic characterization (IR, multinuclear NMR and MS) of all new compounds reported in this manuscript and crystal structure determination of compounds $[Na{\cdot}4H_2O][1\text{-Me-}2\text{-OPH(O)-}1,2\text{-}C_2B_{10}H_{10}]$, $[H_3O][1\text{-Me-}2\text{-OPCl(O)-}1,2\text{-}C_2B_{10}H_{10}]{\cdot}H_2O$, $1\text{-H-}7\text{-P(NMe}_2)_2\text{-}1,7\text{-}C_2B_{10}H_{10}$, and $Na[1\text{-OPH(O)-}1,7\text{-}C_2B_{10}H_{11}]$.

Part of a Special Issue "Women in Chemistry" to celebrate International Women's Day 2016. To view the complete issue, visit: http://dx.doi.org/chem.v22.11.

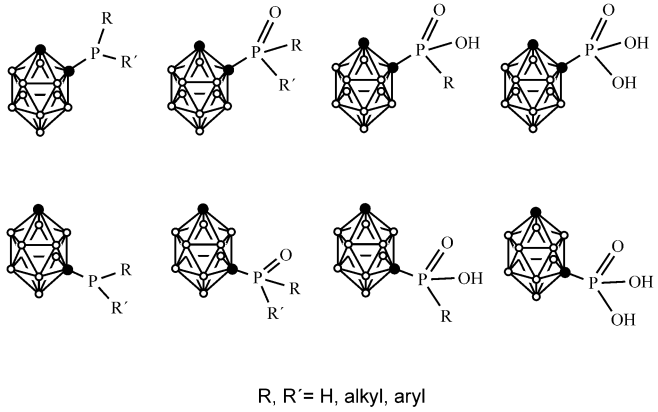

Figure 1. Schematic representation of *ortho*- and *meta*-carboranyl phosphines, carboranyl phosphine oxides, carboranylphosphinic acids, and carboranylphosphonic acids.

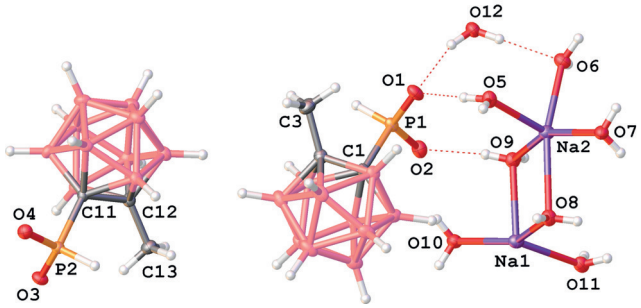

Figure 2. Molecular structure of the sodium salt of *o*-carboranylphosphinic acid (**1**) with selected bond distances [Å] and angles [°]: P(1)–O(1): 1.4917(15), P(1)–O(2): 1.4998(16), P(1)–C(1): 1.844(2), P(1)–H(1): 1.29(2), P(2)–O(3): 1.4918(15), P(2)–O(4): 1.5032(15), P(2)–C(11): 1.856(2), P(2)–H(2A): 1.32(2), C(1)–C(2): 1.664(3), C(11)–C(12): 1.676(3); O(1)-P(1)-O(2): 118.94(9), O(3)-P(2)-O(4): 118.25(9).

molecule that will be capable to coordinate metals producing stable water-soluble systems.

The reaction of 1-Me-2-P$(NMe_2)_2$-1,2-$C_2B_{10}H_{10}$ with dry HCl gas in benzene gave 1-Me-2-PCl_2-1,2-$C_2B_{10}H_{10}$, which after hydrolysis in aqueous solution at room temperature for 20 min, followed by the addition of 10% NaOH solution, gave the sodium salt of the *o*-carboranylphosphinic acid, [Na·4 H_2O][1-Me-2-OPH(O)-1,2-$C_2B_{10}H_{10}$] (**1**), in 70% yield. The general reaction is given in Scheme 1. Compound **1** was characterized by multinuclear NMR and FTIR spectroscopic techniques, mass spectrometry, and elemental analysis. The ^{1}H NMR spectrum displayed a doublet at $\delta = 7.03$ ppm with a coupling constant $^1J(P,H) = 447$ Hz, indicating the presence of a P–H bond in the compound. In addition, the $^{31}P\{^1H\}$ NMR spectrum displayed a resonance at $\delta = 9.21$ ppm that turns into a doublet ($^1J(P,H) = 447$ Hz) in the ^{31}P NMR spectrum, which also supports the existence of the P–H bond. Good crystals of **1** (Figure 2) suitable for X-ray diffraction were grown from water that fully confirmed its molecular structure.[16] The P–C_c bond lengths (1.844(2) and 1.856(2) Å) are similar to those in the *o*-carboranylmonophosphines (1.865(5)–1.884(4) Å),[17] whereas the C_c–C_c bond lengths (1.664(3) and 1.676(3) Å) are slightly shorter (1.702(6) and 1.731(9) A°).[14] The P–H bond lengths (1.29(2) and 1.32(2) Å) compare well with similar bond lengths found in secondary phosphinocarbaboranes (1.31(2) and 1.372(1) Å)[18] or phosphonium salts (1.30(2) and 1.38(4)).[19] The crystal structure of **1** is composed of alternating (001) layers of carboranyl clusters and hydrated Na^+ ions (Figure 3). Hydrogen-bonding interactions link layers together involving coordinated water molecules and phosphonate groups.

With the goal to produce *o*-carboranylphosphonic acid 1-Me-2-OP$(OH)_2$-1,2-$C_2B_{10}H_{10}$, a dry Cl_2 stream was passed through a benzene solution of 1-Me-2-PCl_2-1,2-$C_2B_{10}H_{10}$ over 15 min. It was expected to give 1-Me-2-PCl_4-1,2-$C_2B_{10}H_{10}$ that generates 1-Me-2-OPCl_2-1,2-$C_2B_{10}H_{10}$ by hydrolysis (see the Sup-

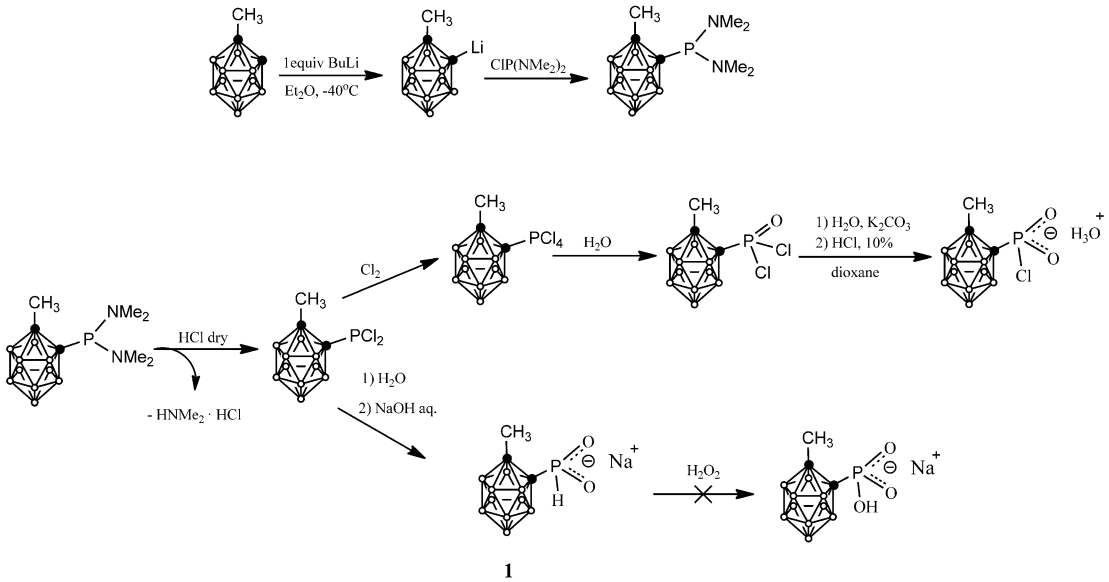

Scheme 1. Synthesis of the sodium salt of *o*-carboranylphosphinic acid (**1**).

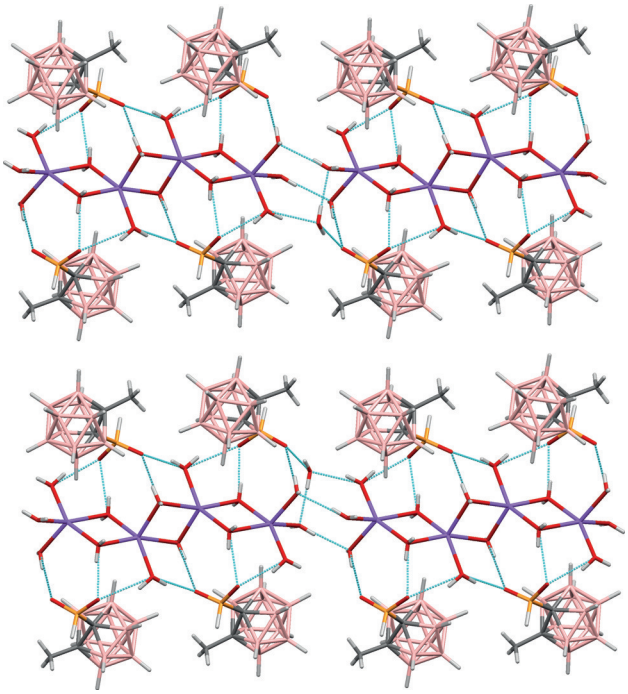

Figure 3. Crystal packing of the sodium salt of *o*-carboranylphosphinic acid (**1**).

porting Information), and from which the target compound 1-Me-2-OP(OH)$_2$-1,2-$C_2B_{10}H_{10}$ would be obtained (Scheme 1). A white solid (in 76% yield) was isolated that produced good crystals from aqueous water solution. Unexpectedly, X-ray diffraction studies showed that the solid corresponds to [H_3O][1-Me-2-OPCl(O)-1,2-$C_2B_{10}H_{10}$]·H_2O.[16] Figure 4 displays its molecular structure. The P–C_c bond length, 1.828(2), is slightly shorter compared with **1**, whereas the C_c–C_c bond length, 1.672(2) Å, is a little longer. The crystal packing is driven by hydrogen-bonding interactions between water molecules and chlorophosphonic groups building a 2D sheet structure. Hydronium molecules reinforced the above referred structure by additional hydrogen bonds (Figure 5).

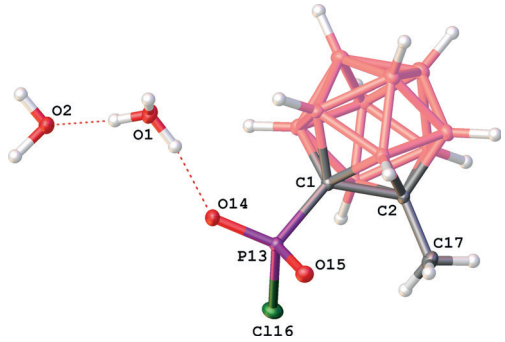

Figure 4. Molecular structure of [H_3O][1-Me-2-OPCl(O)-1,2-$C_2B_{10}H_{10}$] with selected bond distances [Å] and angles [°]: Cl(16)–P(13): 2.0167(7), P(13)–O(15): 1.4927(13), P(13)–O(14): 1.4897(14), P(13)–C(1): 1.8380(18), O(15)-P(13)-Cl(16): 106.64(6), O(15)-P(13)-C(1): 109.51(8), O(14)-P(13)-Cl(16): 107.55(6), O(14)-P(13)-O(15): 117.80(8), O(14)-P(13)-C(1): 108.21(8), C(1)-P(13)-Cl(16): 106.57(6).

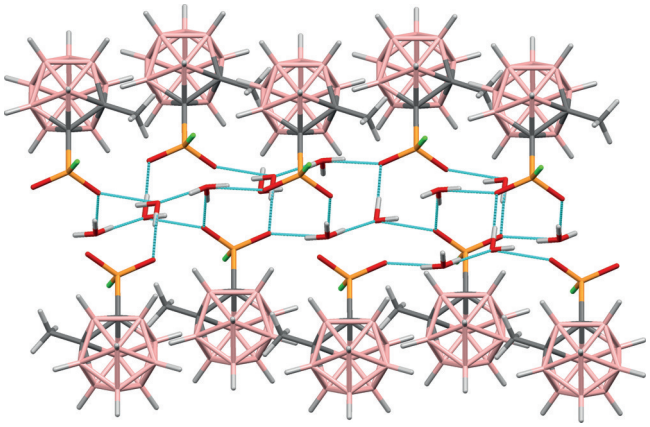

Figure 5. Crystal packing of [H_3O][1-Me-2-OPCl(O)-1,2-$C_2B_{10}H_{10}$].

When forcing the reaction conditions leading to *o*-carboranylphosphonic acid, by oxidation of the sodium salt of the *o*-carboranylphosphinic acid with H_2O_2, only 1-Me-1,2-$C_2B_{10}H_{11}$ was recovered due to the cleavage of the C_c–P bond as it occurs in the deboronation process of *closo* *o*-carboranylphoshines with alkoxide.[20] Looking for alternatives to produce carboranylphosphonic and carboranylphosphinic acid building blocks, we decided to use *m*-carborane as starting framework due to its convenience.

The synthesis of 1-R-7-P(NMe$_2$)$_2$-1,7-$C_2B_{10}H_{10}$ (R = Me, H) was achieved by deprotonation of one of the C_c–H vertices of 1,7-$C_2B_{10}H_{12}$ with *n*BuLi followed by electrophilic reaction with ClP(NMe$_2$)$_2$ (Scheme 2). After workup, compounds with the structure 1-R-7-P(NMe$_2$)$_2$-1,7-$C_2B_{10}H_{10}$ (R = Me, **2**; H, **3**) were isolated in high yield (95 and 90%, respectively). Compounds **2** and **3** were fully characterized by IR and multinuclear NMR spectroscopy. The ^{1}H NMR spectrum of **3** in $CDCl_3$ displays two singlets at $\delta = 2.74$ and 2.77 ppm and a broad singlet at $\delta =$ 2.96 ppm corresponding to the Me groups and C_c–H, respectively. Its ^{31}P NMR spectrum exhibits a singlet at $\delta =$ 105.65 ppm. The ^{11}B and ^{11}B{^{1}H} NMR spectra appears in the δ between −4.4 and −15.3 ppm, which clearly confirms the *closo* cluster nature in **3**. The molecular structure of **3** was unambiguously elucidated by X-ray diffraction (Figure 6) of suitable crystals grown from diethyl ether solution.[16]

As shown in Scheme 2, compounds 1-R-7-PCl$_2$-1,7-$C_2B_{10}H_{10}$ (R = Me, **4**; H, **5**) were obtained in 92 and 95% yields by passing a stream of dry HCl through a benzene solution of **2** and **3**, respectively. Compound 1-OPH(OH)-1,7-$C_2B_{10}H_{11}$ (**6**) was isolated in 90% yield by hydrolysis of **5**. The ^{1}H NMR spectrum of *m*-carboranylphosphinic acid in $CDCl_3$ displays a singlet at $\delta =$ 11.41 ppm that corresponds to the P–OH and a doublet at $\delta =$ 6.88 ppm with a ^1J(P,H) of 633 Hz that corresponds to P–H. The ^{31}P NMR spectrum of **6** in $CDCl_3$ also exhibits a doublet at $\delta =$ 21.06 ppm with a P–H coupling constant of 633 Hz that turns into a singlet in the ^{31}P{^{1}H} NMR spectrum. In the ^{13}C{^{1}H} NMR spectrum of **6**, two doublets are observed for the carbon cluster atoms of the monosubstituted *m*-carbaborane at $\delta = 64.4$ and 68.3 ppm with a ^2J(C,P) and ^1J(C,P) of 108 and 2.3 Hz, respectively. TGA that was run under an argon atmosphere in

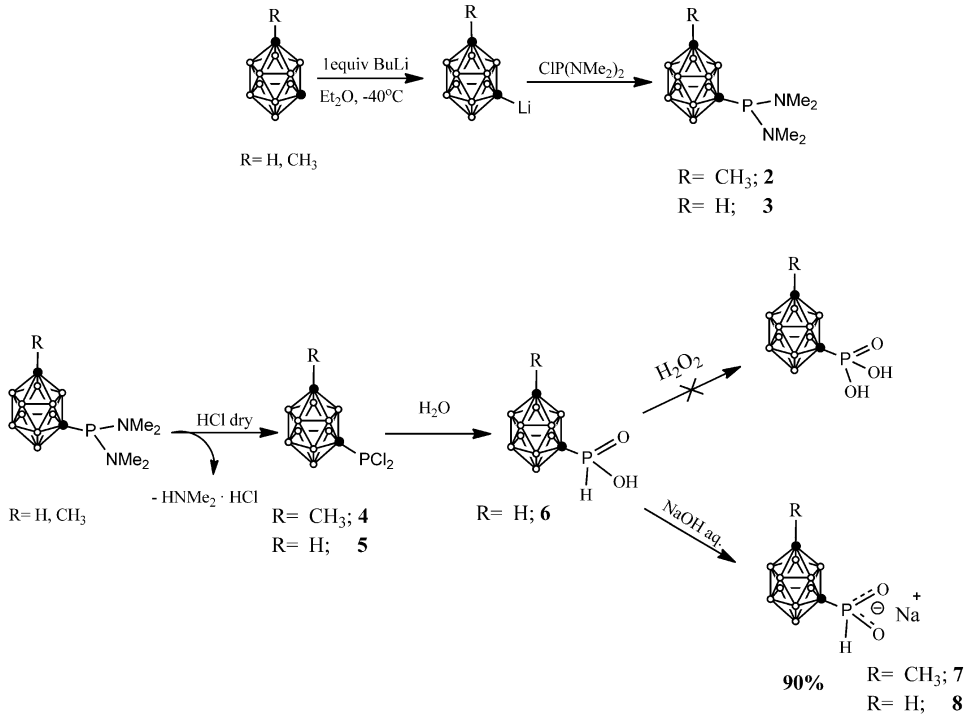

Scheme 2. Synthesis of *m*-carboranylphosphinic acids and their corresponding sodium salts.

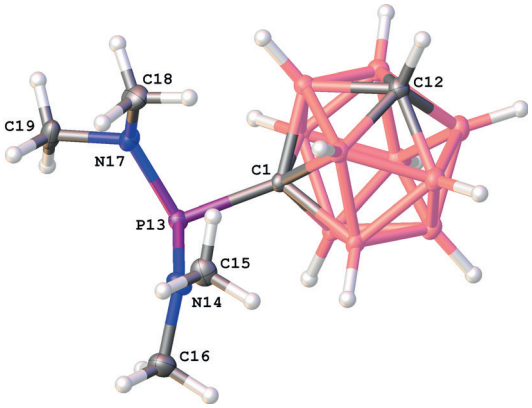

Figure 6. Molecular structure of 1-P(NMe_2)$_2$-1,7-$C_2B_{10}H_{11}$ (**3**) with selected bond distances [Å] and angles [°]. C(1)–P(13): 1.893(2), P(13)–N(14): 1.6730(19), P(13)–N(17): 1.6831(19), N(14)–C(15): 1.460(3), N(14)–C(16): 1.460(3), N(17)–C(18): 1.464(3), N(17)–C(19): 1.467(3); N(14)-P(13)-N(17): 110.81(10),

the range from room temperature to 700 °C showed an exothermic process at 280 °C. The formation of $B(OH)_3$ from the TGA analysis was confirmed by ^{11}B NMR and IR spectroscopy of the solid residue (see the Supporting Information).

The sodium salts of *m*-carboranylphosphinic acid, Na[1-Me-7-OPH(O)-1,7-$C_2B_{10}H_{10}$] (**7**) and Na[1-OPH(O)-1,7-$C_2B_{10}H_{11}$] (**8**) were quantitatively isolated from the corresponding aqueous acid suspensions after adding drop by drop 10% NaOH solution. The ^1H NMR spectrum of Na[1-OPH(O)-1,7-$C_2B_{10}H_{11}$] in D_2O displays a doublet centered at $\delta = 6.72$ ppm with a $^1J(P,H)$ coupling constant of 583 Hz and a broad singlet at $\delta = 3.46$ ppm corresponding to P–H and C_c–H, respectively. Its ^{31}P NMR spectrum exhibits a doublet at $\delta = 14.66$ ppm with the same $^1J(P,H)$ coupling constant of 583 Hz. Good crystals of the sodium salt of the *m*-carboranylphosphinic acid were grown from an *i*PrOH/water solution.[16] Figure 7 displays the asymmetric unit cell that contains two ligands with different P–H bond lengths (1.30(2) and 1.34(2) Å) and two sodium atoms that correspond to [Na_2][1-OPH(O)-1,7-$C_2B_{10}H_{11}$]$_2$ CH(OH)(CH_3)$_2$ (**5**). A sodium atom coordinates to two oxygen atoms, one from each ligand,

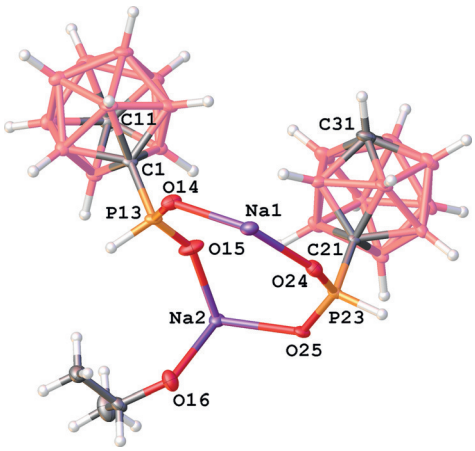

Figure 7. Molecular structure of [Na_2][1-OPH(O)-1,7-$C_2B_{10}H_{11}$]$_2$ CH(OH)(CH_3)$_2$ (**5**) with selected bond lengths [Å] and angles [°]: C(1)–P(13): 1.841(2), P(13)–O(14): 1.4936(15), P(13)–O(15): 1.4787(16), P(23)–O(24): 1.4840(16), P(23)–O(25): 1.5046(14), P(13)–H(13): 1.30(2), P(23)–H(23): 1.34(2); O(15)-P(13)-O(14): 117.98(9), O(24)-P(23)-O(25): 118.87(9), O(15)-Na(2)-O(16): 100.46(7), O(15)-Na(2)-O(25): 102.78(6), O(16)-Na(2)-O(25): 100.22(6), O(24)-Na(1)-O(14): 123.00(6).

with Na–O bond lengths of 2.263 and 2.290 Å, whereas the other sodium (Na1) coordinates to three oxygen atoms, also one from each ligand (2.1602(17) and 2.3570(16) Å), and the third one to one *i*PrOH molecule (2.3108(18) Å). Sodium atoms complete their coordination sphere with O-donor atoms from adjacent asymmetric units, generating 2D chains running along the *a* axis.

In contrast to organic analogues,[21] *m*-carboranylphosphinic acid, 1-OPH(OH)-1,7-$C_2B_{10}H_{11}$, does not oxidize to *m*-carboranylphosphonic acid, 1-OP(OH)$_2$-1,7-$C_2B_{10}H_{11}$. The high stability of *m*-carboranylphosphinic acid against powerful oxidizing agents with respect to the related organic compounds is clear evidence of the cluster influence on the P atom directly bonded to the C_c. The phosphinic acids have one acidic P–OH group; the acidity of organophosphinic acids varies in the range of 1.3–2.5 pK_a.[21b] The pK_a of **6** and its organic analogue phenylphosphinic acid have been calculated in this work and the values are 1.32 and 1.77, respectively, which is a clear indication that the *m*-carboranyl group provides more acidic character to the P–OH than the phenyl organic fragment.

On cooling **6** in $CDCl_3$, the resonance at $\delta = 5.45$ ppm in the room temperature ^{1}H NMR spectrum that corresponds to P–OH shifts to $\delta = 11.41$ ppm at $-60\,^{\circ}$C (see the Supporting Information).

It is reported that the phosphorous-bonded hydrogen of phenylphosphinic acid undergoes isotopic exchange with deuterium from the solvent.[22] It was suggested that this exchange is due to the tautomerism between the pentacoordinated phosphorous ROPH(OH) in organophosphinic acids and the tricoordinated one in RP(OH)$_2$ in organophosphonous acids.[23]

To know the influence of the *m*-carboranyl ligand, the kinetics of this acid- and base-isotopic exchange, between the hydrogen atom bound to phosphorous with deuterium from the D_2O solvent, was studied by means of $^{31}P\{^1H\}$ and ^{31}P NMR spectra for compounds 1-OPH(OH)-1,7-$C_2B_{10}H_{11}$ (**6**), Na[1-Me-7-OPH(O)-1,7-$C_2B_{10}H_{10}$] (**7**), and Na[1-OPH(O)-1,7-$C_2B_{10}H_{11}$] (**8**).

A point to note is that the ^{31}P and $^{31}P\{^1H\}$ NMR spectra of **7** in D_2O exhibit after 3.5 h a triplet (1:1:1) at $\delta = 14.63$ ppm with a ^1J(P,D) of 86 Hz as a result of the completed isotopic exchange, whereas no exchange was observed for **8** after 2 days in D_2O. The phosphinic acid form of 1-OPH(OH)-1,7-$C_2B_{10}H_{11}$ disappears under isotopic exchange but the reaction is not as fast as in the case of Na[1Me-7-OPH(O)-1,7-$C_2B_{10}H_{11}$]. After 48 h in D_2O, a triplet (1:1:1) at $\delta = 12.96$ ppm with a ^1J(P,D) of 87 Hz was observed. The ^{1}H NMR spectrum provided information on the deuterated conversion that was found to be 90% (see the Supporting Information).

In conclusion, this work has shown that, in a similar manner to organic phosphinates, purely inorganic carboranyl phosphinates can be prepared in very good to excellent yields. But this parallelism being true, the preparation of carboranylphosphonates does not follow the same tendency. Carboranylphosphonates cannot be so easily made, at least with our methods. The difficulty of preparation has been made noteworthy with the *o*-carborane isomer, in which the carboranyl-OP(OH)Cl has been isolated instead of the expected carboranyl-OP(OH)$_2$. This is consistent, however, with the electron-withdrawing capacity of the cluster cage through C, which electronically impoverishes the phosphorus, making it more difficult to be oxidized. On the other hand, this is good for the air stability of the carboranylphsophinates, and perhaps on their stability in harsh oxidizing atmospheres. Carboranylphosphinic acids have been prepared both with the *ortho*-, and *meta*-carborane. The hydrogen in the H–P unit of the carboranylphosphinate has been easily exchanged by D from the deuterated NMR solvent, although rate differences have been noticed depending on the adjacent carborane carbon substituent and the salt utilized. The carborane influence has been noticed in the p*K* of the phosphinate, which is more negative for the carboranyl than for the "comparable" phenyl. It is expected that these enhanced electronic properties will be accompanied by others derived from the hydrophobicity and space-filling efficiency of the carboranyl fragment, making the physicochemical properties of the generated metal complexes attractive for applications in medicine or in materials science.

Acknowledgements

The authors thank the Generalitat de Catalunya (2014/SGR/149), Spanish Ministry of Economy and Competitiveness (CTQ2010-16237 and CTQ2013-44670-R) and Intramural CSIC (201530E011) for their support. E.O. is enrolled in the PhD program of the UAB. E.O. thanks the MICINN for an FPU pre-doctoral grant.

Keywords: carboranes · hydrogen bonding · hydrophobicity · phosphinates · phosphonates

[1] J. L. Montchamp, *Acc. Chem. Res.* **2014**, *47*, 77–87.
[2] J. C. Chadwick, R. Duchateau, Z. Freixa, P. W. N. M. van Leeuwen, *Homogeneous Catalysts: Activity, Stability, Deactivation*, Wiley-VCH, Weinheim, **2011**.
[3] J. Lipok, *Ecotoxicol. Environ. Saf.* **2009**, *72*, 1701–1706.
[4] K. A. Kennel, M. T. Drake, *Mayo Clin. Proc.* **2009**, *84*, 632–638.
[5] P. Böger, K. Wakabayashi, K. Hirai, *Herbicide Classes in Development: Mode of Action, Targets, Genetic Engineering, Chemistry*, Springer, Heidelberg, **2002**.
[6] D. G. Kalina, E. P. Horwitz, L. Kaplan, A. C. Muscatello, *Separ. Sci. Technol.* **1981**, *16*, 1127–1145.
[7] a) F. Teixidor, C. Viñas, A. Demonceau, R. Nuñez, *Pure Appl. Chem. Pure App. Chem.***2003**, *75*, 1305–1313; b) M. Scholz, E. Hey-Hawkins, *Chem. Rev.* **2011**, *111*, 7035–7062.
[8] a) R. N. Grimes, *Carboranes*, 2nd ed., Elsevier, New York, **2011**, p. 54; b) M. F. Hawthorne, *Advances in Boron Chemistry*, RSC, Cornwall, **1997**, pp. 261–272.
[9] a) F. Teixidor, R. Núñez, C. Viñas, R. Sillanpää, R. Kivekäs, *Angew. Chem. Int. Ed.* **2000**, *39*, 4290–4292; *Angew. Chem.* **2000**, *112*, 4460–4462; b) R. Núñez, P. Farrás, F. Teixidor, C. Viñas, R. Sillanpää, R. Kivekäs, *Angew. Chem. Int. Ed.* **2006**, *45*, 1270–1272; c) F. Teixidor, G. Barbera, A. Vaca, R. Kivekäs, R. Sillanpää, *J. Am. Chem. Soc.* **2005**, *127*, 10158–10159.
[10] a) M. F. Hawthorne, *Angew. Chem. Int. Ed. Engl.* **1993**, *32*, 950–984; *Angew. Chem.* **1993**, *105*, 997–1033; b) A. H. Soloway, W. Tjarks, B. A. Barnum, F.-G. Rong, R. F. Barth, I. M. Codogni, J. G. Wilson, *Chem. Rev.* **1998**, *98*, 1515–1562; c) J. F. Valliant, K. J. Guenther, A. S. King, P. Morel, P. Schaffer, O. O. Sogbein, K. A. Stephenson, *Coord. Chem. Rev.* **2002**, *232*, 173–230; d) I. B. Sivaev, V. Bregadze, S. Sjöberg, in *Research and Development in Neutron Capture Therapy* (Eds.: W. Sauerwein, R. Moss, A. Wittig), Monduzzi Editore, Bologna, **2002**, pp. 19–23; e) R. Julius, O.

Farha, J. Chiang, L. Perry, M. F. Hawthorne, *Proc. Natl. Acad. Sci. USA* **2007**, *104*, 4808 – 4813.

[11] a) F. Teixidor, C. Viñas, *Science of Synthesis Houben-Weyl Methods of Molecular Transformations* (Eds.: D. E. Kaufmann, D. S. Matteson), Georg Thieme, Stuttgart, **2005**, *6*, p. 1235; b) V. I. Bregadze, *Chem. Rev.* **1992**, *92*, 209 – 223.

[12] a) B. P. Dash, R. Satapathy, J. A. Maguire, N. S. Hosmane, *New J. Chem.* **2011**, *35*, 1955 – 1972; b) L. Schwartz, L. Eriksson, R. Lomoth, F. Teixidor, C. Viñas, S. Ott, *Dalton Trans.* **2008**, *18*, 2379 – 2381; c) J. J. Peterson, M. Werre, Y. C. Simon, E. B. Coughlin, K. R. Carter, *Macromolecules* **2009**, *42*, 8594 – 8598; d) K. Kokado, Y. Chujo, *J. Org. Chem.* **2011**, *76*, 316 – 319; e) Y.-S. Bae, A. M. Spokoyny, O. K. Farha, R. Q. Snurr, J. T. Hupp, C. A. Mirkin, *Chem. Commun.* **2010**, *46*, 3478 – 3480; f) G. Vives, J. M. Tours, *Acc. Chem. Res.* **2009**, *42*, 473 – 487.

[13] a) M. A. Fox, A. K. Hughes, *Coord. Chem. Rev.* **2004**, *248*, 457 – 476; b) H. Jude, H. Disteldorf, S. Fischer, T. Wedge, A. M. Hawkridge, A. M. Arif, M. F. Hawthorne, D. C. Muddiman, P. J. Stang, *J. Am. Chem. Soc.* **2005**, *127*, 12131 – 12139; c) A. V. Puga, F. Teixidor, R. Kivekäs, R. Sillanpää, C. Viñas, *Chem. Eur. J.* **2009**, *15*, 9764 – 9772.

[14] A. R. Popescu, F. Teixidor, C. Viñas, *Coord. Chem. Rev.* **2014**, *269*, 54 – 84 and references therein.

[15] a) L. I. Zakharkin, A. V. Kazantsev, M. N. Zhubekova, *Izv. Akad. Nauk SSSR Ser. Khim.* **1969**, *9*, 2056 – 2057; b) A. V. Kazantsev, M. N. Zhubekova, L. I. Zakharkin, *Zh. Obshch. Khim.* **1971**, *41*, 1570 – 1571.

[16] See the Supporting Information for details for the X-ray structure analyses. CCDC 1434442, 1434443, 1434444 and 1434445 ([Na·4 H_2O][1-Me-2-OPH(O)-1,2-$C_2B_{10}H_{10}$], [H_3O][1-Me-2-OPCl(O)-1,2-$C_2B_{10}H_{10}$], 1-Me-7-P(NMe_2)$_2$-1,7-$C_2B_{10}H_{10}$, and Na[1-OPH(O)-1,7-$C_2B_{10}H_{11}$]) contain the supplementary crystallographic data for this paper. These data are provided free of charge by The Cambridge Crystallographic Data Centre

[17] a) R. Kivekäs, F. Teixidor, C. Viñas, R. Nuñez, *Acta Crystallogr. Sect. C* **1995**, *51*, 1868 – 1870; b) R. Kivekäs, R. Sillanpää, F. Teixidor, C. Viñas, R. Nuñez, *Acta Crystallogr. Sect. C* **1994**, *50*, 2027 – 1870; c) R. Núñez, C. Viñas, F. Teixidor, R. Sillanpää, R. Kivekäs, *J. Organomet. Chem.* **1999**, *592*, 22 – 28.

[18] a) V. P. Balema, M. Pink, J. Sieler, E. Hey-Hawkins, L. Hennig, *Polyhedron* **1998**, *17*, 2087; b) A. Kreienbrink, P. Lonnecke, M. Findeisen, E. Hey-Hawkins, *Chem. Commun.* **2012**, *48*, 9385 – 9387.

[19] a) F. Teixidor, R. Núñez, C. Viñas, R. Sillanpää, R. Kivekäs, *Inorg. Chem.* **2001**, *40*, 2587 – 2594; b) J. P. H. Charmant, M. F. Haddow, R. Mistry, N. C. Norman, A. G. Orpen, P. G. Pringle, *Dalton Trans.* **2008**, 1409 – 1411.

[20] F. Teixidor, C. Viñas, M. M. Abad, R. Núñez, R. Kivekäs, R. Sillanpää, *J. Organomet. Chem.* **1995**, *503*, 193 – 203.

[21] a) G. M. Kosolapoff, *The Synthesis of Phosphonic and Phosphinic Acids*, Wiley, **2011**; b) J.-M. Rueff, G. B. Hix, P.-A. Jaffrès " *Rigid Phosphonic Acids as Building Blocks for Crystalline Hybrid Materials" in Tailored Organic – Inorganic Materials* (Eds.: E. Brunet, J. L. Colón, A. Clearfield), pp. 341 – 393, Wiley, **2015**.

[22] J. Reuben, D. Samuel, B. L. Silver, *J. Am. Chem. Soc.* **1963**, *85*, 3093 – 3096.

[23] a) R. B. Martin, *J. Am. Chem. Soc.* **1959**, *81*, 1574 – 1576; b) R. B. Silver, Z. Luz, *J. Phys. Chem.* **1962**, *66*, 1356 – 1359.

Received: November 2, 2015
Published online on January 7, 2016

Revista de la Societat Catalana de Química, núm. 15 (2016), p. 49-56
Filial de l'Institut d'Estudis Catalans

ISSN: 2013-9853 DOI: 10.2436/20.2003.01.74
http://revistes.iec.cat/index.php/RSCQ

A new class of purely inorganic ligands: carboranylphosphinic acids
Una nova classe de lligands purament inorgànics: els àcids carboranilfosfínics

Elena Oleshkevich, Francesc Teixidor and Clara Viñas
Institut de Ciència de Materials de Barcelona (ICMAB-CSIC)

Abstract: Dicarba-*closo*-dodecaboranes (or carboranes) are icosahedral clusters of empirical formula $C_2B_{10}H_{12}$. Depending on the relative position of the carbon atoms in the cluster, three isomers can be distinguished: *ortho*- (1,2), *meta*- (1,7) and *para*- (1,12). Our group focused this research on the first two: *ortho*- and *meta*-carborane isomers. The high symmetry, remarkable stability and versatile reactivity of these clusters allow their functionalization according to a desired application. Our group and others were interested in carboranylphosphorus compounds, mostly due to their properties as ligands for organometallic chemistry and enantioselective catalysis. Among them are carboranylphosphines and carboranylphosphines with P(V) moieties, except carboranyl phosphinates and carboranyl phosphonates. Few studies are found in the literature on carboranyl phosphinic and phosphonic acids. Our research goal has been devoted to developing preparation and characterization of carboranyl phosphinates, aiming towards the designing of purely inorganic ligands that are capable to coordinate to metals producing stable water-soluble polynuclear systems. The influence of the boron cluster on the reactivity of the phosphinate group was studied as well.

Keywords: Carboranes, phosphinates, phosphonates.

Resum: Els dicarba-*closo*-*carborans (o carborans) són poliedres icosaèdrics de fórmula empírica $C_2B_{10}H_{12}$. Depenent de la posició dels dos àtoms de carboni en els diferents vèrtexs del clúster, podem tenir tres isòmers diferents:* orto- *(1,2-$C_2B_{10}H_{12}$),* meta- *(1,7-$C_2B_{10}H_{12}$) i* para- *(1,12-$C_2B_{10}H_{12}$). Aquests clústers són molt estables i mostren una gran simetria i una capacitat de ser substituïts, sigui als vèrtexs de carboni, als de bor o a ambdós, de manera que s'obtenen així diferents clústers funcionalitzats per emprar-los en l'aplicació desitjada. El grup de recerca té una llarga experiència en la síntesi de lligands tipus fosfina que contenen el clúster de carborà que van emprar-se en la preparació de complexos de metalls de transició per usar-los en catàlisi homogènia. L'oxidació d'aquestes fosfines, de P(III) a P(V), és difícil, cal forçar-la. Aquesta és una propietat important de cara a la seva aplicació com a catalitzadors. Pocs exemples es troben a la literatura sobre àcids fosfònics i fosfínics que continguin clústers de carborà. En aquest treball, s'han sintetitzat i caracteritzat àcids fosfònics i fosfínics de clústers icosaèdrics de carborà fent servir com a reactius de partida els isòmers* orto- *i* meta- *del* closo-*carborà. S'ha estudiat la capacitat coordinant d'aquestes noves famílies de lligands que són purament inorgànics amb metalls amb l'objectiu d'obtenir complexos de coordinació polimèrics solubles en aigua. La influència dels clústers de bor en la reactivitat dels lligands també s'ha estudiat.

Paraules clau: Carborans, àcid fosfònic, àcid fosfínic.

Introduction

In the periodic table of elements, boron lies next to carbon. Both boron and carbon have the property of catenating. Carbon forms cycles and polymers and is the base of organic chemistry. Boron forms clusters and induces a huge discipline of chemistry: Boron science. Boranes, boron clusters and, in particular, icosahedral dicarba-*closo*-dodecaboranes with empirical formula $C_2B_{10}H_{12}$ are of special interest. Boron clusters were considered as electron deficient compounds till Lipscomb's discovery. William N. Lipscomb was awarded with the Nobel Prize in Chemistry 1976 "for his studies on the structure of boranes illuminating problems of chemical bonding". Lipscomb proposed the mechanism to understand the three-center two-electron (3c-2e) bond in boron clusters [1]. In 3c-2e, a pair of electrons is shared between three atoms. The three atoms can be a boron atom at either end and a hydrogen atom in the middle, as in the case of the diborane B–H–B bonds, or the three atoms, can be three boron atoms, as in the polyhedral clusters. 3D aromaticity of boron or carborane clusters gives them unique properties that are not common in organic chemistry [2].

A relation between hydrocarbon and borohydride chemistries has been recently reported [3]. The idea is based on keeping

Contact address: Clara Viñas
Institut de Ciència de Materials de Barcelona (ICMAB-CSIC)
Campus de la UAB, Bellaterra. 08193 Cerdanyola del Vallès
Tel.: +34 935 801 853. Fax: +34 935 805 729
E-mail: *clara@icmab.es*

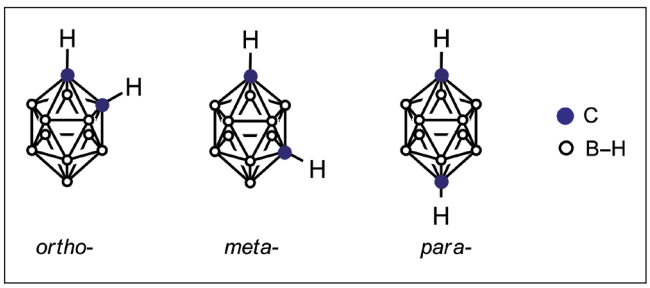

FIGURE 1. The three isomers of icosahedral dicarba-*closo*-dodecarboranes ($C_2B_{10}H_{12}$).

the same number of valence electrons in a confined space. Thus, the «addition» of an extra electron to each boron atom in borohydrides yields molecular analogues of hydrocarbons. As a result, for any given hydrocarbon in organic chemistry, its borohydride analogue can be found in boron chemistry. Along this line, work was recently reported that establishes a direct connection between Wade-Mingos rule of tridimensional aromatic *closo* boron hydride clusters and Hückel's rule of planar aromatic annulenes, showing that they share a common origin regulated by the number of valence electrons in an electronic confined space [4].

Chemical reactivity of *ortho*- and *meta*-carboranes: electrophilic substitutions on *ortho*- and *meta*-carboranes

Although *ortho*- and *meta*-carborane clusters are remarkably stable, in certain reaction conditions they exhibit high synthetic reactivity. From the point of view of electrophilic substitution at the C_c–H vertices (C_c: carbon atom belonging to carborane cluster), both isomers display similar chemical reactivity. In both carborane isomers the hydrogen atoms of the C_c–H units are more acidic than the ones bonded to B–H vertices, due to the more electronegative character of carbon with respect to boron (2.5 and 2.0, respectively, according to the Pauling scale). Thus, hydrogen atoms attached to carbon can be considered acidic while those bonded to boron are considered hydride. The acidity of the C_c–H vertices decreases in the order of *ortho*-, *meta*- and *para*-carborane. Its vulnerability to become deprotonated decreases in the same order.

This relatively acidic character of C_c–H units allows their deprotonation by strong alkali and alkaline earth metal bases, like for example *n*-butyllithium or Grignard reagents. The generated negative charge on the carbon atom of the cluster, C_c, attracts electrophilic reagents, opening the way to the introduction of functional groups at the C_c position of the cluster.

Figure 2 shows the two possible pathways for substitutions at one or both of the C_c atoms. After dilithiation of the carborane cluster (bottom pathway) it is possible to introduce simultaneously twice the same substituent, which leads to symmetrically substituted carborane. The other pathway (top) demonstrates monosubstitution of the carborane cluster or unsymmetrical disubstitution. The synthesis of monosubstituted carborane derivatives is more complicated compared to the sythesis of disubstituted carborane derivatives. The reason is the disproportionation of $Li[1,2\text{–}C_2B_{10}H_{11}]$ into $Li_2[1,2\text{–}C_2B_{10}H_{10}]$ and $1,2\text{–}C_2B_{10}H_{12}$, as it was found for *ortho*-carborane [5]. Several approaches have been developed to overcome this problem. They include the use of protection/deprotection methodol-

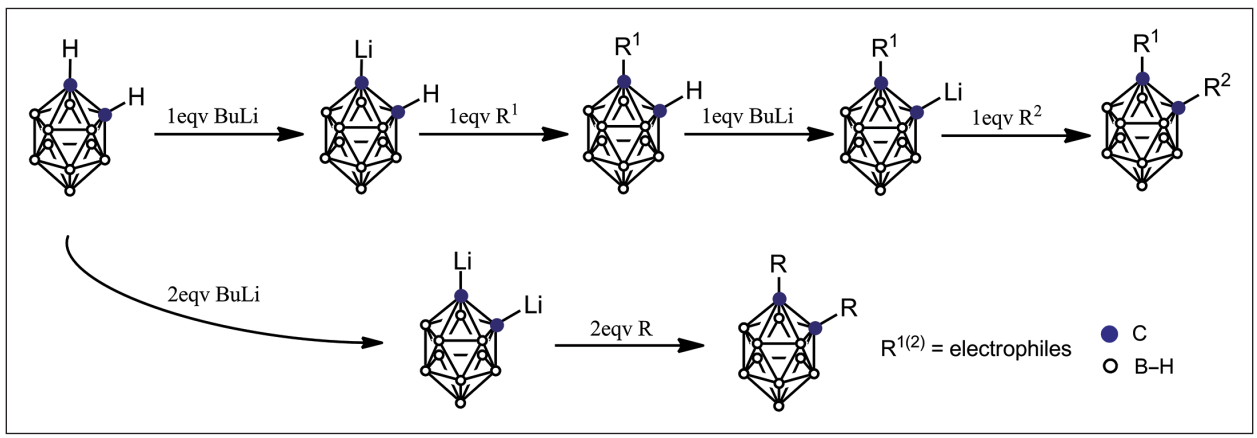

FIGURE 2. Deprotonation reaction of C_c–H units followed by substitution with electrophilic agents.

ogies with dimethoxyethane as the solvent or by doing the reaction at high dilution [6]. Perhaps a simpler method is performing the monosubstitution reactions in ethereal solvents at low temperature and specific carborane concentration. It was suggested that, depending on the type of electrophile, it is possible to find a combination of conditions (ethereal solvent, temperature, carborane concentration) that facilitates the largest degree of monosubstitution [7].

Phosphorus-substituted carboranes and carboranyl phosphinic acids

Substituting conventional organic entities by boron clusters to produce new compounds could deliver remarkable properties such as high rigidity and space occupancy. Carboranylphosphines is one example [8]. Phosphines are prominent ligands in coordination chemistry. By changing groups bonded to phosphorus, the steric and electronic effects are modified, so it is possible to «tailor» properties of the phosphines as ligands.

Our group and others were interested in the exploration of the properties of phosphinate ligands synthesized on the *ortho*-carborane platform [8], including P(III) and P(V) derivatives of *ortho*-carboranylphoshines [9]. The first derivatives that contain pentavalent phosphorus, phosphinic acids of *ortho*- and *meta*-carboranes were synthesized many years ago [10]. However, neither their characterization nor reproducible procedures of their synthesis were available. As a consequence, their coordination chemistry still remained unexplored till recently [11]. A representative drawing of the carboranyl phosphines, carboranyl phosphine oxides, carboranyl phosphinates and carboranyl phosphonates is shown in Figure 3.

Synthetic pathway of carboranyl phosphinic acids

As previously mentioned, due to the acidic character of C_c–H vertices of the cluster, they can be deprotonated with strong bases and then functionalized by means of electrophilic reagents. In our case, the deprotonation of the *meta*-carborane clusters **1–2** by *n*-BuLi followed by reaction with $ClP(NMe_2)_2$ gave *closo*-carboranyldiaminophosphine derivatives **3–4**. The reaction of compounds **3–4** with dry HCl gas in benzene gives *closo*-carboranyldichlorophosphines **5–6** that can be further hydrolyzed to the corresponding phosphinic acids **7–8** in aqueous solution at room temperature. The general reaction is given in Scheme 1.

Compounds **3–10** were characterized by multinuclear NMR and FT-IR spectroscopic techniques, mass spectrometry and elemental analysis. Table 1 shows the ^{31}P chemical shifts of

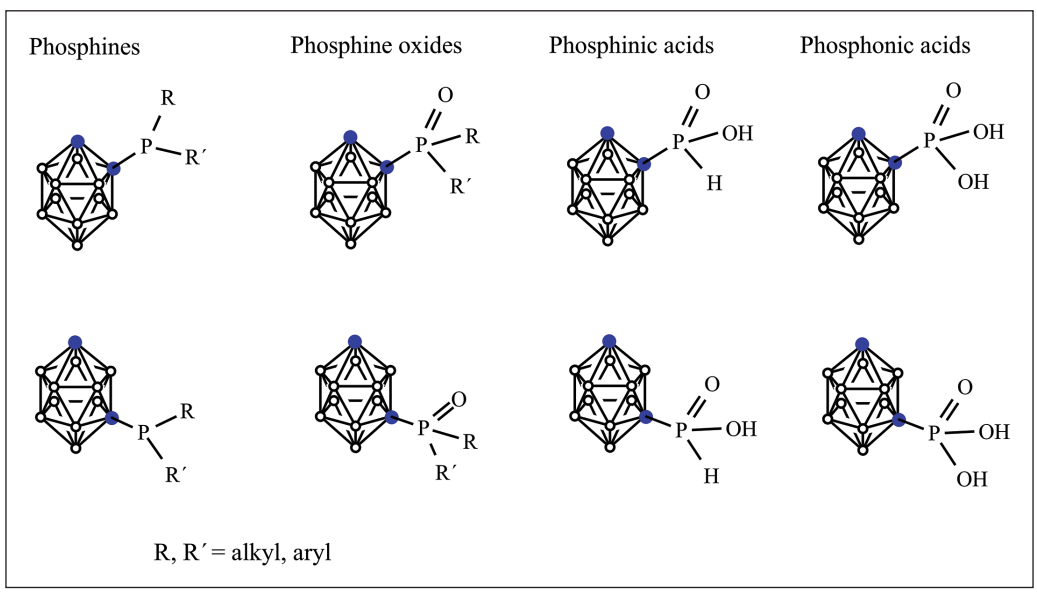

FIGURE 3. Phosphorus-substituted *closo*-carboranes.

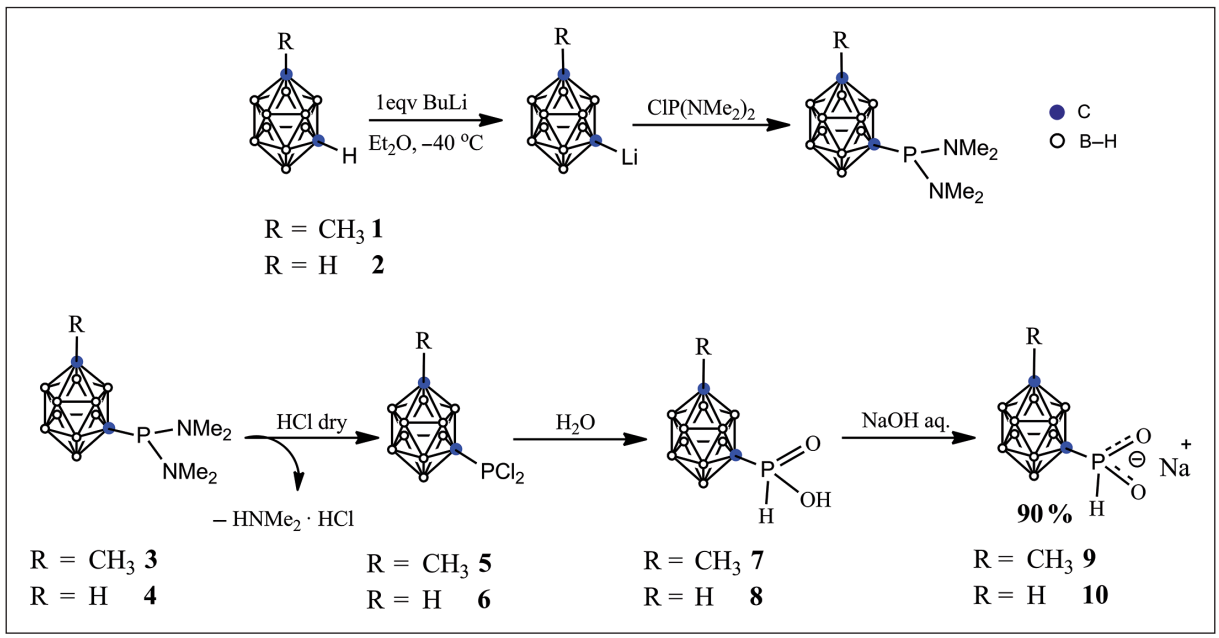

Scheme 1. Synthesis of *closo*-carboranylphosphinic acids.

these phosphorus compounds derived from *ortho*- and *meta*-carborane, which appear in the region between δ +162.20/ +14.66 ppm. The ^{31}P resonances in all *ortho*-carborane derivatives appear at higher frequency compared with those of the *meta*-carborane derivatives. From Table 1, it is clear when comparing the two cluster isomers that the difference in the ^{31}P chemical shift is the same: entries 1 and 2, entries 4 and 5 or entries 7 and 8. These experimental data display that a P(V) atom bonded to a *meta*-carboranyl cluster is more deshielded than if it is bonded to a *ortho*-carboranyl one; the difference being 6.45, 6.82 and 3.70 ppm, respectively. The same trend is observed in the anionic sodium salts, entries 10

Table 1. ^{31}P NMR chemical shifts (in ppm) for intermediates and products

Entry	Compound	Solvent	δ (^{31}P), ppm (*J*, MHz)	Δδ (^{31}P), ppm	
1	1–CH_3–2–$P(NMe_2)_2$–1,2–*closo*–$C_2B_{10}H_{10}$	$CDCl_3$	99.32		
2	1–CH_3–7–$P(NMe_2)_2$–1,7–*closo*–$C_2B_{10}H_{10}$	$CDCl_3$	105.77	+6.45	–0.12
3	1–$P(NMe_2)_2$–1,7–*closo*–$C_2B_{10}H_{11}$	$CDCl_3$	105.65		
4	1–CH_3–2–PCl_2–1,2–*closo*–$C_2B_{10}H_{10}$	$CDCl_3$	155.38		
5	1–CH_3–7–PCl_2–1,7–*closo*–$C_2B_{10}H_{10}$	$CDCl_3$	162.20	+6.82	–0.11
6	1–PCl_2–1,7–*closo*–$C_2B_{10}H_{11}$	$CDCl_3$	162.09		
7	1–CH_3–2–OPH(OH)–1,2–*closo*–$C_2B_{10}H_{10}$	$CDCl_3$	17.08 (640)		
8	1–CH_3–7–OPH(OH)–1,7–*closo*–$C_2B_{10}H_{10}$	$CDCl_3$	20.78 (633)	+3.70	+0.28
9	1–OPH(OH)–1,7–*closo*–$C_2B_{10}H_{11}$	$CDCl_3$	21.06 (635)		
10	$[Na{\cdot}(H_2O)_4][1–CH_3–2–OPH(O)–1,2–closo–C_2B_{10}H_{10}]$	D_2O	9.21 (449)		
11	$[Na][1–CH_3–7–OPH(O)–1,7–closo–C_2B_{10}H_{10}]$	D_2O H_2O	14.63 (t, ^1J(P, D) = 89) 14.65 (d, ^1J(P, H) = 589)	+5.42	+0.01
12	$[Na][1–OPH(O)–1,7–closo–C_2B_{10}H_{11}]$	D_2O	14.66 (d, ^1J(P, H) = 583)		

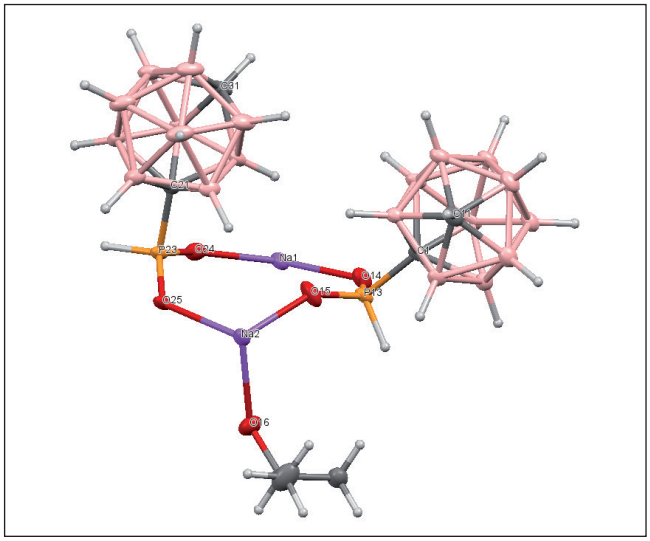

FIGURE 4. Molecular structure of $[Na_2][1\text{–}OPH(O)\text{–}1,7\text{–}closo\text{–}C_2B_{10}H_{10}]_2CH(OH)(CH_3)_2$.

and 11. It is also important to note when comparing entries 2 and 3, entries 5 and 6 or entries 8 and 9 on Table 1 that there is no influence on the nature of the R group (R = Me, H) bonded to the second C_c, the difference being 0.11 ppm in all cases. There is no difference in the chemical shifts for the sodium salts, entries 11 and 12.

Closo-carboranylphosphinic acids, compounds **7–9**, displayed a singlet around 17 ppm (for *ortho*-isomer) and 21 ppm (for *meta*-isomer) on $^{31}P\{^1H\}$ NMR spectrum that turns to a doublet in the ^{31}P NMR spectrum with coupling constant in the range of $^1J(P, H)$ = 635 Hz, indicating the presence of a P–H bond in the compounds.

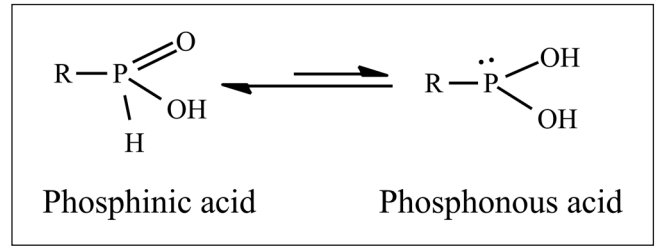

FIGURE 5. Tautomeric equilibrium between phosphinic and phosphonous acid isomers.

Good crystals of sodium salt of *meta*-carboranylphosphinic acid **10** (Figure 4) suitable for X-ray diffraction were grown from *i*PrOH/water solution, fully confirming its molecular structure.

Isotopic exchange with deuterium and tautomerization

It is well known that pentavalent phosphinic acid derivatives R(O)PH(OH) are involved in the tautomerization process with the corresponding trivalent phosphonous acid form $RP(OH)_2$ [12]. This tautomeric equilibrium (Figure 5) is completely shifted to P(V) tautomer, so free phosphonous acid normally cannot be detected by spectroscopic methods.

It was suggested that phosphorus-bonded hydrogen of phenylphosphinic acid undergoes isotopic exchange with deuterium from the deuterated solvent due to the presence of tautomeric equilibrium [13]. The compounds 1–OPH(OH)–1,7–

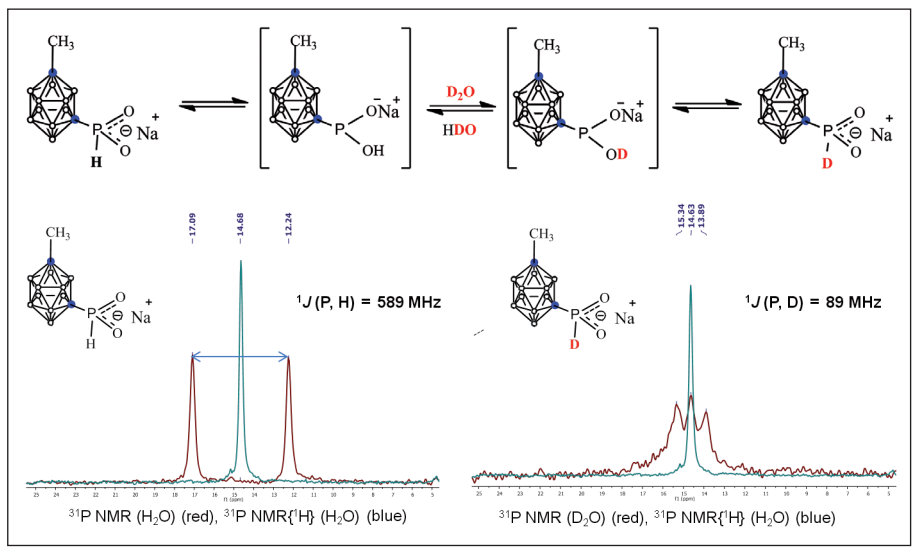

FIGURE 6. P–H/P–D exchange in D_2O observed by ^{31}P NMR spectra for $Na[1\text{–}Me\text{–}7\text{–}OPH(O)\text{–}1,7\text{–}C_2B_{10}H_{10}]$.

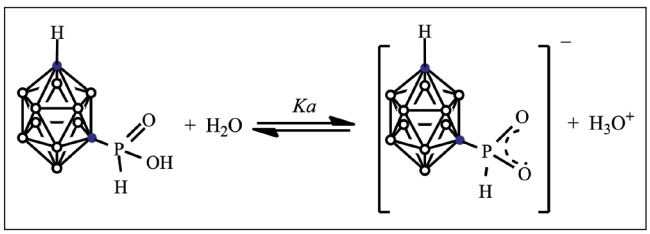

FIGURE 7. *Meta*-carboranylphosphinic acid and the corresponding conjugate base (phosphinate).

$C_2B_{10}H_{11}$ (**8**), Na[1–Me–7–OPH(O)–1,7–$C_2B_{10}H_{10}$] (**9**), and Na[1–OPH(O)–1,7–$C_2B_{10}H_{11}$] (**10**) display the same isotopic exchange.

To know the influence of the *meta*-carboranyl ligand, the kinetics of this acid-base isotopic exchange reaction between the hydrogen atom bound to phosphorus and deuterium from the D_2O solvent, was studied by means of $^{31}P\{^1H\}$ and ^{31}P NMR spectra for the compounds **8–10** (Figure 6).

A point to note is that the ^{31}P and $^{31}P\{^1H\}$ NMR spectra of **9** in D_2O after 3.5 h exhibit a triplet (1:1:1) at d = 14.63 ppm with a ^1J(P, D) of 89 Hz as a result of the completed isotopic exchange, whereas no exchange was observed for **10** after 2 days in D_2O. The phosphinic acid form of 1–OPH(OH)–1,7–$C_2B_{10}H_{11}$ disappears under isotopic exchange but the reaction is not as fast as in the case of Na[1–Me–7–OPH(O)–1,7–$C_2B_{10}H_{11}$]. After 48 h in D_2O, a triplet (1:1:1) at d = 12.96 ppm with a ^1J(P, D) of 87 Hz was observed.

Acidity, pK$_a$ comparison

Phosphinic acids possess one acidic P–OH group; the acidity of organophosphinic acids varies in the range of 1.3-2.5 pK_a.

In a similar way as carboxylic acids, pK_a values of phosphinic acids depend on the backbone molecule and the presence of other functional groups. We compared acid strengths of different carboranylphosphinic acids and their organic analogue phenylphosphinic acid. To our surprise, *meta*-carborane enhances the acidity of corresponding phosphinic acid compared to *ortho*-carborane and phenyl group (Figure 8). Also the presence of CH_3 group on the other C_c decreases the acidity of the corresponding carboranylphosphinic acid.

Conclusions

This work has shown that, in a manner similar to organic phosphinates, purely inorganic carboranyl phosphinates can be prepared in very good to excellent yields. Carboranylphosphinic acids have been prepared with both isomers, *ortho*- and *meta*-carborane. The hydrogen in the H–P unit of the carboranylphosphinate has been easily exchanged by D from the deuterated NMR solvent, although rate differences have been noticed depending on the adjacent carborane carbon substituent and the salt or acid form utilized. The carborane influence has been observed in the pK_a of the phosphinate, which is more negative for the *meta*-carboranyl than for the «comparable» phenyl and *ortho*-carborane. It is expected that these enhanced electronic properties will be accompanied by others derived from the hydrophobicity and space-filling efficiency of the carboranyl fragment, making the physicochemical properties of the generated metal complexes attractive for applications in medicine or in materials science.

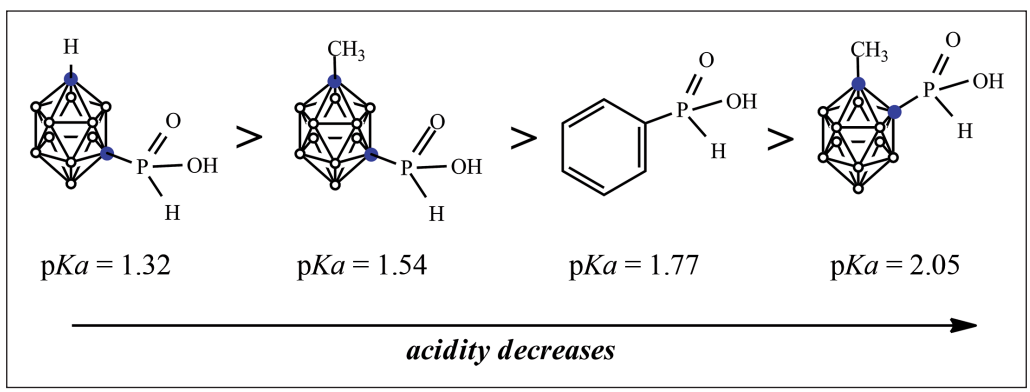

FIGURE 8. pK_a values of *ortho*–, *meta*-carboranylphosphinic acids and phenylphosphinic acid.

Acknowledgements

The authors thank the Generalitat de Catalunya (2014/SGR/149), the Spanish Ministry of Economy and Competitiveness (CTQ2013-44670-R) and the European Union (COST1302) for their financial support. E. Oleshkevich is enrolled in the PhD program of the UAB. E. Oleshkevich thanks the MICINN for an FPU pre-doctoral grant.

References

[1] Eberhardt, W. H.; Crawford, B.; Lipscomb, W. N. "The valence structure of the boron hydrides". *J. Chem. Phys.*, No. 22 (1954), p. 989-1001.

[2] *a*) Teixidor, F.; Viñas, C.; Demonceau, A.; Núñez, R. "Boron clusters: do they receive the deserved interest?". *Pure App. Chem.*, No. 75 (2003), p. 1305-1313. *b*) Scholz, M.; Hey-Hawkins, E. "Carbaboranes as pharmacophores: properties, synthesis, and application strategies". *Chem. Rev.*, No. 111 (2011), p. 7035-7062.

[3] *a*) Poater, J.; Solà, M.; Viñas, C.; Teixidor, F. "A simple link between hydrocarbon and borohydride chemistries". *Chem. Eur. J.*, No. 19 (2013), p. 4169-4175. *b*) Poater, J.; Solà, M.; Viñas, C.; Teixidor, F. "π aromaticity and three-dimensional aromaticity: two sides of the same coin?". *Angew. Chem. Int. Ed.*, No. 53 (2014), p. 12191-12195.

[4] Poater, J.; Solà, M.; Viñas, C.; Teixidor, F. "Hückel's rule of aromaticity categorizes aromatic *closo* boron hydride clusters". *Chem. Eur. J.* (2016). DOI: 10.1002/chem.201600510.

[5] Grimes, R. N. *Carboranes*. 2nd ed. Burlington: Academic Press, 2011.

[6] *a*) Gómez, F. A.; Hawthorne, M. F. "A simple route to C-monosubstituted carborane derivatives". *J. Org. Chem.*, No. 57 (1992), p. 1384-1390. *b*) Viñas, C.; Benakki, R.; Teixidor, F.; Cassabó, J. "Dimethoxyethane as a solvent for the synthesis of C-monosubstituted o-carborane derivatives". *Inorg. Chem.*, No. 34 (1995), p. 3844. *c*) Valliant, J. F.; Guenther, K. J.; King, A. S.; Morel, P.; Schaffer, P.; Sogbein, O. O.; Stephenson, K. A. "The medicinal chemistry of carboranes". *Coord. Chem. Rev.*, No. 232 (2002), p. 173.

[7] Popescu, A. R.; Musteti, A. D.; Ferrer-Ugalde, A.; Viñas, C.; Núñez, R.; Teixidor, F. "Influential role of ethereal solvent on organolithium compounds: the case of carboranyllithium". *Chem. Eur. J.*, No. 18 (2012), p. 3174-3184.

[8] Popescu, A. R.; Teixidor, F.; Viñas, C. "Metal promoted charge and hapticities of phosphines: the uniqueness of carboranylphosphines". *Coord. Chem. Rev.*, No. 269 (2014), p. 54-84 and cited references.

[9] Popescu, R.; Laromaine, A.; Teixidor, F.; Sillanpää, R.; Kivekäs, R.; Llambias, J. I.; Viñas, C. "Uncommon coordination behaviour of P(S) and P(Se) units when bonded to carboranyl clusters: experimental and computational studies on the oxidation of carboranyl phosphine ligands". *Chem. Eur. J.*, No. 17 (2011), p. 4429-4443.

[10] *a*) Zakharkin, L. I.; Kazantsev, A. V.; Zhubekova, M. N. *Izv. Akad. Nauk SSSR, Ser. Khim.*, No. 9 (1969), p. 2056-2057. *b*) Kazantsev, A. V.; Zhubekova, M. N.; Zakharkin, L. I. *Zh. Obshch. Khim.*, No. 42 (1971), p. 1570-1571.

[11] Oleshkevich, E.; Teixidor, F.; Choquesillo-Lazarte, D.; Sillanpää, R.; Viñas, C. "Carboranylphosphinic acids: a new class of purely inorganic ligands". *Chem. Eur. J.*, No. 11 (2016), p. 3665-3670.

[12] *a*) Martin, R. B. "The rate of exchange of the phosphorus bonded hydrogen in phosphorous acid". *J. Am. Chem. Soc.*, No. 81 (1959), p. 1574-1576. *b*) Silver, R. B.; Luz, Z. "Oxidation of phosphorous acid". *J. Phys. Chem.*, No. 66 (1962), p. 1356-1359.

[13] Reuben, J.; Samuel, D.; Silver, B. L. "Deuterium exchange between phenylphosphonous acid and water". *J. Am. Chem. Soc.*, No. 85 (1963), p. 3093-3096.

E. Oleshkevich

F. Teixidor

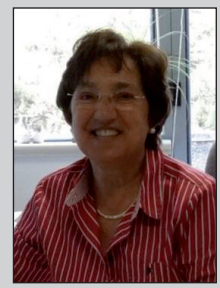

C. Viñas

Elena Oleshkevich is a graduate in Chemical Technology of Biologically Active Synthetic Substances (2011) at the D. I. Mendeleev University of Chemical Technologies of Russia (Российский химико-технологический университет имени Д. И. Менделеева). She is now preparing her doctoral thesis under the direction of Prof. Clara Viñas at the Institute of Materials Science of Barcelona (ICMAB-CSIC). The subject of her thesis is the synthesis of carboranyl phosphinic acids for use as purely inorganic ligands and the study of the properties of their metallic complexes for their possible application in medicine and in materials science.

Francesc Teixidor graduated in Chemistry at the Autonomous University of Barcelona (UAB) in 1975 and took his doctorate there in 1979. Then he did a post-doctoral fellowship at the University of Michigan with Prof. Ralph W. Rudolph for two and half years. Back in Barcelona, he joined the UAB as lecturer in Chemistry. In 1987 he won a place as scientific researcher of the Higher Council of Scientific Research (CSIC) at the Institute of Materials Science of Barcelona and he has been a research professor there since 1999. He has directed 25 doctoral theses and 24 research projects, and he has published over 350 scientific papers in SCI journals, 24 book chapters and one encyclopedia chapter, among other scientific contributions. His field of research is inorganic chemistry, with a special focus on the formation of B–C and B–P bonds and the application of boron clusters as molecular materials for energy production.

Clara Viñas is a graduate in Chemistry at the Autonomous University of Barcelona (UAB, 1975) and in Pharmacy at the University of Barcelona (UB, 1980). She began her research work at the laboratories of Prof. Ralph W. Rudolph at the University of Michigan for one year. On returning to Barcelona, she worked in industry and subsequently won a place at the Municipal Laboratory of Sabadell, where she came to be the director. She took a PhD in Pharmacy at the University of Barcelona in 1991. In 1992 she won a place as tenured scientist of the Higher Council of Scientific Research (CSIC) at the Institute of Materials Science of Barcelona. There she was promoted to the category of scientific researcher in 2002 and she has been a research professor at this institution since 2006. Over the course of her scientific career she has directed 11 doctoral theses and 12 research projects, and she has published over 295 scientific papers in SCI journals, 17 book chapters and one encyclopedia chapter, among other contributions. Her research is based on the synthesis of boron compounds, carboranes and metallacarboranes for use in advanced medical applications.

Inorganic Chemistry

Communication

pubs.acs.org/IC

m-Carboranylphosphinate as Versatile Building Blocks To Design all Inorganic Coordination Polymers

Elena Oleshkevich,[†] Clara Viñas,[†] Isabel Romero,[‡] Duane Choquesillo-Lazarte,[§] Matti Haukka,[∥] and Francesc Teixidor*[,†]

[†]Institut de Ciència de Materials de Barcelona (ICMAB-CSIC), Campus UAB, 08193 Bellaterra, Spain

[‡]Departament de Química and Serveis Tècnics de Recerca, Universitat de Girona, Campus de Montilivi, E-17071 Girona, Spain

[§]Laboratorio de Estudios Cristalográficos, IACT (CSIC-UGR), Av de las Palmeras 4, 18100 Armilla (Granada), Spain

[∥]Department of Chemistry, University of Jyväskylä, FIN-40014 Jyväskylä, Finland

Supporting Information

ABSTRACT: The first examples of coordination polymers of manganese(II) and a nickel(II) complex with a purely inorganic carboranylphosphinate ligand are reported, together with its exhaustive characterization. X-ray analysis revealed 1D polymeric chains with carboranylphosphinate ligands bridging two manganese(II) centers. The reactivity of polymer **1** with water and Lewis bases has also been studied.

Coordination polymers (CPs) are different from organic polymers because metal atoms participate in their backbone, resulting in different properties.[1] They require ligands, and among these, carboxylic ligands are frequent choices for metal−organic network spacers.[2] Although phosphorus is an essential element in materials science and inorganic chemistry, as well as a key building block in all known forms of life[3] (e.g., DNA is a fundamental life polymer), phosphorus chemistry is not receiving much attention to construct CPs. This is somewhat surprising because the coordinating motif of organic phosphorus oxoacids reminds one very much of the carboxylic acid site. Perhaps one possible clue to the weak presence of organic phosphorus oxoacids in CPs is that hypophosphorous acid is a powerful reducing agent that strongly limits its coordination to metal ions.[4] Phosphorus oxoacids are the most common form of phosphorus acids. Within the mononuclear phosphorus oxoacids, those that have only one phosphorus and whose representative examples are hypophosphorous acid, phosphorous acid, and phosphoric acid, the phosphorus oxidation states are 1+, 3+, and 5+, respectively (Chart 1). Substitution of one hydrogen or OH by organic groups leads to the corresponding organophosphonic and organophosphinic acids; their salts are known as phosphinates and phosphonates, respectively.

Chart 1. Schematic Representations of Phosphorous Oxoacids

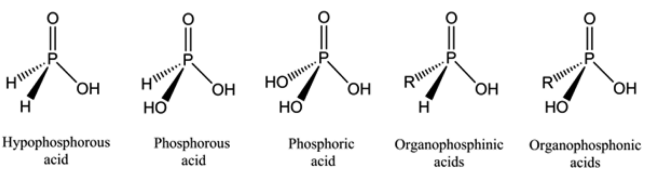

Phosphinates are made on an industrial scale (~50.000 tons/year) but have not yet been employed in general industrial organophosphorus synthesis.[5] Althought phosphonic and phosphinic acids are seemingly good competitors to carboxylic acids in the sense of the complexation capacity and stability of produced complexes,[6] a search of the Cambridge Structural Database[7] shows just 375 hits for phosphonic acid R-PO(OH)$_2$ (R = alkyl, aryl) and >2200 hits for its transition-metal complexes,[8] while only 20 hits for phosphinic acids R-P(H)O(OH) (R = alkyl, aryl) and 47 hits for its transition-metal complexes were found.[9]

The 12-vertex *closo*-$C_2B_{10}H_{12}$ icosahedral carboranes, *o*-(1,2), *m*-(1,7), or *p*-(1,12), are like spheres of exceptional thermal and chemical stability that can be functionalized at the carbon and/or boron vertices by different straightforward reactions.[10] All of these peculiarities and the fact that they can be produced at large scale[10b] make them valuable ligands in coordination chemistry. *o*- and *m*-carboranylphosphinates (Figure 1) were prepared as a new

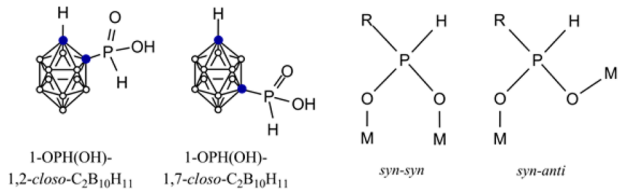

Figure 1. Schematic drawing of *o*- and *m*-carboranylphosphinic acid and their coordination modes: syn−syn and syn−anti.

class of purely inorganic ligands, and the influence of the cluster on the reactivity of the phosphinate group was studied.[11] The electron-withdrawing character of the carboranyl carbon atoms of the cluster cage, combined with their spherical space-filling efficiency, that have a volume similar to that of a rotating phenyl group with enhanced 3D aromaticity[12] renders the phosphorus more difficult to oxidize. This enables carboranylphosphinates to survive against strong oxidizing elements, a property that is uncommon for organic phosphinates.[4]

To date, no examples of carboranylphosphinic acid complexes or CPs with this motif have ever been described. This is not

Received: March 13, 2017

DOI: 10.1021/acs.inorgchem.7b00610
Inorg. Chem. XXXX, XXX, XXX−XXX

surprising because, as we have already noted above, very few complexes of phosphinate exist. The use of carboranes in supramolecular chemistry is a topic that generates great interest for their particular properties, which may induce unconventional characteristics in the supramolecular structures in which they are inserted.[13] The geometrical features found in the complexes of $[1\text{-}CO_2\text{-}1,2\text{-}closo\text{-}C_2B_{10}H_{11}]^-$ with manganese(II),[14] copper(II),[15] and cobalt(II)[16] could not be compared with those of derivatives of conventional monocarboxylate ligands. The carboranyl group with its spherical shape is difficult to compare with organic fragments if we do not consider C_{60} or dodecahedrane $C_{20}H_{20}$; besides, it displays good hydrophobicity and electron-withdrawing properties through the carbon-atom vertices. There is a remarkable difference between the two isomers 1,2-*closo*-$C_2B_{10}H_{12}$ and 1,7-*closo*-$C_2B_{10}H_{12}$ that induces higher chemical stability to the P−C_c bond in 1,7-*closo*-carboranylphosphinic acids (Figure 1). All of these characteristics of the icosahedral carborane, not found in imaginable organic fragments, suggest that a marked distinct behavior can be suspected in most of the generated complexes compared with aryl- and/or alkylphosphinic acids. In this paper, we show that inorganic CPs uniquely made with inorganic fragments are possible. Only organic solvent molecules occupying non-structural sites have been needed. This has been possible by using the recently available *m*-carboranylphosphinate ligand $[1\text{-}OPH(O)\text{-}1,7\text{-}closo\text{-}C_2B_{10}H_{11}]^-$, with manganese(II) and nickel(II). The reactivity of the 1D polymer manganese(II) complex versus water and nitrogen heterocyclic aromatic ligands such as 2,2′-bipyridine (2,2′-bpy) is also presented.

Synthesis of All-Inorganic-Made Inorganic CPs. The strategic procedures for the synthesis of the manganese(II), **1**−**3**, and nickel(II), **4**, complexes, all of them containing the anionic *m*-carboranylphosphinate ligand $[1\text{-}OPH(O)\text{-}1,7\text{-}closo\text{-}C_2B_{10}H_{11}]^-$, are outlined in Scheme 1. The manganese(II) complex **1** was obtained by mixing methanol solutions of $Na[1\text{-}OPH(O)\text{-}1,7\text{-}closo\text{-}C_2B_{10}H_{11}]$ salt with $MnCl_2{\cdot}4H_2O$ in a 2:1 ratio after stirring for 2 h at room temperature. Afterward, NaCl was filtered and the solvent evaporated under a vacuum to obtain a white solid **1**. When **1** was dissolved in ^{i}PrOH/H_2O, compound **2** was obtained. However, when an equimolar ethanol solution of bidentate 2,2′-bpy was added to **1**, a slightly yellow solution of **3** was formed. The polymeric structure of **3** is lost in a mixture of ^{i}PrOH/H_2O, producing lower-nuclearity species, as supported by $^{11}B\{^1H\}$ NMR spectroscopy (see Supporting Information, SI).

Scheme 1. Synthetic Strategy for the Preparation of Manganese(II) Compounds 1−3

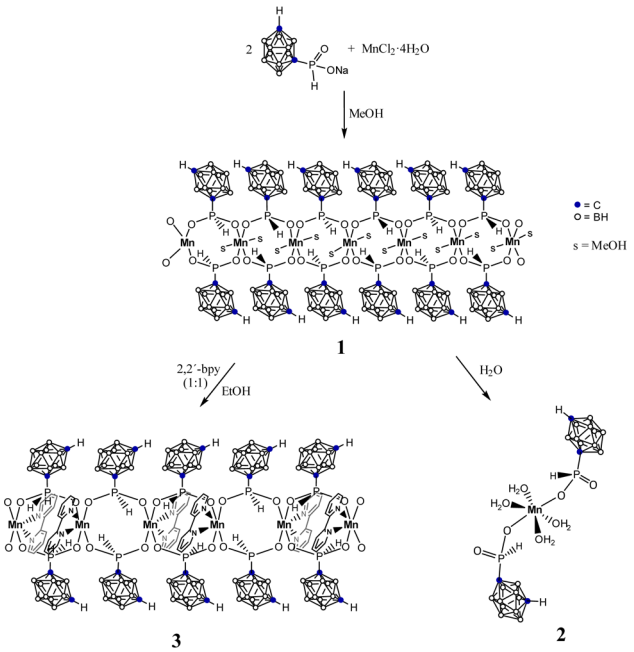

On the other hand, the reaction of $Na[1\text{-}OPH(O)\text{-}1,7\text{-}closo\text{-}C_2B_{10}H_{11}]$ and $NiCl_2$ in a 2:1 ratio in ethanol at room temperature leads to the formation of compound **4** after NaCl filtration and solvent evaporation. Elemental analyses and electrospray ionization mass spectroscopy confirm the stoichiometries of all of these complexes.

Spectroscopic Evidence of the All-Inorganic-Made Inorganic CPs. The IR spectra of **1**−**4** display typical ν(B−H) absorption at frequencies above 2580 cm^{-1}, characteristic of *closo*-carborane derivatives.[17] Strong absorptions observed in the region 1225−1000 cm^{-1} indicate the presence of P═O and M−O−P linkages, and the absorption around 2330−2400 cm^{-1} is associated with ν(P−H) in all cases.[18] The $^{11}B\{^1H\}$ NMR spectra of complexes **2**−**4** are observed in the range −2 to −15 ppm. The nickel(II) compound shows a 2:2:4:2 pattern, whereas ^{11}B and $^{11}B\{^1H\}$ NMR spectra of manganese(II) complex **1** displays a downfield spectrum (+14.0/+1.7 ppm) with boron resonances overlapping. The phosphorus resonance of **1**−**3** at the $^{31}P\{^1H\}$ NMR spectra was not observed because of the paramagnetism as well as the quadrupole moment of the metal nuclei ($I = {}^5/_2$ for ^{55}Mn; natural abundance = 100%), while the nickel(II) complex **4** displays a very broad resonance around 13 ppm (see the SI).

Crystal Structures. The polymeric nature of **1** and **3** could not be absolutely defined unless good crystals were grown. Compounds **1** and **3**, in addition to be the first examples of all-inorganic-made inorganic CPs, are also the first described coordination polynuclear manganese(II) polymers with phosphinate ligands bridging each of the two manganese(II) centers. The backbone is strictly made of manganese and the all-inorganic-made carboranylphosphinate that runs in a zigzag 1D chain. In **1**, the two μ-OO′ phosphinate groups in the "$Mn_2(\mu\text{-}OOPR)_2$" core are different; one of them is coordinated to manganese(II) atoms in a syn−syn conformation and the other one in a syn−anti conformation (Figure 1). To fill the two vacant manganese(II) positions that do not have a structural function, both methanol (**1**) and 2,2′-bpy (**3**) have been utilized. To the best of our knowledge, no similar structure has been found in the literature with other phosphinate ligands.[19] Interestingly, the structure of **3** is the same as that for **1**, except in one noticeable fact. In **1**, the methanol molecules are trans, whereas in **3**, 2,2′-bpy necessarily occupies a cis disposition. The fact that the structure of **3** is similar to that of **1** is in contrast to the fate of manganese coordination complexes with carboranylcarboxylate that, upon reaction with 2,2′-bpy, the initial polymeric nature is lost to develop species with much lower nuclearity. The result of dissolving **1** in ^{i}PrOH/H_2O leads to **2**. The crystal structure indicates that the former polymeric structure in **1** is broken, leading to a mononuclear manganese(II) compound, $[Mn(H_2O)_4(1\text{-}OPH(O)\text{-}1,7\text{-}closo\text{-}C_2B_{10}H_{11})_2]$. In **2**, the carboranylphosphinate ligand is monodentate, whereas it is bridging in **1** and **3**. The molecular structures of **1**−**3** are shown in Figure 2.

For nickel(II), the affinity to the carboranylphosphinate ligand is very weak, much less than that for water. The polymeric structure is not generated in this case, and a salt of $[Ni(H_2O)_6]^{2+}$

DOI: 10.1021/acs.inorgchem.7b00610
Inorg. Chem. XXXX, XXX, XXX−XXX

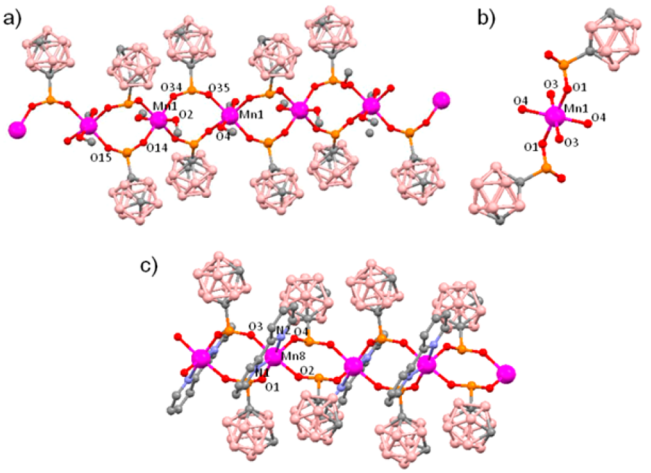

Figure 2. X-ray structures of manganese compounds **1**−**3** (a−c, respectively), showing a monodimensional arrangement.

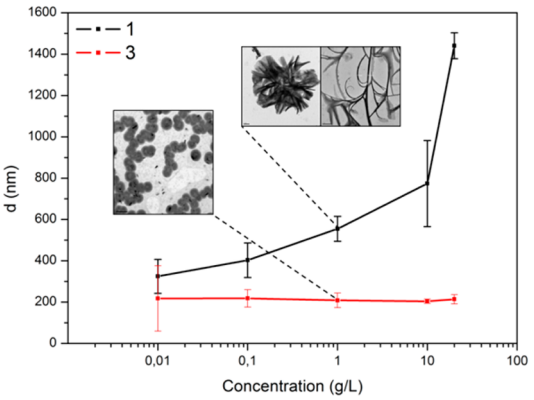

Figure 3. DLS study of polymers **1** and **3** from methanol at different concentrations with their TEM images from methanol at the same concentration (1 g/L).

compensating for the carboranylphosphinate ligand is generated. Noticeable is the packing of **4** along the *a* axis in which the hydrophobic layers pack one on top of the other. Views of the packing along the *a*, *b*, and *c* axes are displayed in the SI.

Physical Studies of the All-Inorganic-Made Inorganic CPs. *Thermal Stability.* Because these polymers can be interpreted as made of a fully inorganic scaffold structure plus solvating or ancillary ligands, the thermogravimetric analysis (TGA)/differential scanning calorimetry (DSC) studies were made to interpret whether these solvating elements were really the easiest ones to remove. Some information had been drawn from the **1** to **3** reaction process, by which the initial scaffold had been retained and only the initial solvating ligands had been exchanged. TGA/DSC data are displayed in the SI. For **1**, the best fit for a weight loss of 38.49% in the range from room temperature to 483 °C is the removal of two methanol coordinated molecules and one 1,7-*closo*-$C_2B_{10}H_{12}$ per manganese(II). For **2**, a weight loss of 40.90% in the range from room temperature to 507 °C corresponds to four coordinated water molecules and one 1,7-*closo*-$C_2B_{10}H_{12}$ per manganese(II). Finally, a weight loss of 47.71% in the range from room temperature to 430 °C observed for **3** can be assigned to the loss of one bpy molecule and one 1,7-*closo*-$C_2B_{10}H_{12}$.

Dynamic Light Scattering (DLS) and Transmission Electron Microscopy (TEM) of 1 and 3. Methanol solutions of **1** and **3** at different concentrations (from 0.01 to 20 g/L) were measured by DLS, indicating that aggregation/cleavage processes of polymeric structures **1** and **3** in methanol strongly depend on the concentration (Figure 3). This dynamic process causes polydispersity; however, an estimation of the dimensions of the polymer/aggregates can be obtained. The TEM images of a methanol solution of CPs **1** and **3** at the same concentration (1 g/L) corroborate that either polymeric or aggregate structures exist in solution (Figure 3). For **1**, long strands of 100−200 nm width are formed, whereas **3** aggregates in spherical structures whose dimensions are in the range 1700−2000 nm.[20]

To date, organophosphinate CPs with transition metals were not available because of the reducing power of the ligands. Here, we report on the first 1D phosphinate CPs of manganese(II) (**1** and **3**). This goal has been achieved by using a unique purely inorganic ligand, *m*-carboranylphosphinate, which is not a reducing agent because of the electron-withdrawing character of the *closo*-carboranyl cluster. In addition, *m*-carboranylphosphinate is an amphiphilic ligand as a result of the hydrophilic site of the coordinating group and the lypophilic properties of the *closo*-carboranyl cluster. The central wire is made of manganese(II) ions linked by bridging PO_2 units. Each PO_2 unit is also linked to a spherical *closo*-carborane overall, producing an all-inorganic-made inorganic CP. Only organic solvent molecules occupying nonstructural sites have been needed. In contrast to manganese(II), nickel(II) possesses a higher affinity for water than for the *m*-carboranylphosphinate ligand; consequently, no polymeric structure is generated, but the salt $[Ni(H_2O)_6][1\text{-}OPH(O)\text{-}1,7\text{-}closo\text{-}C_2B_{10}H_{11}]$ with a supramolecular hydrophobic/hydrophilic structure is obtained. Work is now underway to explore the coordination capability of *m*-carboranylphosphinate with other first- and second-row transition metals.

■ ASSOCIATED CONTENT

Supporting Information

The Supporting Information is available free of charge on the ACS Publications website at DOI: 10.1021/acs.inorgchem.7b00610.

Synthesis and characterization, TGA/DSC, TEM images of complexes **1**−**4** and their crystallographic data, selected bond distances and angles, and packing structures (PDF)

■ AUTHOR INFORMATION

Corresponding Author

*E-mail: teixidor@icmab.es.

ORCID

Clara Viñas: 0000-0001-5000-0277
Isabel Romero: 0000-0003-4805-8394
Duane Choquesillo-Lazarte: 0000-0002-7077-8972
Matti Haukka: 0000-0002-6744-7208
Francesc Teixidor: 0000-0002-3010-2417

Notes

The authors declare no competing financial interest.

■ ACKNOWLEDGMENTS

Thanks to MINECO (CTQ2015-66143-P, CTQ2010-16237 and SEV-2015-0496), Generalitat de Catalunya (2014/SGR/149), and COST CM1302. E.O. who is enrolled in the PhD program of the UAB thanks for FPU grant.

DOI: 10.1021/acs.inorgchem.7b00610
Inorg. Chem. XXXX, XXX, XXX−XXX

REFERENCES

(1) (a) Moulton, B.; Zaworotko, M. J. Coordination polymers: toward functional transition metal sustained materials and supermolecules. *Curr. Opin. Solid State Mater. Sci.* **2002**, *6*, 117−123. (b) Janiak, C. J. Engineering coordination polymers towards applications. *Dalton Trans.* **2003**, 2781−2804. (c) Yan, Y.; Zhang, J.; Ren, L.; Tang, C. Metal-containing and related polymers for biomedical applications. *Chem. Soc. Rev.* **2016**, *45*, 5232−5263. (d) Housecroft, C. E. Carboranes as guests, counterions and linkers in coordination polymers and networks. *J. Organomet. Chem.* **2015**, *798*, 218−228. (e) Nuñez, R.; Romero, I.; Teixidor, F.; Viñas, C. Icosahedral boron clusters: a perfect tool for the enhancement of polymer features. *Chem. Soc. Rev.* **2016**, *45*, 5147−5173. (g) Huang, F.; Anslyn, E. V. Introduction: Supramolecular Chemistry. *Chem. Rev.* **2015**, *115*, 6999−7000.

(2) (a) Cahill, C. L.; de Lill, D. T.; Frisch, M. Homo- and heterometallic coordination polymers from the f elements. *CrystEngComm* **2007**, *9*, 15−26. (b) Loiseau, T.; Mihalcea, I.; Henry, N.; Volkringer, C. The crystal chemistry of uranium carboxylates. *Coord. Chem. Rev.* **2014**, *266-267*, 69−109.

(3) Kochian, L. V. Rooting for more phosphorus. *Nature* **2012**, *488*, 466−467.

(4) (a) Gordon, P. E.; Fry, A. J.; Hicks, L. D. Further studies on the reduction of benzylic alcohols by hypophosphorous acid/iodine. *Arkivoc* **2005**, *6*, 393−400. (b) Hicks, L. D.; Han, J. K.; Fry, A. J. Hypophosphorous acid−iodine: a novel reducing system. *Tetrahedron Lett.* **2000**, *41*, 7817−7820.

(5) (a) Büchel, K. H.; Moretto, H.-H.; Woditsch, P. *Industrial Inorganic Chemistry*, 2nd ed.; Wiley VCH: New York, 2000; pp 65−101. (b) Kroschwitz, J.; Seidel, A. *Kirk−Othmer Encyclopedia of Chemical Technology*, 4th ed.; Wiley: New York, 1999; Vol. *18*.

(6) Montchamp, J. L. Phosphinate Chemistry in the 21st Century: A Viable Alternative to the Use of Phosphorus Trichloride in Organophosphorus Synthesis. *Acc. Chem. Res.* **2014**, *47*, 77−87.

(7) (a) On February 28, 2017. (b) Bruno, J.; Cole, J. C.; Edgington, P. R.; Kessler, M.; Macrae, C. F.; McCabe, P.; Pearson, J.; Taylor, R. New software for searching the Cambridge Structural Database and visualizing crystal structures. *Acta Crystallogr., Sect. B: Struct. Sci.* **2002**, *58*, 389−397.

(8) A total of 84 crystal structures with the ligand being monodentate, 549 bidentate, and >1600 binding as the tridentate mode.

(9) A total of 7crystal structures in a monodentate binding mode and 40 for bidentate bridging. Importantly, only 15 of the 47 phosphinic acid complexes are CPs.

(10) (a) Grimes, R. N. *Carboranes*, 3rd ed.; Elsevier Inc., 2016. (b) Scholz, M.; Hey-Hawkins, E. Carbaboranes as Pharmacophores: Properties, Synthesis, and Application Strategies. *Chem. Rev.* **2011**, *111*, 7035−7062. (c) *Boron Science*; Hosmane, N. S., Ed.; CRC Press: New York, 2012. (d) Olid, D.; Nuñez, R.; Viñas, C.; Teixidor, F. Methods to produce B−C, B−P, B−N and B−S bonds in boron clusters. *Chem. Soc. Rev.* **2013**, *42*, 3318−3336. (e) Armstrong, A. F.; Valliant, J. F. The bioinorganic and medicinal chemistry of carboranes: from new drug discovery to molecular imaging and therapy. *Dalton Trans.* **2007**, 4240−4251. (f) Sivaev, I. B.; Bregadze, V. V. Polyhedral Boranes for Medical Applications: Current Status and Perspectives. *Eur. J. Inorg. Chem.* **2009**, *2009*, 1433−1450. (g) Fox, M. A. Polyhedral Carboranes. In *Comprehensive Organometallic Chemistry III*; Crabtree, R. H., Mingos, D. M. P., Eds.; Elsevier: Oxford, U.K., 2007; Vol. *3*, Chapter 3.02, pp 49−112. (h) Yao, Z.-J.; Deng, W. Half-sandwich late transition metal complexes based on functionalized carborane ligands. *Coord. Chem. Rev.* **2016**, *309*, 21−35.

(11) Oleshkevich, E.; Teixidor, F.; Choquesillo-Lazarte, D.; Sillanpää, R.; Viñas, C. Carboranylphosphinic Acids: A New Class of Purely Inorganic Ligands. *Chem. - Eur. J.* **2016**, *22*, 3665−3667.

(12) Poater, J.; Solà, M.; Viñas, C.; Teixidor, F. π-aromaticity and tridimensional aromaticity. Two sides of the same coin? *Angew. Chem., Int. Ed.* **2014**, *53*, 12191−12195.

(13) (a) Farha, O. K.; Spokoyny, A. M.; Mulfort, K. L.; Galli, S.; Hupp, J. T.; Mirkin, C. A. Gas-Sorption Properties of Cobalt(II)−Carborane-Based Coordination Polymers as a Function of Morphology. *Small* **2009**, *5*, 1727−1731. (b) Huang, S. L.; Weng, L. H.; Jin, G. X. Bottom-up synthesis of coordination polymers based on carborane backbones and $Cu_2(CO_2)_4$ paddle-wheel: ligand metathesis with metallotecons. *Dalton Trans.* **2012**, *41*, 11657−11662. (c) Kennedy, R. D.; Krungleviciute, V.; Clingerman, D. J.; Mondloch, J. E.; Peng, Y.; Wilmer, C. E.; Sarjeant, A. A.; Snurr, R. Q.; Hupp, J. T.; Yildirim, T.; Farha, O. K.; Mirkin, C. A. Carborane-Based Metal−Organic Framework with High Methane and Hydrogen Storage Capacities. *Chem. Mater.* **2013**, *25*, 3539−3543. (d) Li, J.-R.; Sculley, J.; Zhou, H.-C. Metal−Organic Frameworks for Separations. *Chem. Rev.* **2012**, *112*, 869−932. (e) Boldog, I.; Bereciartua, P. J.; Bulanek, R.; Kucerakova, M.; Tomandlova, M.; Dusek, M.; Machacek, J.; De Vos, D. E.; Base, T. 10-Vertex *closo*-carborane: a unique ligand platform for porous coordination polymers. *CrystEngComm* **2016**, *18*, 2036−2040. (f) Rodríguez-Hermida, S.; Tsang, M. Y.; Vignatti, C.; Stylianou, K. C.; Guillerm, V.; Pérez-Carvajal, J.; Teixidor, F.; Viñas, C.; Choquesillo-Lazarte, D.; Verdugo-Escamilla, C.; Peral, I.; Juanhuix, J.; Verdaguer, A.; Imaz, I.; Maspoch, D.; Giner Planas, J. Switchable Surface Hydrophobicity−Hydrophilicity of a Metal−Organic Framework. *Angew. Chem., Int. Ed.* **2016**, *55*, 16049−16053.

(14) (a) Fontanet, M.; Rodriguez, M.; Romero, I.; Fontrodona, X.; Teixidor, F.; Viñas, C.; Aliaga-Alcalde, N.; Matějíček, P. A water soluble Mn(II) polymer with aqua metal bridges. *Dalton Trans.* **2013**, *42*, 7838−7841. (b) Fontanet, M.; Rodriguez, M.; Romero, I.; Fontrodona, X.; Teixidor, F.; Viñas, C.; Aliaga-Alcalde, N.; Matějíček, P. Water-Soluble Manganese Inorganic Polymers: The Role of Carborane Clusters and Producing Large Structural Adjustments from Minor Molecular Changes. *Chem. - Eur. J.* **2014**, *20*, 13993−14003.

(15) (a) Fontanet, M.; Popescu, A. R.; Fontrodona, X.; Rodriguez, M.; Romero, I.; Teixidor, F.; Viñas, C.; Aliaga-Alcalde, N.; Ruiz, E. Design of Dinuclear Copper Species with Carboranylcarboxylate Ligands: Study of Their Steric and Electronic Effects. *Chem. - Eur. J.* **2011**, *17*, 13217−13229. (b) Fontanet, M.; Rodriguez, M.; Fontrodona, X.; Romero, I.; Teixidor, F.; Viñas, C. Intramolecular hydrogen bonding stabilizes the nuclearity of complexes. A comparative study based on the H-carborane and Me-carborane framework. *Dalton Trans.* **2015**, *44*, 10399−10409.

(16) Fontanet, M.; Rodriguez, M.; Fontrodona, X.; Romero, I.; Teixidor, F.; Viñas, C.; Aliaga-Alcalde, N. Carving a 1D Co^{II}-carboranylcarboxylate system by using organic solvents to create stable trinuclear molecular analogues: complete structural and magnetic studies. *Dalton Trans.* **2016**, *45*, 10916−10927.

(17) Leites, L. A. Vibrational spectroscopy of carboranes and parent boranes and its capabilities in carborane chemistry. *Chem. Rev.* **1992**, *92*, 279−323.

(18) (a) Pothiraja, R.; Sathiyendiran, M.; Butcher, R. J.; Murugavel, R. Non-Interpenetrating Transition Metal Diorganophosphate 2-Dimensional Rectangular Grids from Their 1-Dimensional Wires: Structural Transformations under Mild Conditions. *Inorg. Chem.* **2005**, *44*, 6314−6323. (b) Pothiraja, R.; Shanmugan, S.; Walawalkar, M. G.; Nethaji, M.; Butcher, R. J.; Murugavel, R. Structural Diversity in Zinc Phosphates and Phosphinates: Observation of a Lattice Water Dimer Sandwiched Between Phosphoryl Oxygen Atoms. *Eur. J. Inorg. Chem.* **2008**, *2008*, 1834−1845.

(19) Kostakis, G. E.; Ako, A. M.; Powell, A. K. Structural motifs and topological representation of Mn coordination clusters. *Chem. Soc. Rev.* **2010**, *39*, 2238−2271.

(20) Rich, J.; Castillo, C. E.; Romero, I.; Rodríguez, M.; Duboc, C.; Collomb, M.-N. Investigation of the Zero-Field Splitting in Six- and Seven-Coordinate Mononuclear Mn^{II} Complexes with N/O-Based Ligands by Combining EPR Spectroscopy and Quantum Chemistry. *Eur. J. Inorg. Chem.* **2010**, *2010*, 3658−3665.

DOI: 10.1021/acs.inorgchem.7b00610
Inorg. Chem. XXXX, XXX, XXX−XXX

ADDENDUM II

Articles d'aquesta tesi doctoral que estan enviats o en procés de elaboració.

Merging Icosahedral Boron Clusters and Magnetic Nanoparticles: Aiming towards Multifunctional Nanohybrid Materials.

Elena Oleshkevich,[a] Francesc Teixidor,[a] Anna Rosell[b] and Clara Viñas[a,]*.

[a] Institut de Ciència de Materials de Barcelona (ICMAB-CSIC), Campus UAB, 08193 Bellaterra, Spain.

[b] Neurovascular Research Laboratory, Vall d'Hebron Research Institute, Universitat Autònoma de Barcelona, Passeig Vall d'Hebron 119-129, 08035 Barcelona, Spain.

KEYWORDS: m-carboranyl, phosphinate, MNPs, iron oxide nanoparticles.

ABSTRACT: All-inorganic-made nanohybrid icosahedral Boron cluster magnetic nanoparticles have been prepared. These MNPs consist of a magnetic core and an inorganic carboranylphosphinate shell. The phosphinate is directly bonded to the iron atoms of the surface in a bidentated coordination mode. The nanoparticles have been characterized by TEM, X-ray powder diffraction, infrared spectroscopy, energy dispersive X-ray analysis, high resolution X-ray photoelectron spectroscopy, magnetometry measurements and redox titration, among other techniques. These studies have led to a composition (1-OPH(O)-1,7-*closo*-$C_2B_{10}H_{11})_8(2Fe_3O_4{\bullet}Fe_2O_3)_{13}$ that implies a surface coverage of 61.3±7.4% by the ligand. When these MNPs go through sterilization in one autoclave the magnetic hysteresis studies suggest minimal change before and after sterilization; this could erroneously indicate that there has not been any changes in the MNP composition. However, the Fe^{2+} titration demonstrates that after sterilization only 1/7 of the Fe is Fe^{2+} leading to a core formula $Fe_3O_4.2Fe_2O_3$ with concomitant loss of ligand to a final ratio of 1:70 (carborane: Fe), and a final coverage by the ligand of 16.9±1.9% . These studies bring relevant information on the behavior of the widely used MNPs and clearly show how the sterilization process needed for biological tests may alter the composition of the core and the loading of peripheral ligand. In the particular case reported here, the liberated ligand has not been oxidized nor altered through the sterilization process.

Introduction.

The synthesis of magnetic nanoparticles (MNPs) has thoroughly flourished for copiuos technological[1] and medical applications during the past decades.[2] To understand ferrofluid behaviour careful studies related to fluid stability, control of surfactants, particle sizes, materials, and physical behaviour are essential. Typical MNPs obtained by the bottom-up synthesis consist of a magnetic core and an organic or inorganic shell that provides a barrier between the core and its environment. This is generally a layer of capping molecules that bind directly to the surface ideally preventing particles aggregation and disperses them in water at a range of different pH values, among other tasks. While physical properties of MNPs are determined by their inorganic magnetic core, their surface properties play an important role, especially in effective interfacing (e.g., ensuring biocompatibility and specific site) with biological systems. Superparamagnetic iron oxide nanoparticles (SPIONs or MNPs) have been extensively investigated for numerous *in vivo* applications, such as magnetic resonance imaging (MRI) contrast enhancement,[3] tissue repair, and immunoassay, detoxification of biological fluids, hyperthermia, drug delivery, and cell separation.[4] Further developments in the synthesis and bioorthogonal chemistry of nanoparticles have broadened MNPs applications to the therapeutic areas.[5]

The most studied carborane is the icosahedral 1,2-dicarba-*closo*-dodecaborane, 1,2-*closo*-$C_2B_{10}H_{12}$, and its isomers (1,7 and 1,12-) that can be viewed as "superaromatic" systems[6] whose volume approximates that displayed by a benzene molecule rotating on one of its twofold axes.[7]

These carboranes exhibit an unusual combination of properties such as low nucleophilicity, chemical inertness, thermal stability,[8] electron-withdrawing via bonding at the carboranyl carbon atoms,[9] and electron-donating via bonding at the carborane boron atoms,[10] stability and low toxicity in biological systems.[11]

Chart 1. Schematic representation of *m*-carboranylphosphinic acid (H[**1**]), its sodium salt (Na[**1**]), and bidentate bridging mode of coordination of [**1**]$^-$ onto the surface of MNPs.

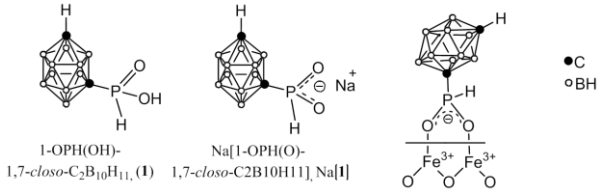

These properties have stimulated the development of a wide range of potential applications based on a molecular approach for the preparation of materials. Moreover, the rigid geometry and the relative easiness of derivatization at the carbon vertexes of the carborane cluster[9a],[12] allow the preparation of a wide number of compounds potentially useful as precursors of more complex materials.[8a],[13] Further, the use of carboranes in supramolecular chemistry is a topic that raises great interest for

their particular properties that may induce an unexpected behaviour in the supramolecular structures in which they are inserted.[9a],14 Our vision of the carboranyl substituent, however, is that it is unique as a ligand because it is a rigid sphere appended to a metal coordinating site; this along with its hydrophobicity and electron withdrawing properties through the carbon cluster, C_c, suggest the possibility of inducing distinct geometrical behavior in boron rich macromolecules or particles of significance for Boron Neutron Capture Therapy (BNCT)[15] and for drug delivery.[16] Particular to this work is the carborane derivative utilized, *m*-carboranylphosphinate, which deserves some comments. Organophosphinic acids, HOP(O)HR, are derivatives of the strong reducing agent phosphinic acid $HOP(O)H_2$, after substituting the one hydrogen atom directly bound to phosphorus by organic groups. Althought phosphonic and phosphinic acids are seemingly good competitors to carboxylic acids in the sense of complexation capacity and stability of pro-duced complexes, it is of notice that few metal complexes exist either of phosphinic or of organophosphinic acids, $HOP(O)H_2$ and HOP(O)HR, respectively. A search at the Cambridge Structural Database (CSD version 5.38, November 2016 updates)[17] shows only 47 hits found for phosphinic acids R-P(H)O(OH) (R=alkyl, aryl) transition metal complexes. The reason may be due to the strong tendency to become oxidized.[18] Recently, *m*-carboranylphosphinates (Chart 1) were synthesized as a new class of purely inorganic ligands,[19] and the reactivity of the phosphinate group throughout Mn^{II} studied.[20] The phosphinate coordinating group is subjected to the properties bestowed by the *m*-carborane, perhaps the most noticeable in what refers to the results obtained in this work being the reduced tendency to be oxidized of the functional group, the spherical nature of the carborane and the hydrophobicity of the carboranyl unit.

In this paper, boron cluster-MNPs nanohybrids coated with *m*-carboranylphosphinate (**1**) (Chart 1) are reported. These MNPs have been prepared by classic co-precipitation synthesis and have been characterized by different techniques (transmission electron microscopy images, electron diffraction, X-ray powder diffraction, infrared spectroscopy, energy dispersive X-ray analysis, high resolution X-ray photoelectron spectroscopy, and magnetometry measurements) that have provided information on structural and physicochemical distinctive properties of these unique **1**-MNPs.

Experimental section.

Methods. Infrared spectra (IR) were obtained on PerkinElmer® Universal ATR Accessory. Transmission Electron Microscopy (TEM): TEM specimens were prepared by depositing a few drops of water suspensions of **1**-MNPs onto copper grids. Then samples were left to get dry at room temperature. Images of **1**-MNPs were obtained using a transmission electron microscope JEOL 1210 at 120 kV. The particle size distribution was determined by measuring diameter of nearly 200 particles with ImageJ software. Particle diameters were derived by assuming all the particles are ideal spheres. X-ray powder diffraction (XRD) measurements were performed in a Powder X-ray diffractometer SIEMENS D-5000. X-ray Tube: ceramic tube DRX, Cu anode, 2, 2K, 2K (λ (CuKα1) = .540560 Å), (λ (CuKα2) = 1.544390 Å) in the 2Θ range from 5º to 125º, with a step 0.02º/0.5s. Dynamic Light Scattering (DLS) and Zeta Potential: The hydrodynamic diameter of **1**-MNPs dispersed in water and in several biological media were investigated with a ZETASIZER NANO ZS (Malvern Instruments Ltd) equipped with a He-Ne 633nm laser using 1 mL of particle dispersion in a disposable plastic cuvette. Measurements were run in triplicate at ambient temperature and at 37ºC for samples in biological media. Number of scans was set up in automatic mode. Laser Doppler Microelectrophoresis is the technique used to measure zeta potential. The zeta potential of the **1**-NMP colloidal suspension in aqueous media was obtained by filling a disposable cell with 1 mL of colloidal suspension. Measurements were run in triplicate at ambient temperature. Number of scans was set up in automatic mode. Magnetic characterization of **1**-MNPs was carried out in a Superconductive Quantum Interference Device (SQUID) magnetometer (Quantum Design MPMS5XL). Magnetization *vs* magnetic field measurements were performed at 300K and 5K in a field 6T. Zero-field cooling (ZFC) and field cooling (FC) temperature dependent magnetization measurements were carried in a field of 50 Oe. The sample was prepared using a polycarbonate capsule filled with 1 mg of **1**-MNPs and compacted cotton. High resolution X-ray photoelectron spectroscopy (HRXPS) was performed with a Phoibos 150 analyzer (SPECS GmbH, Berlin, Germany)) in ultra-high vacuum conditions (base pressure 4E-10mbar) with a monochromatic aluminium K alpha X-ray source (1486.74eV)). The energy resolution as measured by the FWHM of the Ag 3d5/2 peak for a sputtered silver foil was 0.8 eV. Scanning Electron Microscope (SEM) images and Energy Dispersive X-ray Spectroscopy (EDX) analysis were done using the QUANTA FEI 200 FEG-ESEM device. **1**-MNPs samples were prepared by dispersing a small amount of powder in Milli-Q water. Afterwards, the drop dispersion was dried onto a carbon coated TEM grid.

Materials. Starting 1-OPH(OH)-1,7-*closo*-$C_2B_{10}H_{11}$ (**1**) was synthesized as reported.[19] $FeCl_2$, $FeCl_3{\cdot}6H_2O$, aqueous $[NMe_4]OH$ solution (25 wt.%) were purchased from Sigma–Aldrich. $[NH_4]OH$ (30% as NH_3) was purchased from Panreac AppliChem and used as received. Milli-Q water was used to do all preparations and dilutions.

Preparation of solid *m*-carboranylphosphinate-capped MNPs, 1-MNPs. *m*-Carboranylphosphinate coated magnetite nanoparticles (**1**-MNPs) were prepared in two steps as follow: i) the preparation of the core of MNPs was carried out under inert (nitrogen) atmosphere using the aqueous co-precipitation method. $FeCl_2$ (50 mg, 0.39 mmol) and $FeCl_3{\cdot}6H_2O$ (213.25 mg, 0.79 mmol) were dissolved in 30 mL deionized and degassed water at room temperature. After stirring for 20 minutes, 2.0 mL (15.43 mmol) of $[NH_4]OH$ aqueous solution (30 wt.%) was added at once to the above mixture under vigorous stirring. Immediately a black suspension was formed, which suggested the formation of magnetic nanoparticles. The reaction mixture was then stirred vigorously for 2 h. The precipitate was isolated from the aqueous solution by magnetic decantation, and washed with distilled water (10 mL) three times. ii) Then, the aqueous solution was removed and a saturated solution of 1-OPH(OH)-1,7-*closo*-$C_2B_{10}H_{11}$ H[**1**] (25 mg, 0.12 mmol) in H_2O (10 mL) was added. Next, the mixture was sonicated for 2 h. The **1**-MNPs were separated from the aqueous solution by magnetic decantation; washed with distilled water (10 mL) three times and dried at 50ºC for 2 h *in vacuum*.

Preparation of 1-MNPs aqueous suspension at the fisiological pH. Stable **1**-MNPs (0.5 mg/mL) colloidal aqueous dispersion was prepared as follows. **1**-MNPs (5 mg) were re-

dispersed in deionized H_2O (10 mL) containing 1μL of [NMe_4]OH by using ultrasound radiation. The as-prepared dispersion has a pH about 5.5-6.5, and then pH was adjusted to 7.3-7.5 by using additional aqueous [NMe_4]OH solution (25 wt.%).

Results and discussion.

Preparation of 1-MNPs. The preparation of magnetite nanoparticles coated with *m*-carboranylphosphinate was performed in two steps as described above. The first one was the preparation of non functionalized iron oxide super paramagnetic nanoparticles by co-precipitation. This method, which is the concomitant precipitation from ferrous and ferric iron (in a 1:2 ratio) in alkaline aqueous solution, is the most widely applied synthesis route for the MNPs formation. It was shown by TEM that nucleation and growth of magnetite proceeds through rapid agglomeration of nanometric primary particles within the framework of classical nucleation theory.[21] The second step was the funtionalization of the MNPs with the *closo*-carboranyl ligand[**1**]$^-$. To obtain the superparamagnetic iron oxide nanoparticles coated with *closo*-carboranylphosphinate ligands **1**-MNPs, a saturated aqueous solution of H[**1**] was added to the formed non functionalized core of MNPs. After sonicating the mixture for 2 hours, the **1**-MNPs were isolated by magnetic decantation, washed with water and dried at 50ºC in vacuum.

Chemical characterization of 1-MNPs. The **1**-MNPs were characterized by FTIR Spectroscopy, EDX analysis, high resolution XPS, and $Fe^{2+/3+}$ chemical titration. The FTIR spectra of H[**1**], its sodium salt Na[**1**], **1**-MNPs and non functionalized core of MNPs are shown in Figure 1. Strong absorptions at 2594 cm^{-1} in all three the pure *m*-carboranylphosphinic ligand **1,** Na[**1**] and **1**-MNPs, due to B–H stretches, dominate the IR spectra and support the presence of a *closo*-carboranyl cluster structure in the molecules as well as onto the surface of **1**-MNPs.[22] It is worth noting that the P=O stretching band of the phosphinate group, which was present at 1210 cm^{-1} in the spectrum of **1** is absent in the spectrum of **1**-MNPs but, two new bands at 1189 and 1068 cm^{-1} appeared, which were ascribed to asymmetric $\nu_{as(POO-)}$ and symmetric $\nu_{s(POO-)}$ stretch of coordinated phosphinate group (Figure 1).[23] This result revealed that **1** was chemisorbed onto the surface of magnetite nanoparticles as a phosphinate bidentated bridging ligand coordinated to the iron atoms of the iron oxide super paramagnetic nanoparticles (see Chart 1). In addition, the IR spectrum of pristine MNPs shows a peak at 1629 cm^{-1} that remains in the **1**-MNPs spectrum and is associated to coordinated water to the Fe centers of the core.

This is in agreement with a mechanistic study and its spectroscopic identification[24] that was performed by infrared reflection absorption spectroscopy (IRAS) on the interaction of water with a well-defined model Fe_3O_4(111) surface.

To further verify that **1** is attached onto the surface of **1**-MNPs, EDX analysis of **1**-MNPs was performed. Phosphorus was detected by EDX analysis (Figure 2) proving that **1** was coating MNPs surface with an atomic composition for **1**-MNPs of 92.89 and 7.13% for Fe and P, respectively. This corresponds to a ratio 13:1 (Fe:P), indicating that the composition of the **1**-MNPs can be referred to as (1-OPH(O)-1,7-*closo*-$C_2B_{10}H_{11})_8(2Fe_3O_4{\cdot}Fe_2O_3)_{13}$.

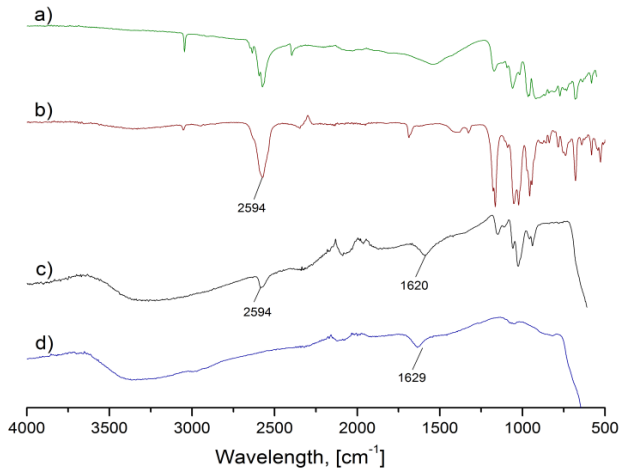

Figure 1. Comparison between the IR spectra of the *m*-carboranylphosphinic acid (**1** in green), its sodium salt (Na[**1**] in red), **1**-MNPs (in black) and none functionalized core of MNPs (in blue).

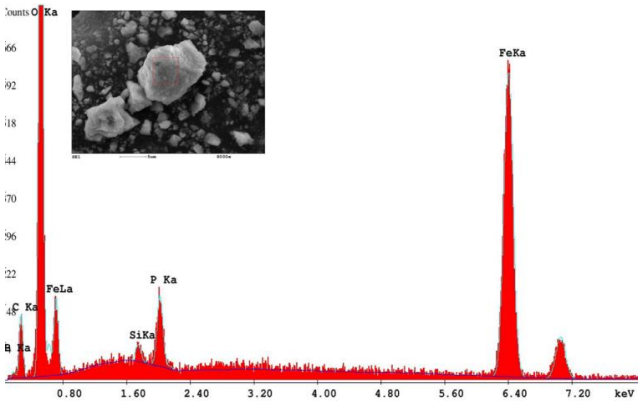

Figure 2. EDX analysis of **1**-MNPs

The high resolution XPS analysis performed on **1**-MNPs (Figure 3) displays peaks at 189 and 133eV, which are characteristic of a B-B[25] and P-O bonds (Figure 3b, 3c), confirming the presence of *m*-carboranyl and phosphinate groups as well as the peaks at 711.2 and 724.9 eV indicating Fe in the Fe_3O_4 phase at the MNP core[26] (Figure 3d).

Chemical titration: The iron oxide nanoparticles, the most explored magnetic nanoparticles up to date, are composed of Fe^{2+} and Fe^{3+} oxides. In order to evaluate the amount of Fe^{2+} and Fe^{3+} ions forming the core of the **1**-MNPs nanoparticles, redox titrations were performed as described at the S. I. The chemical titration indicated an amount of 25.08% of Fe^{2+} to the total amount of $Fe^{2+/3+}$; while for pure magnetite (Fe_3O_4=$FeO{\cdot}Fe_2O_3$) it is expected a 33%. This result revealed that the iron oxide core of the synthesized **1**-MNPs consists of a mixture of both magnetite and maghemite phases, with a composition $2Fe_3O_4{\cdot}Fe_2O_3$.

Morphological, structural and physicochemical characterization of the 1-MNPs. The magnetic properties of nanoparticles depend upon their physical structure: the size and the shape of the particles, their microstructure, and the chemical phases in which they are present. Moreover, the biological behaviour of magnetic nanoparticles also strongly depends

upon their size and shape as well as their polydispersity, charge, and nature of the coating. Several techniques were used to determine these parameters.

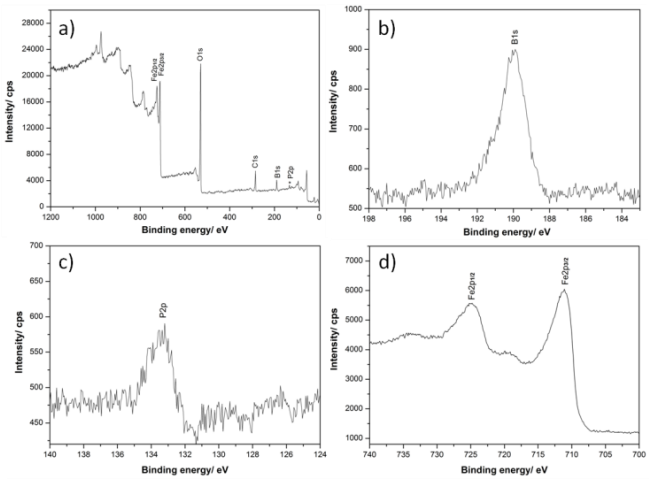

Figure 3. a) XPS spectrum of **1**-MNPs. High resolution XPS spectrum of **1**-MNPs in the B 1s, P 2p and Fe 2p regions, b), c) and d) respectively.

The morphological and structural characterization of **1**-MNPs was performed by using TEM and XRD. Particle imaging and sizing of synthesized **1**-MNPs was investigated by TEM analysis. **1**-MNPs nanoparticles are observed to have spherical shape (Figure 4). Mean particle diameters ($Ø_{TEM}$) were statistically calculated for each sample by counting 200 particles and fitting the particle size histogram from three different batches, prepared following the same way of synthesis, to a Gaussian function, producing a mean particle diameter of 7.6 ± 0.6 nm. The 8% polydispersity indicates the narrow particle size distribution, although **1**-MNPs were prepared by the aqueous co-precipitation method. The electron diffraction of **1**-MNPs shows well defined diffraction rings confirming that the particle core composition is made of magnetite/maghemite spinel structure (Figure 4). The line profile was fitted for observed six peaks with the following Miller indices: (220), (311), (400), (422), (511), and (440). The XRD pattern of **1**-MNPs revealed the average crystallite size, D, calculated from the peak broadening refinements, resulted as 9.0 ± 0.6 nm. This result is in a good agreement with the mean particle diameter from TEM of 7.6 ± 0.6 nm.

The magnetic property of iron oxide (Fe_3O_4) nanoparticles is affected by the distribution of iron ions in octahedral and tetrahedral sites of spinel structure.[27] The magnetic spins of the ions in the octahedral sites are ferromagnetically coupled to each other and antiferromagnetically coupled with tetrahedral sites. Because the numbers of Fe^{3+} ions in the octahedral sites and the tetrahedral sites are the same, their magnetic spins cancel each other. Consequently, the magnetic spins of only Fe^{2+} ions in the octahedral sites contribute to the net magnetic moment. Ferromagnetic iron, that is 100% composed by Fe^{2+}, has the highest saturation magnetization (218 emu g-1) because of the absence of cancelled magnetic spins.[28]

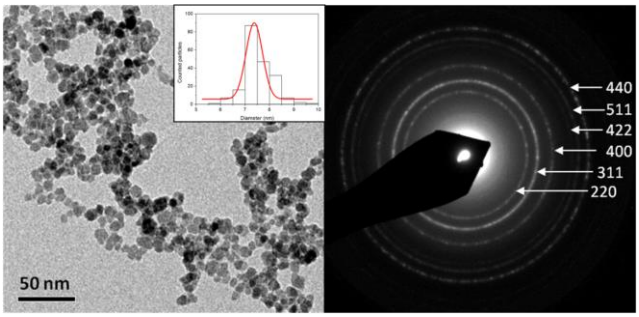

Figure 4. TEM micrograph with particle size distribution histogram and electron diffraction pattern of synthesized **1**-MNPs.

However, Fe^{2+} can be oxidized upon harsh conditions of temperature, moisture and oxygen as these that can be found in an autoclave for sterilization. Thus one important point to be addressed in the use of MNPs for medical applications and consequently on their autoclave sterilization for their application on cultures, is to learn on the fate of the MNPs and their ligands, particularly on what occurs to Fe^{2+} upon the autoclave sterilization process, and to this purpose it is necessary to learn on the fate of functionalized MNPs at room temperature and after the autoclave sterilization process. To this aim, magnetic measurements of freshly prepared **1**-MNPs were done and the results are displayed in Figure 5. Figures 5a and 5b show a typical magnetization curve at 300 K for superparamagnetic nanoparticles in which neither remanent magnetization (magnetization at zero field, M_R) nor coercivity (hysteresis loop, H_c) were observed. The saturation magnetization value of **1**-MNPs at 300 K was 65 emu/g that indicates a high degree of crystallinity, as well as 29.8% of Fe^{2+} by comparison with the ferromagnetic iron. This value is comparable to the 25.1% of Fe^{2+} of the total $Fe^{2+/3+}$ that was obtained by chemical titration of freshly prepared **1**-MNPs; this indicates that **1**-MNP is made of a ratio of 2:1 mols of magnetite (Fe_3O_4) per 1 mol of maghemite (Fe_2O_3). Maghemite exhibits ferrimagnetic ordering and as magnetite is also used in biomedicine. As expected, saturation magnetization was higher at 5K (76 emu/g **1**-MNPs) and the **1**-MNPs present M_R ferromagnetic features of 12 emu/g (Figure 5b). Superparamagnetism was also proved by the ZFC-FC magnetization curves (Figure 5c). The ZFC increased with temperature until reaching the maximum value corresponding to the blocking temperature (TB) at 111 K. The FC curve increases as the temperature decreases and never reaches saturation at low temperature, suggesting that interparticles' interactions do not significantly affect the relaxation dynamics. These studies were done with the **1**-MNPs before autoclave sterilization.

On the other hand, little information is available on MNPs after sterilization in autoclave, and definitively is necessary for their medical application. We will take advantage of the chemical nature of the carboranylphosphinic acid, having uncommon atoms B and P, to learn on the evolution of the ligand's shell following autoclave sterilization. Three main targets are thus sought: Is the initial $Fe^{2+/3+}$ pre-sterilization distribution of the MNPs core maintained after autoclave sterilization? What happens with the ligand shell? Is the magnetic response comparable to the starting one?. To answer the previous questions, magnetic properties of **1**-MNPs were measured after the autoclave sterilization process. Magnetization curves of **1**-MNPs

before (blue) and after (red) autoclave sterilization process at 5K and 300K as function of the applied 6 Tesla magnetic field are displayed in (Figure 5d). The graph demonstrates that the autoclave sterilization process does not produce significant changes on magnetic properties of **1**-MNPs. The saturation magnetization value of **1**-MNPs at 300K was 65 emu/g and 66 emu/g before and after autoclave sterilization, respectively. As expected, saturation magnetization was higher at 5 K (76 emu/g before and 80 emu/g after autoclave sterilization, respectively). These results would suggest that no changes or just minor modifications in the structure and composition would have occurred upon applying the autoclave sterilization conditions, but we shall see that this is not the case.

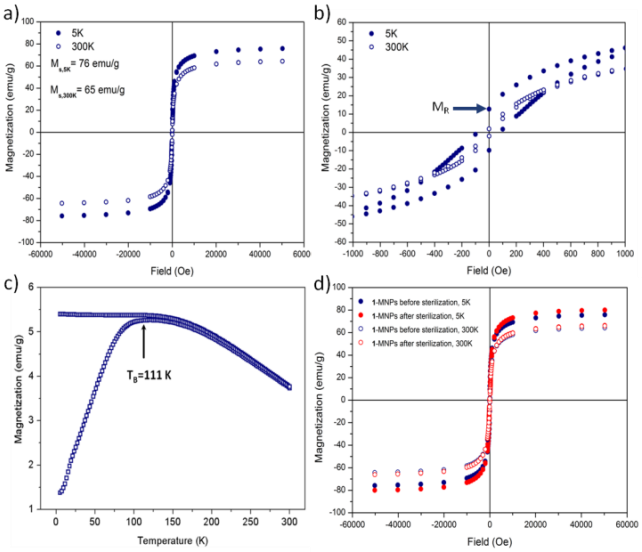

Figure 5. a) Hysteresis cycles recorded at low temperature (5 K) and room temperature (300K) for **1**-MNPs; b) zoom of the hysteresis cycle at low fields; c) ZFC and FC curves of **1**-MNPs at 50 Oe; d) Hysteresis cycles recorded at low temperature (5 K) and room temperature (300K) for **1**-MNPs before (blue) and after (red) the autoclave sterilization process.

A redox titration of an aqueous suspension of **1**-MNPs (following autoclave sterilization) was performed and shows that the Fe^{2+} content decreases from 25.1% to 14.7% to the total amount of $Fe^{2+/3+}$ indicating that autoclave sterilization process of **1**-MNPs leads to partial oxidation of Fe^{2+} to $Fe^{3+}$of the **1**-MNPs core, and increases the amount of maghemite. This leads to a chemical composition $Fe_3O_4{\cdot}2Fe_2O_3$. Does this affect the ligands shell in the **1**-MNPs? The answer is yes, as the EDX ratio before autoclave sterilization was 1P:13Fe, and after autoclave sterilization was 1P:70Fe indicatng that practically 80% of the ligand shell had been removed from the surface. Using a spherical geometrical model and considering the major circle area of the carborane, the first ratio corresponds to a surface coverage of 61.3±7.4% whereas after autoclave sterilization the surface coverage by the carboranyl ligands has been reduced to 16.9±1.9% (S. I.). What has happened with the removed ligand? ^{11}B-NMR and ^{31}P-NMR of the mother liquor indicated that the liberated carboranylphosphinate ligand that was released from the **1**-MNPs remained intact after the autoclave sterilization process (S.I.).

The control of the monodisperse size of magnetic nanoparticles is very important because their biological properties strongly depend on their polydispersity, charge, and nature of the coating in addition to their size and shape. The surface charge of the nanoparticles was determined by measuring their ζ-potential values at different pH, by means of DLS. DLS technique also provides information on the hydrodynamic diameter and, thus, on the colloidal behaviour of the **1**-MNPs in a different environment. As the mean effective diameter of the particles depends on the size of the core, the size of the shell, particle concentration as well as the type of ions in the medium, the influence of pH on the stability of colloidal aqueous dispersion of **1**-MNPs was studied and their results collected in Table 1.

Table 1. Hydrodynamic diameter, Zeta potential and Diffusion coefficient values of **1**-MNPs colloidal aqueous dispersion at different pH measured by DLS.

pH	$Ø_{HYD}$, (nm)	PdI	Zeta potential, ζ (mV)	Diffusion Coefficient, ($\mu m^2/s$)
5.30	> 60	0.446	+17	1.77
7.45	45 ± 20	0.454	-30 ± 4	3.77
9.21	23 ± 11	0.482	-44 ± 5	7.49

The pH of the solution was adjusted using aqueous $[NMe_4]OH$ solution (25 wt.%). DLS analysis reveals that the hydrodynamic diameter of the particle increases when decreasing the pH, which indicates the particles aggregate when pH decreas

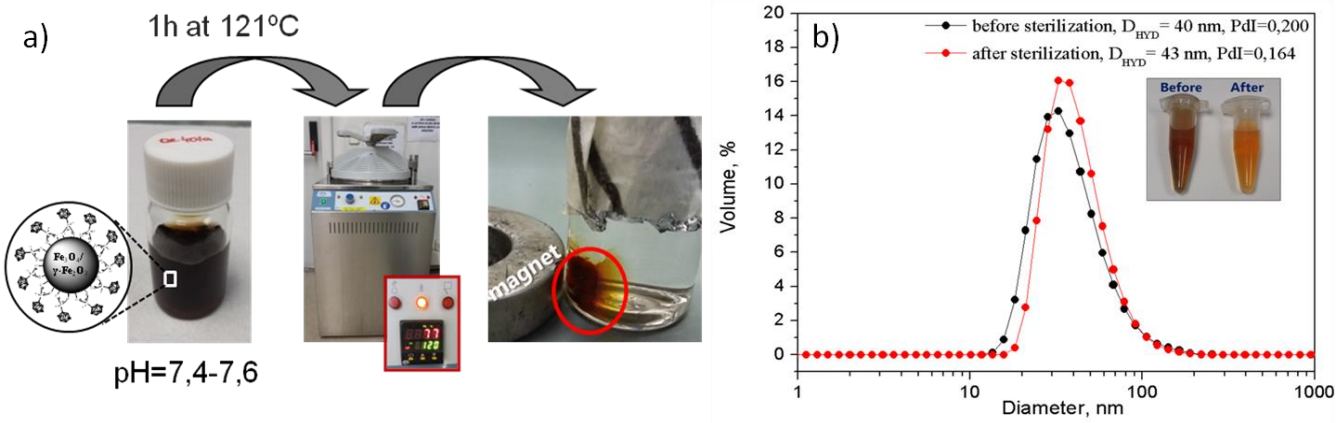

Figure 6. a) **1**-MNPs display magnetic properties after the autoclave sterilization process. b) DLS of **1**-MNPs before and after the autoclave sterilization process.

es. On the other hand, when pH is basic, the electrostatic repulsion force seems to be higher (ζ= -44 ± 5 mV), therefore the dimensions of the aggregates ($Ø_{HYD}$ = 23 ± 11 nm) are closer to the size of particles determined by TEM ($Ø_{TEM}$) that is 7.6 ± 0.6 nm. At physiological pH, the size of aggregates are $Ø_{HYD}$= 45 ± 20nm and Zeta potential value, ζ= -30 ± 4 mV, that was enough to avoid the aggregation with further precipitation of colloid. This fact can be attributed to the negatively charged surface of the core of magnetic nanoparticles and by the hydrophobicity due to the carboranyl spheres coordinated to the surface $Fe^{2+/3+}$ ions through the phosphinate binding sites.

Studies of colloidal stability of the 1-MNPs suspension during the autoclave sterilization process.

The colloidal behaviour of an aqueous solution at the pH range 7.4-7.6 of the **1**-MNPs (0.5 mg/mL) that had been under autoclave sterilization process conditions (steam heated to 121°C under pressure during 1 hour) were studied by DLS measurements.

Figure 6 shows that the dimensions of the aggregates are the same before and after the autoclave sterilization process and, as said earlier, the magnetic properties of **1**-MNPs remain unaltered after the autoclave sterilization process. What has changed is the composition of the MNPs from $2Fe_3O_4{\cdot}Fe_2O_3$ before autoclave sterilization to $Fe_3O_4{\cdot}2Fe_2O_3$ following autoclave sterilization. It has also changed the degree of ligands' MNPs coverage that has been reduced nearly a 80%.

Conclusions.

Magnetite/Maghemite MNPs decorated with the carboranylphosphinate ligand have been prepared. Two characteristics need to be highlighted in this ligand: the phosphinate coordinating group and the hollow sphere carborane that define the characteristics of these **1**-MNPs. No previous examples of MNPs with phosphinic acid derivatives had been previously reported, probably due to the reducing character of the phosphinic group that is weakened by the carborane. The carborane itself contributes the MNPs with a hydrophobic layer tHAT IS POROUS TO CERTAIN IONS. This work deals on the capacity of the novel carboranylphosphinate ligAND to bind onto the surface of magnetic nanoparticles via coordination to the iron atoms as a phosphinate bidentated bridging ligand, and provides an understanding of how the environment influences on the strength of this bond. Of particular relevance is what refers to the stability of MNPs before and after sterilization under autoclave conditions. These studies have shown that the magnetic properties are left unaltered albeit the ratio of Fe^{2+} in the MNPs has been reduced drastically, and the shell of ligands has been weakened considerably. Thereby, the chosen way of AUTOCLAVE sterilization that is required for biological studies *in vitro* and *in vivo* can play a crucial role in the properties of the final material altering its surface and nanoparticle core composition, and consequently its colloidal behavior and physical properties. In summary, we believe that these new nanohybrid Icosahedral boron cluster-MNPs might offer a broad scope for exciting research and future biomedical applications.

Supporting Information

The Supporting Information is available free of charge on the ACS Publications website. Redox titration analysis description, particle size distribution histograms from three batches, prepared following the same synthesis, and mean particle size diameter, XRD patterns, calculations of surface coverage of **1**-MNPs before and after autoclave sterilization, ^{1}H-NMR, ^{1}H{^{11}B}-NMR, ^{11}B-NMR, ^{11}B{^{1}H}-NMR ^{31}P-NMR of the mother liquor from **1**-MNPs after autoclave sterilization (in PDF).

AUTHOR INFORMATION

Corresponding Author

* clara@icmab.es

Author Contributions

The manuscript was written through contributions of all authors. All authors have given approval to the final version of the manuscript.

Funding Sources

This work has been supported by the Spanish Ministerio de Economía y Competitividad CTQ2013-44670-R, European Union (FP7-OCEAN-2013: Proposal number: 614168) and the Generalitat de Catalunya (2014/SGR/149).

Notes

The authors declare no competing financial interests.

ACKNOWLEDGMENT

E. O. is enrolled in the PhD program of the UAB. E. O. thanks MICINN for FPU predoctoral grant. C. V. thanks COST CM1302 project.

REFERENCES

(1) a) Faivre, D.; Bennet, M.; *Nature* **2016**, *535*, 235–236. b) Kaittanis, C.; Santra, S.; Santiesteban, O. J.; Henderson, T. J.; Perez, J. M. *J. Am. Chem. Soc.* **2011**, *133*, 3668−3676. c) Haun, J. B.; Yoon, T.-J.; Lee, H.; Weissleder, R. *Wiley Interdiscip. Rev.: Nanomed. Nanobiotechnol.* **2010**, *2*, 291−304.

(2) a) Pankhurst, Q. A.; Thanh, N. T. K.; Jones, S. K.; Dobson, J. *J. Phys. D: Appl. Phys.* **2009**, *42*, 224001. b) Lee, N.; Yoo, D.; Ling, D; Cho, M. H.; Hyeon, T; Cheon, J. *Chem. Rev.* **2015**, *115*, 10637−10689.

(3) a) Lee, N.; Hyeon, T. *Chem. Soc. Rev.* **2012**, *41*, 2575−2589. b) Casula, M. F.; Floris, P.; Innocenti, C.; Lascialfari, A.; Marinone, M.; Corti, M.; Sperling, R. A.; Parak, W. J.; Sangregorio, C. *Chem. Mater.* **2010**, *22*, 1739−1748.

(4) a) Jun, Y.-W.; Lee, J.-H.; Cheon, J. *Angew. Chem., Int. Ed.* **2008**, *47*, 5122−5135. b) Yoo, D.; Lee, J.-H.; Shin, T.-H.; Cheon, J. *Acc. Chem. Res.* **2011**, *44*, 863−874. c) Ling, D.; Hyeon, T. *Small* **2012**, *9*, 1450− 1466.

(5) a) Sosnovik, D. E.; Nahrendorf, M.; Weissleder, R. *Circulation* **2007**, *115*, 2076−2086. b) Mahmoudi, M.; Sahraian, M. A.; Shokrgozar, M. A.; Laurent, S. *ACS Chem. Neurosci.* **2011**, *2*, 118−140.

(6) Poater, J.; Solà, M.; Viñas, C.; Teixidor, F. *Angew. Chem. Int. Ed.* **2014**, *53*, 12191 –12195.

(7) a) Teixidor, F.; Viñas, C.; Demonceau, A.; Nuñez, R. *Pure App. Chem.* **2003**, *75*, 1305–1313. b) Scholz, M.; Hey-Hawkins, E.; *Chem. Rev.* **2011**, *111*, 7035–7062.

(8) a) Grimes, R.N.; *Carboranes Third Edition:* Elsevier Inc., New York/Oxford, 2016. b) Hawthorne, M.F.; *Advances in Boron Chemistry*; The Royal Society of Chemistry: Cornwall, U.K., 1997, 261-272. c) Plesek, *J. Chem. Rev.* **1992**, *92*, 269-278.

(9) a) Teixidor, F.; Núñez, R.; Viñas, C.; Sillanpää, R.; Kivekäs, R. *Angew. Chem., Int. Ed.* **2000**, *39*, 4290-4292. b) Núñez, R.; Farrás, P.; Teixidor, F.; Viñas, C.; Sillanpää, R.; Kivekäs, R. *Angew. Chem.,Int. Ed.* **2006**, *45*, 1270-1272.
(10) a) Teixidor, F.; Barbera, G.; Vaca, A.; Kivekäs, R.; Sillanpää, R. *J. Am. Chem. Soc*. **2005**, *127*, 10158- 10159. b) Spokoyny, A. M.; Machan, C. W.; Clingerman, D. J.; Rosen, M. S.; Wiester, M. J.; Kennedy, R. D.; Stern, C. L.; Sarjeant, A. A.; Mirkin, C. A. *Nat. Chem.* **2011**, *3(8)*, 590-596.
(11) a) Hawthorne, M. F. *Angew. Chem. Int. Ed.*, **1993**, *32*, 950-984. b) Soloway, A. H.; Tjarks, W.; Barnum, B. A.; Rong, F-G.; Barth, R.F.; Codogni, I. M.; Wilson, J. G. *Chem. Rev.* **1998**, *98*, 1515-1562. c) Valliant, J. F.; Guenther, K. J.; King, A. S.; Morel, P.; Schaffer, P.; Sogbein, O. O.; Stephenson, K. A. *Coord. Chem. Rev.* **2002**, *232*, 173-230. d) Sivaev, I. B.; Bregadze, V.; Sjöberg, S. in *Research and Development in Neutron Capture Therapy* (Eds.: W. Sauerwein, R. Moss and A. Wittig) Monduzzi Editore, Bologna, **2002**, 19–23. e) Julius, R.; Farha, O.; Chiang, J.; Perry, L.; Hawthorne, M. F.; *Proc. Natl. Acad. Sci. U.S.A.* **2007**, *104*, 4808-4813.
(12) a) Teixidor, F.; Viñas, C.; Science of Synthesis, Houben-Weyl Methods of Molecular Transformations; Kaufmann, D. E., Matteson, D. S. Eds.; Georg Thieme Verlag: Stuttgart-New York, **2005**, 6, 1235. b) Bregadze, V. I.; *Chem. Rev.* **1992**, *92*, 209-223.
(13) a) Dash, B. P.; Satapathy, R.; Maguire, J. A.; Hosmane, N. S.; *New J. Chem.* **2011**, *35*, 1955–1972 b) Schwartz, L.; Eriksson, L.; Lomoth, R.; Teixidor, F.; Viñas, C.; Ott, S. *Dalton Trans.* **2008**, *18*, 2379-2381. c) Peterson, J. J.; Werre, M.; Simon, Y. C.; Coughlin, E. B.; Carter, K. R. *Macromolecules*, **2009**, *42*, 8594-8598. d) Kokado, K.; Chujo, Y. *J. Org. Chem.* **2011**, *76*, 316-319. e) Bae, Y.-S.; Spokoyny, A. M.; Farha, O. K.; Snurr, R. Q.; Hupp, J. T.; Mirkin, C. A. *Chem. Commun.* **2010**, *46*, 3478-3480. f) Vives, G.; Tours, J. M. *Acc. Chem. Res.* **2009**, *43*, 473-487. g) Morin, J. F.; Shirai, Y.; Tour, J. M. Org. Lett. 2006, 8(8), 1713-1716. h) Kahlert, J. U.; Rawal, A.; Hook, J. M.; Rendina, L. M.; Choucair, M. Chem. Commun., 2014,50, 11332-11334. i) Núñez, R.; Romero, I.; Teixidor, F.; Viñas, C. Chem. Soc. Rev., 2016, 45, 5147-5173. j) Lamrani, M.; Hamasaki, R.; Mitsuishi, M.; Miyashita, T.; Yamamoto, Y. *Chem. Commun.* 2000, 17, 1595-1596.
(14) a) Fox, M. A.; Hughes, A. K.; *Coord. Chem. Rev*. **2004**, *248*, 457-476. b) Jude, H.; Disteldorf, H.; Fischer, S.; Wedge, T.; Hawkridge, A. M.; Arif, A. M.; Hawthorne, M. F.; Muddiman, D. C.; Stang, P. J.; *J. Am. Chem. Soc.* **2005**, *127*, 12131-12139. c) Puga, A.V.; Teixidor, F.; Kivekäs, R.; Sillanpää, R.; Viñas, C.; *Chem. Eur. J.* **2009**, *15*, 9764-9772. d) Hardie, M. J.; Raston, C. L., *Chem. Commun.* **2001**, *10*, 905-906. e) Yao, Z.-J.; Jin, G. X. *Coord. Chem. Rev.* **2013**, *257(17-18)*, 2522-2535. f) Scheer, M.; Schindler, A.; Groger, C.; Virovets, A. V.; Peresypkina, E. V. *Angew. Chem. Int. Ed.* **2009**, *48(27)*, 5046-5049.
(15) a) Heber, E. M.; Hawthorne, M. F.; Kueffer, P. J.; Garabalino, M. A.; Thorp, S. I.; Pozzi, E. C. C.; Hughes, A. M.; Maitz, C. A.; Jalisatgi, S. S.; Nigg, D. W.; Curotto, P.; Trivillin, V. A.; Schwint, A. E. *Proc. Natl. Acad. Sci. U.S.A.* **2014**, *111(45)*, 16077-16081. b) Otero, R.; Seoane, S.; Sigueiro, R.; Belorusova, A. Y.; Maestro, M. A.; Perez-Fernandez, R.; Rochel, N.; Mourino, A. *Chem. Sci*, **2016**, *7(2)*, 1033-1037. c) Zhu, Y.; Lin, Y.; Zhu, Y. Z.; Lu, J.; Maguire, J. A.; Hosmane, N. S.; *J. Nanomater.* **2010**, 409320-409327. d) Xuan, S.; Zhao, N.; Zhou, Z. H.; Fronczek, F. R.; Vincente, M. G. H. J. *Med. Chem.* **2016**, *59(5)*, 2109-2117. e) A. M. Cioran, A. D. Musteti, F. Teixidor, Ž. Krpetić, I. A. Prior, Q. He, C. J. Kiely, M. Brust, C. Viñas *J. Am. Chem.Soc.* **2012**, *134*, 212−221. f) Ferrer-Ugalde, A.; Juarez-Perez, E. J.; Teixidor, F.; Viñas, C.; Nuñez, R. *Chem. Eur. J.* **2013**, *19(50)*, 17021-17030. g) Calabrese, G.; Nesnas, J. J.; Barbu, E.; Fatouros, D.; Tsibouklis, J. *Drug Discov Today*. **2012**, *17*, 153-159. h) Justus, E.; Awad, D.; Hohnholt, M.; Schaffran, T.; Edwards, K; Karlsson, G.; Damian, L.; Gabel, D. *Bioconjugate Chem*. **2007**, *18(4)*, 1287-1293. i) Koganei, H.; Ueno, M.; Tachikawa, S.; Tasaki, L.; Ban, H. S.; Suzuki, M.; Shiraishi, K.; Kawano, K.; Yokoyama, M.; Maitani, Y.; Ono, K.; Nakamura, H. *Bioconjugate Chem*. **2013**, *24(1)*, 124-132. j) Sauerwein, W. A. G.; Wittig, A.; Moss, R.; Nakagawa, Y. (Eds.) *Neutron Capture Therapy. Principles and Applications*. Springer Science & Business Media **2012**. k) Byun, Y.; Yan, J. H.; Al-Madhoun, A. S.; Johnsamuel, J.; Yang, W. L.; Barth, R. F.; Eriksson, S.; Tjarks, W. *J. Med. Chem.* **2005**, *48(4)*, 1188-1198. l) Ciani, L.; Bortolussi, S.; Postuma, I.; Cansolino, L.; Ferrari, C.; Panza, L.; Altieri, S.; Ristori, S. *Int. J. Pharm*. **2013**, *458*, 340–346. m) Barth, R.; Vicente, M. G. H.; Harling, O. K.; Kiger, W. S.; Riley, K. J.; Binns, P. J.; Wagner, F. M.; Suzuki, M.; Aihara, T.; Kato, I.; Kawabata, S. *Radiation Oncology* **2012**, *7*, 146 (pp. 21).
(16) a) Luderer, M. J.; Puente, P.; A. K. Azab, A. K. *Pharm Res*. **2015**, *32*, 2824–2836. b) Sun, T; Li, Y. Y.; Huang, Y. L.; Zhang, Z. Z.; Yang, W. L.; Du, Z. W.; Zhou, Y. X. *Oncotarget* **2016**, *7(28)*, 43095-43108. c) Gao, Z. Y.; Horiguchi, Y.; Nakai, K.; Matsumura, A.; Suzuki, M.; Ono, K.; Nagasaki, Y. *Biomaterials* **2016**, *104*, 201-212. d) Gianpiero, C.; Anis, D.; Aikaterini, R.; Eirini, T.; Ioannis, V. S.; Dimitrios, F. G.; John, T.; *Med. Chem. Commun.* **2017**, *8*, 67-72. e) Bialek-Pietras, M.; Olejniczak, A. B.; Tachikawa, S.; Nakamura, H.; Lesnikowski, Z. J. *Bioorg. Med. Chem*. **2013**, *21(5)*, 1136-1142.
(17) a) On February 28th 2017. b) Bruno, J.; Cole, J. C.; Edgington, P. R.; Kessler, M.; Macrae, C. F.; McCabe, P.; Pearson J.; Taylor, R. *Acta Crystallogr*. **2002**, *B58*, 389-397.
(18) a) Gordon, P. E.; Fry, A. J.; Hicks, L. D. *ARKIVOC* **2005**, *6*, 393-400. b) Hicks, L. D.; Han, J. K.; Fry, A. J. *Tetrahedron Lett*. **2000**, *41*, 7817-7820.
(19) Oleshkevich, E.; Teixidor, F.; Choquesillo-Lazarte, D.; Sillanpää, R.; Viñas, *C. Chem. Eur. J*. **2016**, *22*, 3665-3667.
(20) Oleshkevich, E.; Viñas, C.; Romero, I; Choquesillo-Lazarte, D.; Haukka, M.; Teixidor, F. *Inorg. Chem*. **2017** DOI: 10.1021/acs.inorgchem.7b00610.
(21) Baumgartner, J.; Dey, A.; Bomans, P. H. H.; Coadou, C. L.; Fratz, P.; Sommerdijk, N. A. J. M.; Faivre, D. *Nat. Mater*. **2013**, *12*, 310-314.
(22) Leites, L. A. *Chem. Rev.* **1992**, *92*, 279-323.
(23) a) Pothiraja, R.; Sathiyendiran, M.; Butcher, R. J.; Murugavel, R. *Inorg. Chem.* **2005**, *44*, 6314. (b) Pothiraja, R.; Shanmugan, S.; Walawalkar, M. G.; Nethaji, M.; Butcher, R. J.; Murugavel, R. *Eur. J. Inorg. Chem.* **2008**, 1834.
(24) Dementyev, P.; Dostert, K.-H.; Ivars-Barcelý, F.; O´Brien, C. P.; Mirabella, F.; Schauermann, S.; Li, X.; Paier, J.; Sauer, J.; Freund, H.-J. *Angew. Chem. Int. Ed.* **2015**, *54*, 13942 –13946.
(25) Lu, X.; Liu, W.; Ouyang, J.; Tian, Y. *Applied Surface Science* **2014,** *311*, 749-752.
(26) Joseph, D.; Sachar, S.; Kishore, N.; Chandra, S. *Colloids and Surfaces B: Biointerfaces*, **2015**, *135*, 596–603.
(27) O'Handley, R. C.; *Modern Magnetic Materials: Principles and Applications*; Wiley: New York, **1999**.
(28) Ho, D.; Sun, X.; Sun, S. *Acc. Chem. Res.* **2011**, *44*, 875−882.

SUPPORTING INFORMATION

Merging Icosahedral Boron Clusters and Magnetic Nanoparticles: Aiming towards Multifunctional Nanohybrids Materials.

Elena Oleshkevich,[a] Francesc Teixidor,[a] Anna Rosell[b] and Clara Viñas[a,*]

[a] *Institut de Ciència de Materials de Barcelona (ICMAB-CSIC), Campus UAB, 08193 Bellaterra, Spain.*

b Neurovascular Research Laboratory, Vall d'Hebron Research Institute, Universitat Autònoma de Barcelona, Passeig Vall d'Hebron 119-129, 08035 Barcelona, Spain.

Redox titration analysis.

Geometry calculations.

Surface coverage values calculations.

Figure S1. Particle size distribution histograms from three batches of freshly prepared **1**-MNPs, prepared following the same synthesis, and mean particle size diameter.

Figure S2. X-ray diffraction patterns corresponding to **1**-MNPs (black) and the typical magnetite/maghemite spinel structure (red).

Figure S3. a) Images of **1**-MNP colloidal suspension in water at different pH. b) DLS studies in water at different pH.

Figure S4. ^{1}H-NMR, ^{1}H{^{11}B}-NMR, ^{11}B-NMR, ^{11}B{^{1}H}-NMR, ^{31}P-NMR spectra of the mother liquor after **1**-MNPs sterilization. Spectra were run in D_2O.

Redox titration analysis.

The ratio of Fe^{2+} and Fe^{3+} ions forming **1**-MNPs nanoparticle core was determined by redox titration analysis.

Samples of freshly prepared **1**-MNPs: Powder samples of **1**-MNPs (about 0.5 mg) before sterilization were decomposed in 0.1 mL HCl (37 wt.%) and diluted to 1mL by Milli-Q water giving a yellowish solution (with Fe^{2+} and Fe^{3+} ions).

Preparation of the **1**-MNPs samples after sterilization: About 0.1 mL HCl (37 wt.%) was added to 1 mL of **1**-MNPs suspensions after sterilization to decompose the nanoparticles.

In both samples, each of the obtained clear yellow solutions was analyzed by titration with $K_2Cr_2O_7$ (oxidizing solution) (5 mM). To know the end point of titration (oxidation of all Fe^{2+} to Fe^{3+}) the indicator sodium diphenylamine sulphonate was added to the prepared solution. The Fe^{2+} content was determined by the first titration. Then by addition of $SnCl_2$ (reductive agent) Fe^{3+} was reduced to Fe^{2+}. The total iron content $Fe^{2+/3+}$ was determined by the second titration. The Fe^{3+} content was calculated as follows: $Fe^{2+/3+}{}_{content}$ - $Fe^{2+}{}_{content}$. Titration was done in triplicate (n=3).

Before sterilization:

n	$W_{1\text{-}MNPs}$, µg	Fe^{2+} content, $wt.\%_{Fe2+/totFe}$	Fe^{3+} content, $wt.\%_{Fe3+/totFe}$
1	540	23.57	76.43
2	528	26.67	73.33
3	546	25.00	75.00
MEAN	538	25.08	74.92

25.08 % of Fe^{2+} content corresponds to magnetite/maghemite ratio $2Fe_3O_4.Fe_2O_3$ (Fe_8O_{11}).

*After sterilization in 1mL of suspension of **1**-MNPs:*

n	Fe^{2+} content, $wt.\%_{Fe2+/totFe}$	Fe^{3+} content, $wt.\%_{Fe3+/totFe}$
1	14.31	85.69
2	15.94	84.05
3	13.89	86.11
MEAN	14.71	85.28

14.71 % of Fe^{2+} content corresponds to magnetite/maghemite ratio $Fe_3O_4.2Fe_2O_3$ (Fe_7O_{10})

Geometry calculations

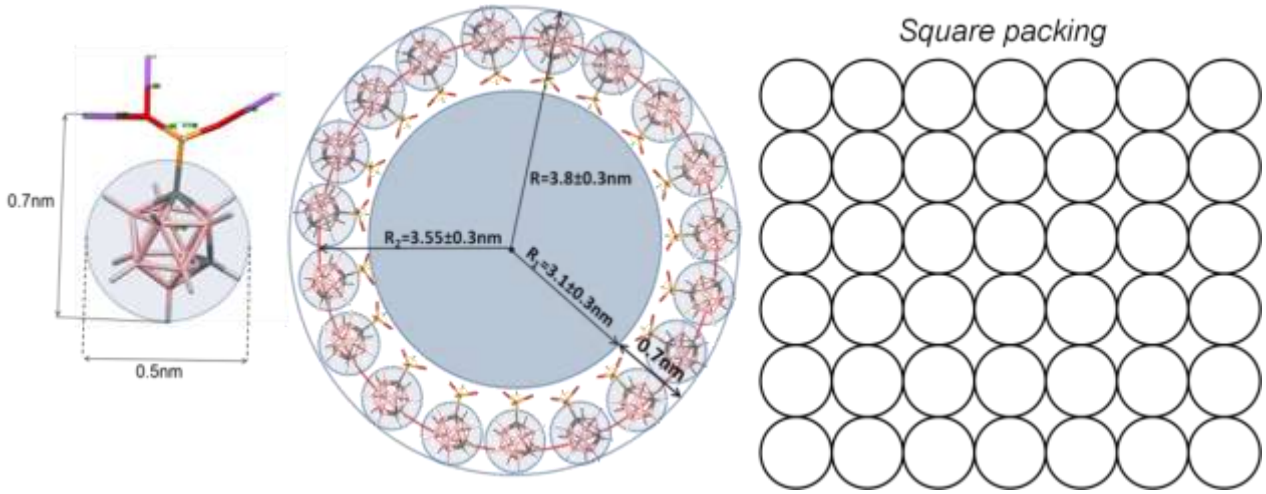

R_2=3.55±0.3 nm

$A_2 = 4\pi R_2^2$ = 132.732 ÷ 186.265 nm^2 (158 ± 27 nm^2)

For square packing: $A_{[\textbf{carboranylphosphate}]}$ = 0.5 x 0.5 = 0.25nm^2

n_{max} =$A_2/A_{[\textbf{carboranylphosphate}]}$= 530.928 ÷ 745.060 (638 ± 107) – maximum number of *meta*-carboranylphosphates that can fit one nanoparticle with core diameter of 6.2 ± 0.6 nm.

Surface coverage values calculations.

Energy Dispersive X-ray (EDX) analysis of **1**-MNPs before sterilization was performed for 3 (n = 3) bathes, prepared following the same synthesis. Average:

Fe 92,89 (At%) – 13 Fe

P 7.11 (At%) – 1 P

Fe:P = 13:1

For freshly prepared **1**-MNPs the core composition is $2Fe_3O_4{\cdot}Fe_2O_3$ (Fe_8O_{11}).

Fe_8O_{11} : $C_2B_{10}H_{11}$-P(H)OO^- = 1.625 : 1

(from geometry calculations) d = 6.2 ± 0.6 nm - diameter of nanoparticle core.

$m_{MNPs} = (1/6)\pi d^3 \rho_{MNPs}$ = (66.4 ± 19)E-20 g (taking the density of magnetite to be $\rho_{Magnetite}$=5.175g/cm^3 according to https://www.mindat.org/min-2538.html).

$Mole_{MNPs} = m_{MNPs}/M_{2Fe3O4{\cdot}Fe2O3} = N_{Fe8O11}/N_A$, where M_{Fe8O11} = 622.75 g/mol is molecular weight of magnetite/maghemite couple $2Fe_3O_4{\cdot}Fe_2O_3$, N_{Fe8O11} – number of Fe_8O_{11} units that contain one nanoparticle core with diameter 6.2 ± 0.6 nm.

$N_{Fe8O11} = m_{MNPs} N_A/M_{Fe8O11}$ = 642 ± 182 Fe_8O_{11}/NP

Taking into account EDX results before sterilization, Fe_8O_{11} : $C_2B_{10}H_{11}$-P(H)OO^- = 1.625 : 1, each nanoparticle bears $n_{[\textbf{carboranylphosphate}]} = N_{Fe8O11}$ / 1.625 = 395 ± 112 *meta*-carboranylphosphinates.

The saturation of surface of the nanoparticles core (%) $s_{CBP} = n_{[\mathbf{carboranylphosphate}]}/n_{max} \cdot 100\% = 61.29 \pm 7.43$ %.

$$\mathbf{s_{[carboranylphosphate](ICP)} = 61.29 \pm 7.43}$$

$$\mathbf{\%,\ n_{CBP} = 395 \pm 112\ CBP/NP}$$

Energy Dispersive X-ray (EDX) analysis of **1**-MNPs after sterilization was performed for 3 (n = 3) bathes, prepared following the same synthesis. Average:

Fe 55,34 (At%) – 70 Fe

P 0.79 (At%) – 1 P

Fe:P = 70:1

For **1**-MNPs after sterilization the core composition is $Fe_3O_4{\cdot}2Fe_2O_3$ (Fe_7O_{10}).

Fe_7O_{10} : $C_2B_{10}H_{11}$-P(H)OO^- = 10 : 1. $Mole_{MNPs} = m_{MNPs}/M_{Fe7O10} = N_{Fe7O10}/N_A$, where M_{Fe7O10} = 550.91 g/mol is molecular weight of magnetite/maghemite couple Fe_7O_{10}, N_{Fe7O10} – number of Fe_7O_{10} units that contain one nanoparticle core with diameter 6.2 ± 0.6 nm.

$N_{Fe7O10} = m_{MNPs} N_A/M_{Fe7O10} = 726 \pm 205\ Fe_7O_{10}$/NP

Taking into account EDX results after sterilization, Fe_7O_{10} : $C_2B_{10}H_{11}$-P(H)OO^- = 10 : 1, each nanoparticle bears $n_{[\mathbf{carboranylphosphate}]}$ = 73 ± 21 *meta*-carboranylphosphinates. The saturation of surface of the nanoparticles core (%)) $s_{[\mathbf{carboranylphosphate}]} = n_{[\mathbf{carboranylphosphate}]}/n_{max} \cdot 100\% = 11.21 \pm 1.41$ %.

$$\mathbf{s_{[carboranylphosphate](ICP)} = 11.21 \pm 1.41\ \%.}$$

$$\mathbf{\%,\ n_{[carboranylphosphate]\ (ICP)} = 73 \pm 21\ _{[carboranylphosphate]}/NP}$$

Figure S1. Particle size distribution histograms from three batches of freshly prepared **1**-MNPs, prepared following the same synthesis, and mean particle size diameter.

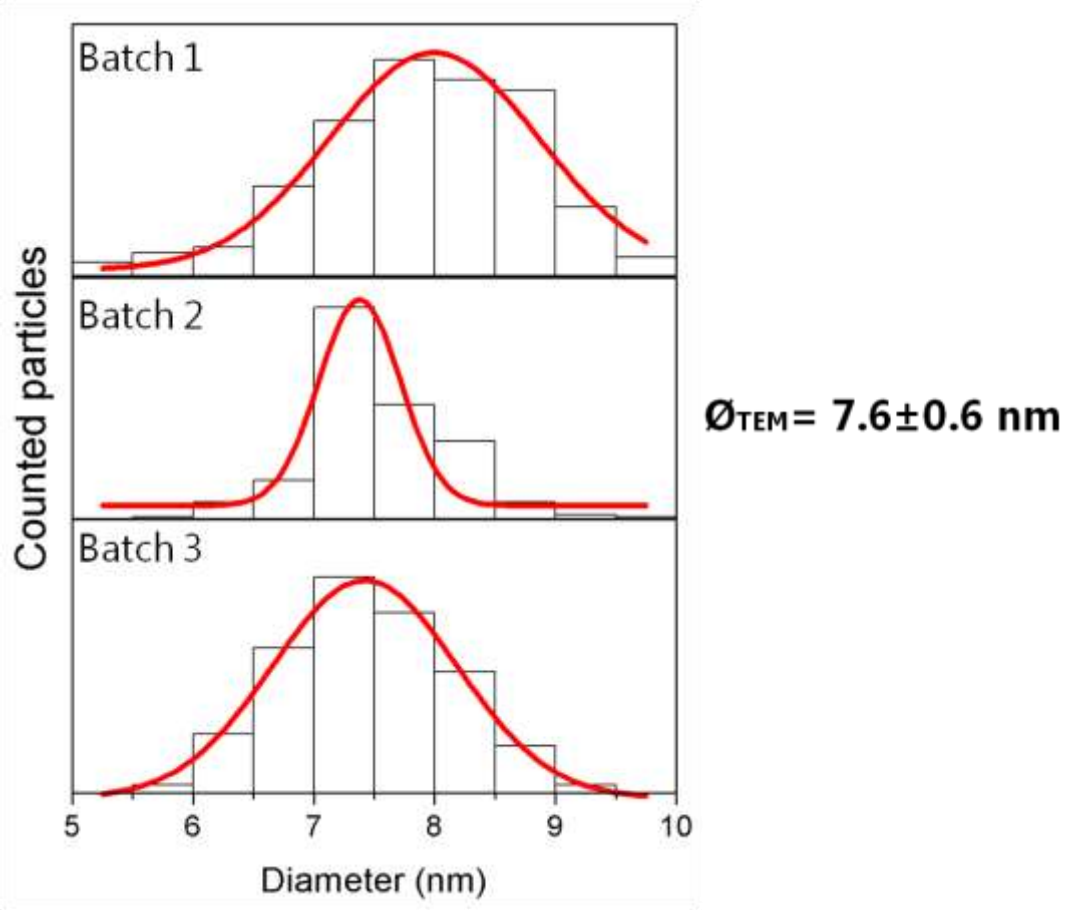

Figure S2. X-ray diffraction patterns corresponding to **1**-MNPs (black) and the typical magnetite/maghemite spinel structure (red).

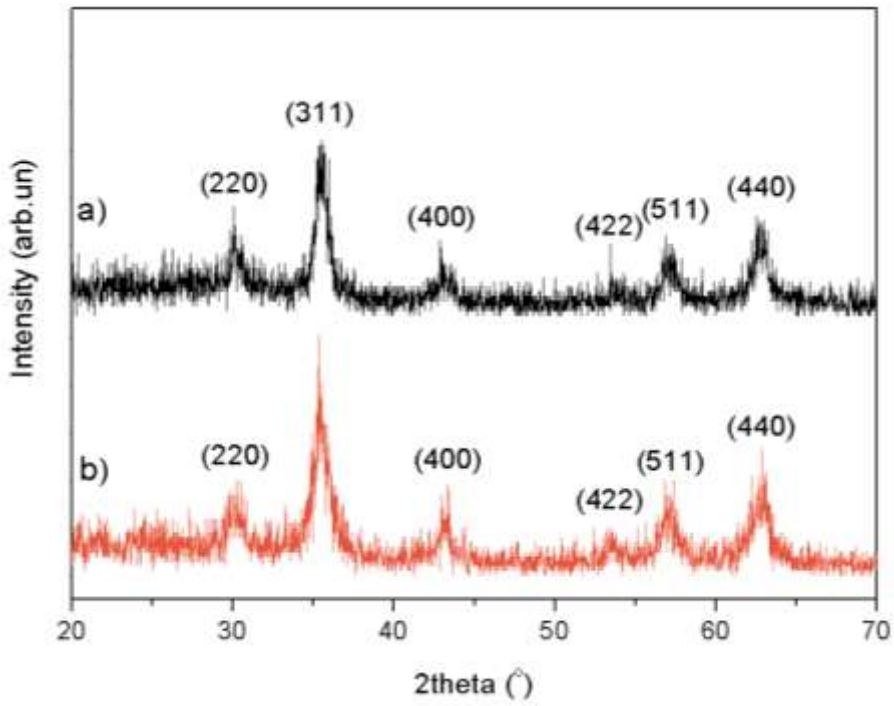

Figure S3. a) Images of **1**-MNP colloidal suspension in water at different pH. b) DLS studies in water at different pH.

a) b)

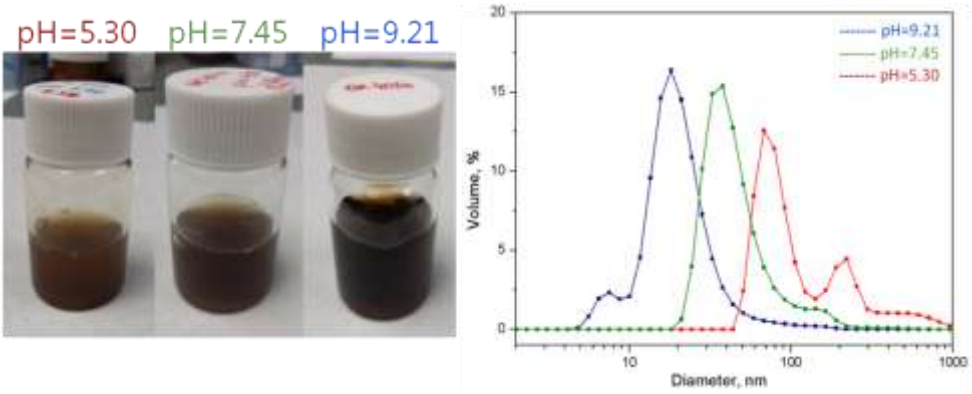

Figure S4. ^{1}H-NMR, ^{1}H{^{11}B}-NMR, ^{11}B-NMR, ^{11}B{^{1}H}-NMR, ^{31}P-NMR spectra of the mother liquor after **1**-MNPs sterilization. Spectra were run in D_2O.

^{1}H-NMR

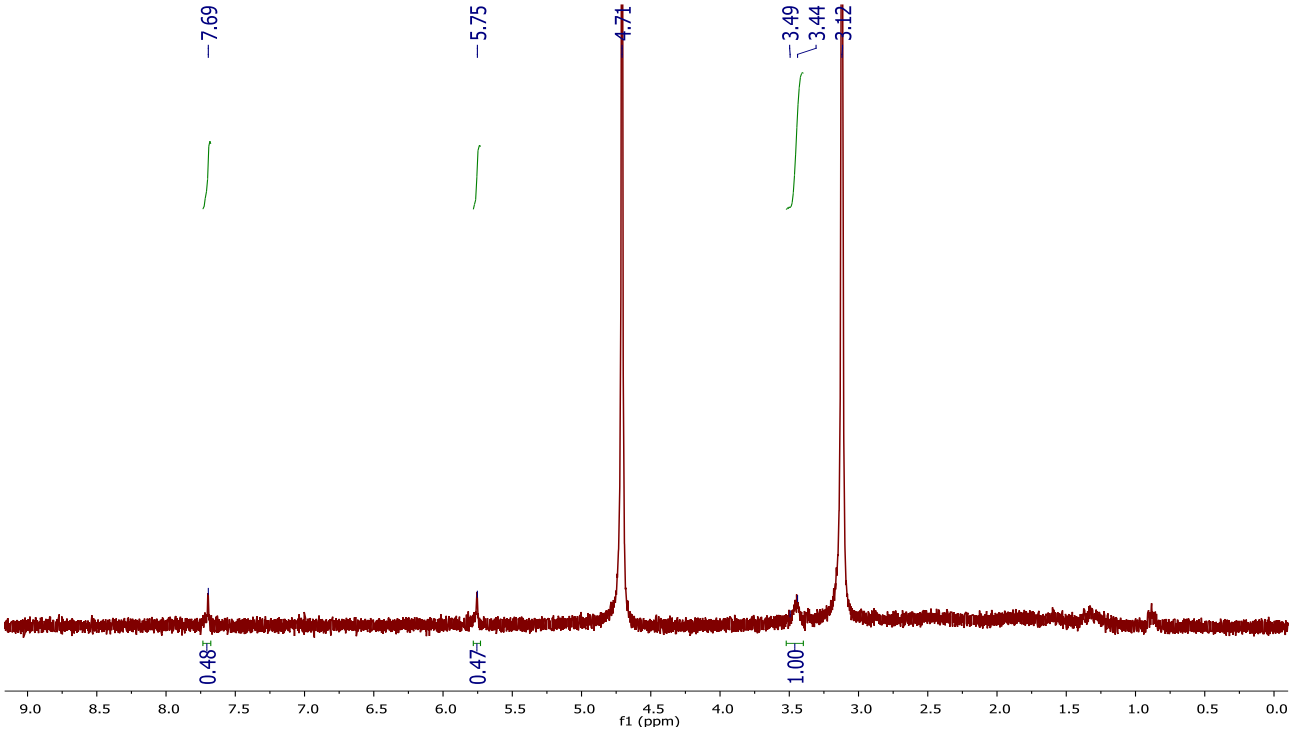

^{1}H{^{11}B}-NMR

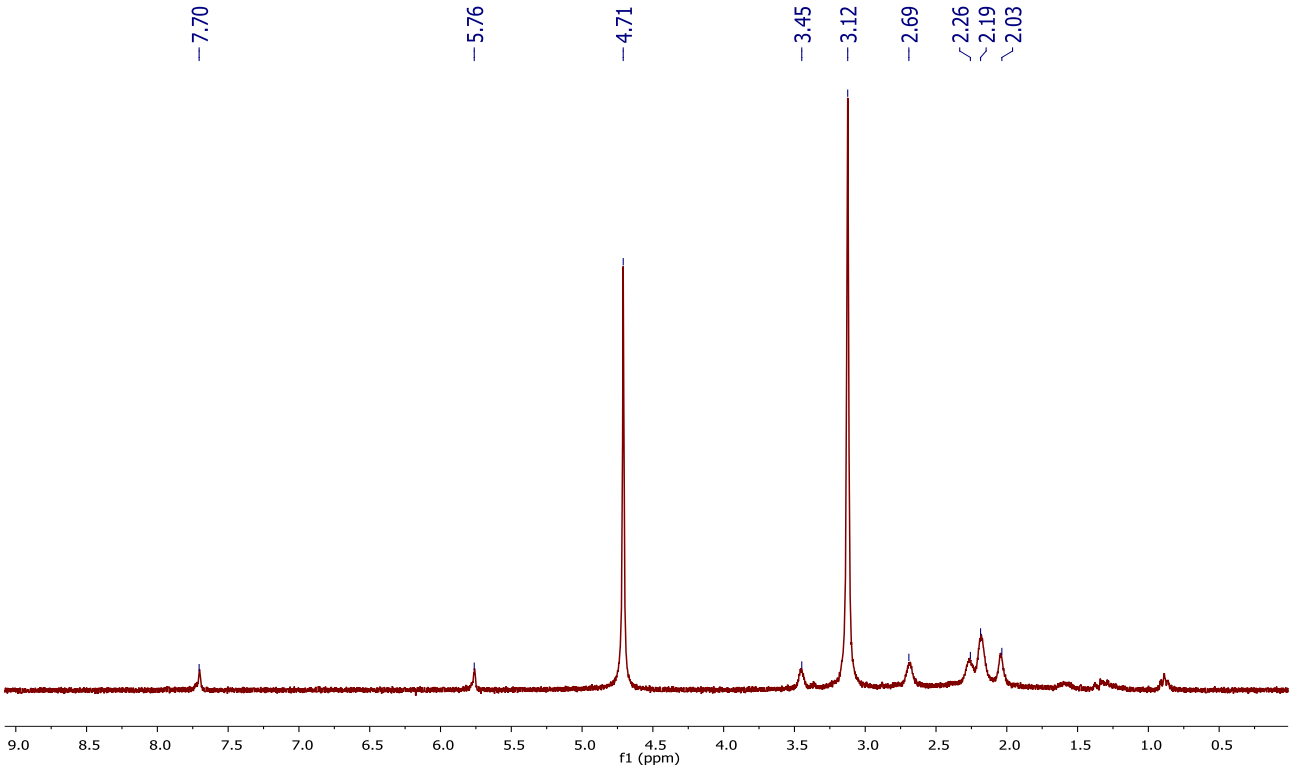

$^{11}B\{^{1}H\}$-NMR

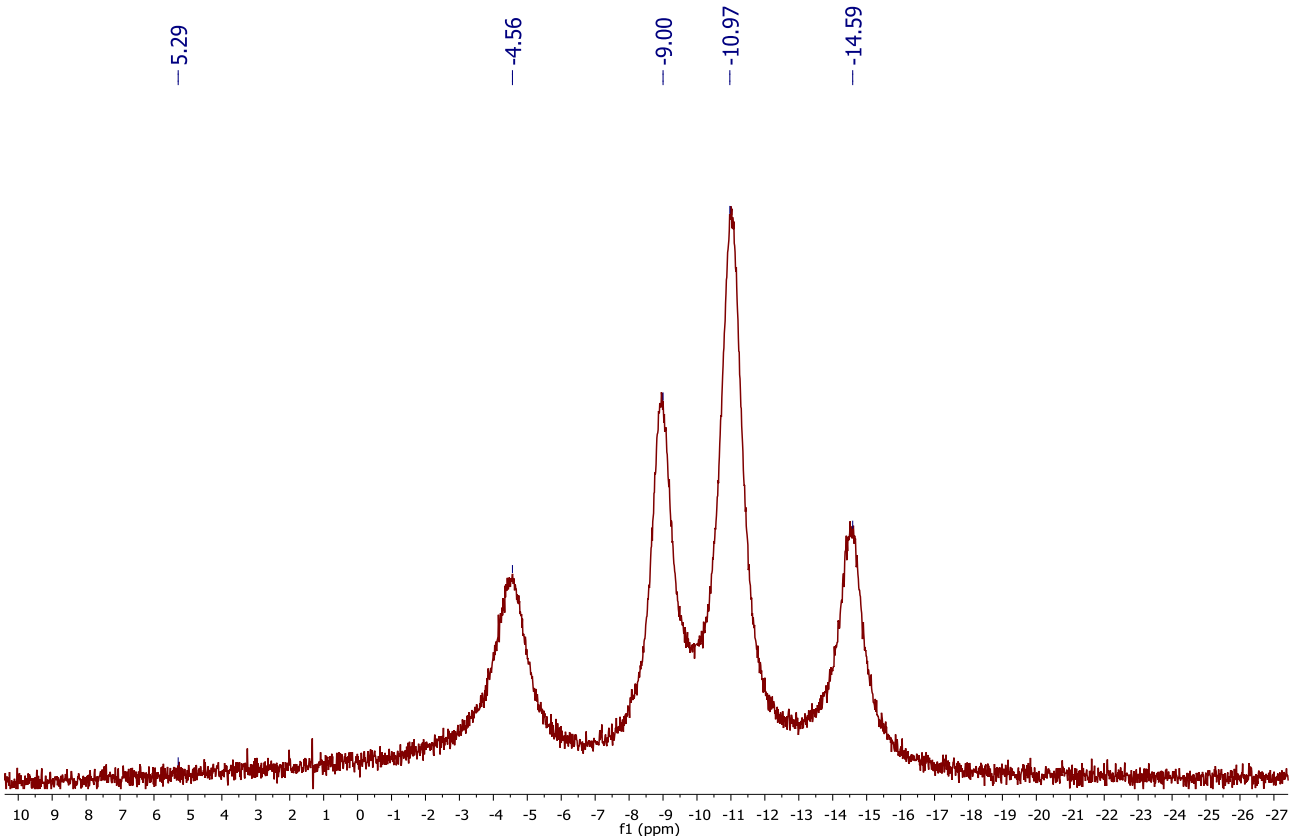

^{11}B-NMR

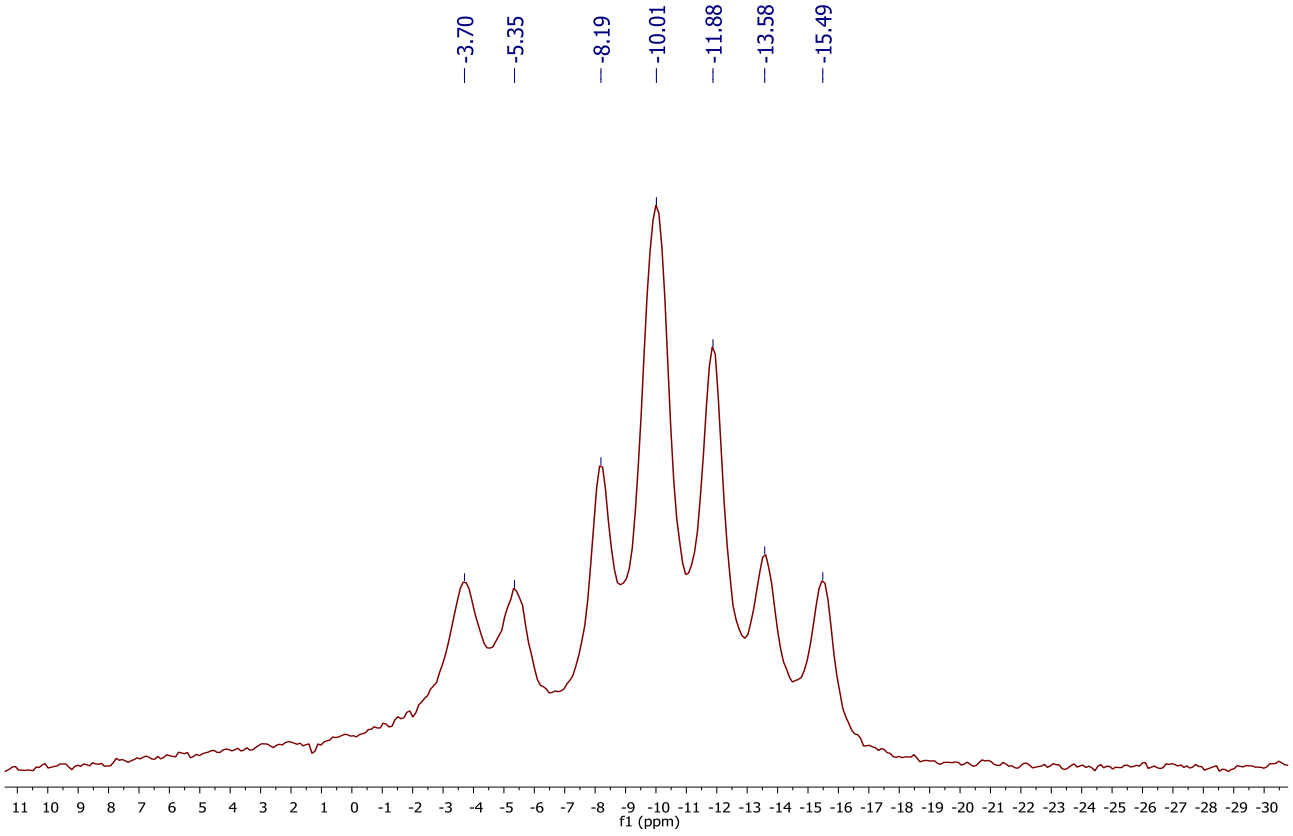

^{31}P-NMR

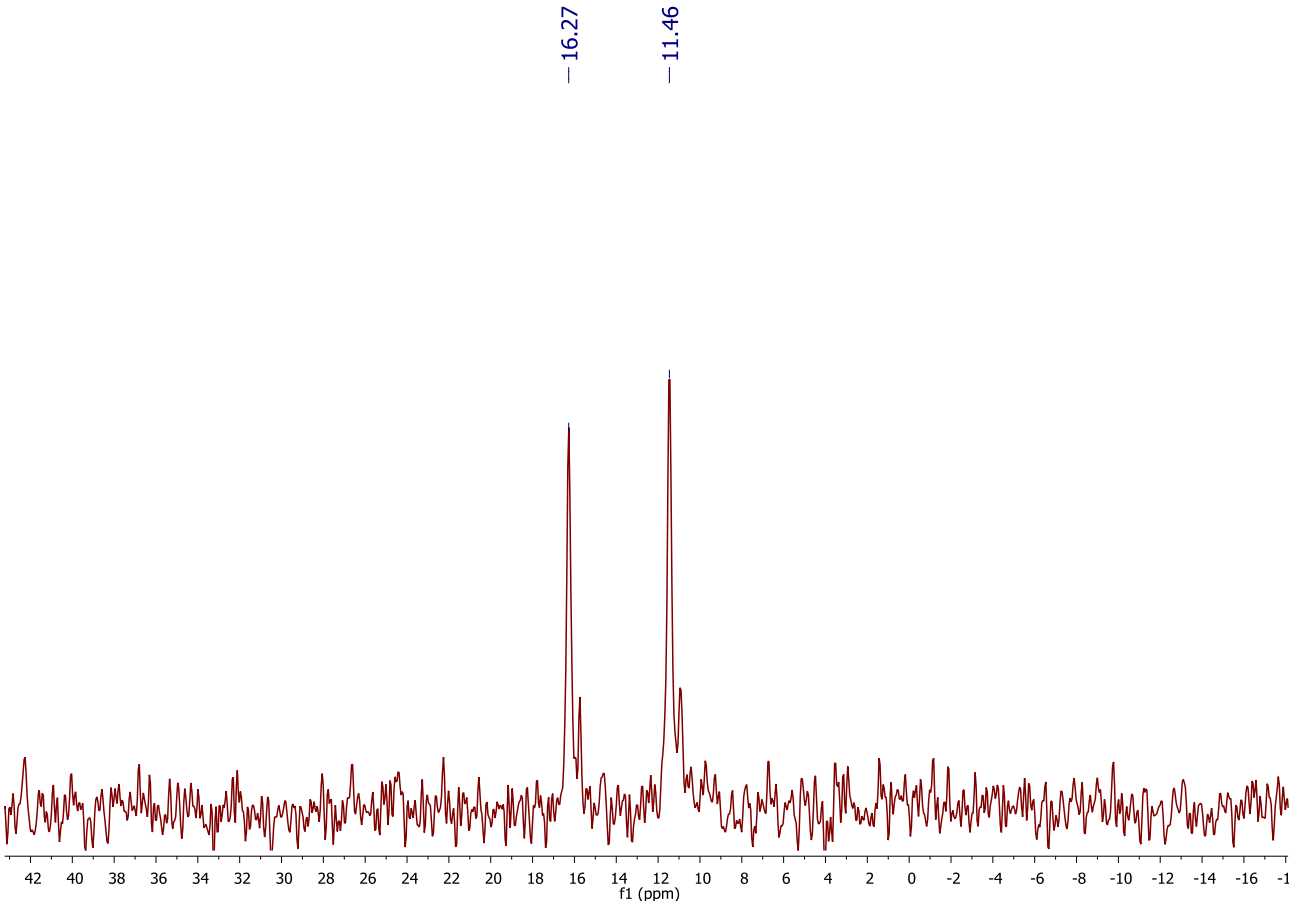
16.27
11.46
42 40 38 36 34 32 30 28 26 24 22 20 18 16 14 12 10 8 6 4 2 0 -2 -4 -6 -8 -10 -12 -14 -16 -1
f1 (ppm)

Biocompatible Fully Inorganic Nanohybrids for Biomedical Applications: Combining Magnetic Nanoparticles and Icosahedral Boron Clusters.

Elena Oleshkevich,[a] Anna Morancho,[b] Koen M. O. Galenkamp,[c,d,e] Alba Grayston,[b] Joan X. Comella,[c,d,e] Francesc Teixidor,[a] Anna Rosell,[b,*] Clara Viñas[a,*].

[a] Institut de Ciència de Materials de Barcelona (ICMAB-CSIC),Campus UAB, 08193 Bellaterra, Spain.

[b] Neurovascular Research Laboratory, Vall d'Hebron Research Institute, Universitat Autònoma de Barcelona, Passeig Vall d'Hebron 119-129, 08035 Barcelona, Spain.

[c] Cell Signaling and Apoptosis Group, Institut de Recerca de l'Hospital Universitari de la Vall d'Hebron (VHIR), Barcelona, Spain

[d] Institut de Neurociències, Departament de Bioquímica i Biologia Molecular, Facultat de Medicina, Universitat Autònoma de Barcelona, Bellaterra, Spain

[e] Centro de Investigación Biomédica en Red sobre Enfermedades Neurodegenerativas (CIBERNED), Madrid, Spain

KEYWORDS. m-carborayl, phosphinate, MNPs, cancer, cytotoxicity, theranostics, drug delivery, nanomedicine, iron oxide nanoparticles.

ABSTRACT: In this paper, we assess the *in vitro* and *in vivo* properties of newly synthesized boron cluster-MNPs nanohybrids (**1**-MNPs) coated with *m*-carboranylphosphinate ([**1**]$^-$), prepared by classic co-precipitation synthesis. To illustrate their potential biomedical applications, we demonstrate the cellular uptake of these **1**-MNPs from culture media by the human cell line of capillary-derived human brain endothelial cells (hCMEC/D3) and by the glioblastoma multiforme cell line A172 together with their toxicity profile. Prior to testing the *in vitro* toxicity of **1**-MNPs, studies of colloidal stability of the **1**-MNPs suspension at different culture media and temperatures (room temperature and 37 °C) have been carried out. TEM images and chemical titration confirmed that the **1**-MNPs penetrate into these cells in cytoplasmatic membrane-vesicles. Additionally, to explore its potential use in Boron Neutron Capture Therapy (BNCT) for treating cancer locally, we show that with the MNPs uptake it is proven the presence of the *m*-carboranyl cluster coordinated at the MNPs core by high resolution XPS and EELS spectra. Importantly, we also demonstrate that the systemic administration of these **1**-MNPs in adult mice is well tolerated with no major signs of toxicity after 10 days.

INTRODUCTION

In the past decade, the synthesis of magnetic nanoparticles (MNPs) has been intensively developed for many technological[1] and medical applications.[2] Typical MNPs obtained by the bottom-up synthesis consist of a magnetic core and an organic or inorganic shell that provides a barrier between the core and its environment dispersing them in water at a range of different pH values, among other tasks. While physical properties of MNPs are determined by their inorganic magnetic core, their surface properties also play an important role, especially in effective interfacing (e.g., ensuring biocompatibility and specific site) with biological systems. Superparamagnetic iron oxide nanoparticles (SPIONs or MNPs) have been extensively investigated for numerous *in vivo* and *in vitro* applications, such as magnetic resonance imaging (MRI) contrast enhancement,[3] tissue repair, and detoxification of biological fluids, hyperthermia, drug delivery, immunoassays and cell separation techniques.[4]

All these biomedical applications require that MNPs have high magnetization values, a size smaller than 100 nm, and a narrow particle size distribution. These applications also require a demanding surface coating of the MNPs, which has to be nontoxic and biocompatible.[5] Such MNPs have been bound to drugs, proteins, enzymes, antibodies, or nucleotides and can be directed to an organ, tissue, or tumor using an external magnetic field.[6]

The most studied carborane is the icosahedral 1,2-dicarba-*closo*-dodecaborane, 1,2-*closo*-$C_2B_{10}H_{12}$, and its isomers (1,7 and 1,12-) that can be viewed as 3D aromatic systems[7] whose volume approximates that of one displayed by a benzene molecule rotating on one of its twofold axes.[8] These carboranes exhibit an unusual combination of properties such as low nucleophilicity, chemical inertness, thermal stability,[9] as well as stability and low toxicity in biological systems.[10] The rigid geometry and the relative easiness of derivatization at the carbon vertexes of the carborane cluster[9a,11] allow the preparation of a wide number of compounds potentially useful as precursors of more complex materials.[8a,12] Furthermore, the use of carboranes in supramolecular chemistry is a topic that raises great interest for their particular properties[9a,13] that may induce an unexpected behavior in the supramolecular structures in which they are inserted. Our vision of the carboranyl substituent, however, is that it is unique as a ligand because it is a rigid sphere appended to a metal coordinating site. This, along with its hydrophobicity and electron withdrawing properties through

the carbon cluster, C_c,[14] suggests the possibility of inducing distinct geometrical behavior in boron rich macromolecules or particles of significance for Boron Neutron Capture Therapy (BNCT)[15] for certain types of cancer, and for drug delivery.[16] Particular to this work is the carborane derivative utilized, *m*-carboranylphosphinate and its *m*-carboranylphosphinic acid (Chart 1), which were recently reported.[17] The ligand is subjected to the properties bestowed by the *m*-carborane, perhaps the most noticeable in what refers to the results obtained in this work being the reduced tendency to be oxidized of the coordinating group, the spherical nature of the carborane and the hydrophobicity of the carboranyl unit.

In this paper, we assessed the *in vitro* and *in vivo* properties of the boron cluster-MNPs nanohybrids coated with *m*-carboranylphosphinate ([**1**]$^-$), which were prepared (**1**-MNPs)[18] by classic co-precipitation synthesis.

Chart 1. Schematic representation of *m*-carborane, *m*-carboranylphosphinic acid (H[**1**]), its sodium salt (Na[**1**]), and bidentate bridging mode of coordination of [**1**]$^-$ onto the surface of MNPs.

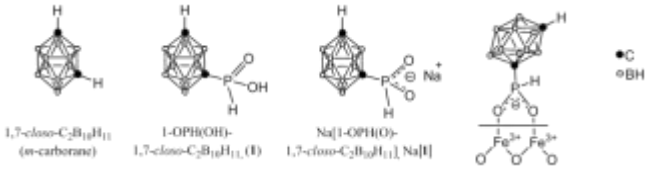

To illustrate their potential biomedical applications, we have demonstrated the cellular uptake of these **1**-MNPs from culture media by a human cell line of capillary-derived human brain endothelial cells (hCMEC/D3). We show by TEM images that the **1**-MNPs penetrate into these cells in membrane-vesicles and remain within the cells' cytoplasm. Additionally, to explore its potential ability to penetrate into malignant tumors as drug carriers or in Boron Neutron Capture Therapy (BNCT) for treating cancer locally, we have shown that these **1**-MNPs are taken up from culture media by the glioblastoma multiforme cell line A172. Finally, we demonstrate that the systemic administration of these **1**-MNPs in adult mice is well tolerated at mid-term with no major signs of toxicity.

EXPERIMENTAL SECTION

Methods.

Dynamic Light Scattering (DLS) and Zeta Potential: The hydrodynamic diameter ($Ø_{HYD}$) of **1**-MNPs dispersed in water and in several biological media was investigated with a ZETASIZER NANO ZS (Malvern Instruments Ltd) equipped with a He-Ne 633 nm laser using 1 mL of particle dispersion in a disposable plastic cuvette. Measurements were run in triplicate at ambient temperature and at 37 °C for samples in biological media. Number of scans was set up in automatic mode. Laser Doppler Micro-electrophoresis is the technique used to measure zeta potential. The zeta potential of a colloidal suspension in aqueous media was obtained by filling a disposable cell with 1 mL of the colloidal suspension. Measurements were run in triplicate at ambient temperature. Number of scans was set up in automatic mode. Magnetic characterization of **1**-MNPs was carried out in a Superconductive Quantum Interference Device (SQUID) magnetometer (Quantum Design MPMS5XL). Magnetization *vs* magnetic field measurements were performed at 300 K and 5 K in a field 6 T. Zero-field cooling (ZFC) and field cooling (FC) temperature dependent magnetization measurements were carried in a field of 50 Oe. The samples were prepared using a polycarbonate capsule filled with 1 mg of **1**-MNPs and compacted cotton. High resolution X-ray photoelectron spectroscopy (HRXPS) was performed with a Phoibos 150 analyzer (SPECS GmbH, Berlin, Germany) in ultra-high vacuum conditions (base pressure 4E-10 mbar) with a monochromatic aluminium K alpha X-ray source (1486.74 eV). The energy resolution as measured by the FWHM of the Ag 3d5/2 peak for a sputtered silver foil was 0.8 eV. Scanning Transmission Electron Microscopy (STEM) images were acquired at 200 keV on an FEI Tecnai G2 F20 microscope using a high angle annular dark field (HAADF) detector. Energy Dispersive X-Ray (EDX) spectra were obtained with an EDAX super ultra-thin window (SUTW) X-ray detector. Electron Energy-Loss Spectroscopy (EELS) and Energy Filtered TEM (EFTEM) experiments were performed using a Gatan Imaging Filter (GIF) Quantum SE 963 fitted with a 2k x 2k CCD camera. **1**-MNPs and cell samples were prepared by dispersing a small amount of powder in Milli-Q water. Afterwards, the drop dispersion was dried onto a carbon coated TEM grid.

TEM of cells: The presence of cytoplasmatic and intracellular localization of **1**-MNPs into human brain endothelial cells hCMEC/D3 and glioblastoma A172 cells was done by using a JEOL JEM-1400 microscope operating at 120 kV.

Materials

Starting compounds 1-OPH(OH)-1,7-*closo*-$C_2B_{10}H_{11}$ (**1**), Na[1-OPH(O)-1,7-*closo*-$C_2B_{10}H_{11}$] (Na[**1**]) and **1**-MNPs were synthesized as reported.[17,18] 3-[4,5-dimethylthiazol-2-yl]-2,5-diphenyltetrazolium bromide was purchased from Sigma-Aldrich. Milli-Q water was used to do all preparations and dilutions.

The culture media used for cell growing and treatments were EGM-2 (Clonetics, Lonza) and DMEM (Thermo Fisher), with 2% and 10% FBS respectively. Phosphate buffer saline (PBS) was prepared from 10x concentrated solution (Sigma-Aldrich) in sterile Milli-Q water. Cultured cells were hCMEC/D3 (as human cerebral microvascular endothelial cells),[19] and A172 (as human glioblastoma cell line) purchased at ATCC (Manassas, VA, USA). Collagen I coating purchased at BD Biosciences was used for hCMEC/D3 cultures.

*Preparation of **1**-MNPs aqueous suspension at the physiological pH*: A stable **1**-MNPs (0.5 mg/mL) colloidal aqueous dispersion was prepared as follows. **1**-MNPs (5 mg) were redispersed in deionized H_2O (10 mL) containing 1 µL of [NMe_4]OH by using ultrasound radiation. The as-prepared dispersion has a pH about 5.5-6.5, and then pH was adjusted to 7.3-7.5 by using additional [NMe_4]OH aqueous solution. The corresponding vehicle media used in control conditions consisted of equal content of *m*-carboranylphosphinic acid (**1**) and [NMe_4]OH as in a **1**-MNPs colloidal suspension.

*Cellular uptake of **1**-MNPs*: **1**-MNPs (first sonicated for 10 minutes) were tested at concentrations from 0 to 100 µg/mL of total iron $Fe^{2+/3+}$ or with vehicle solution, and incubated at 37 °C in a CO_2 incubator as follows: Brain endothelial cells (hCMEC/D3, $1x10^4$ cells) were cultured in 24-well plates, and after 48 hours, cells were washed with PBS twice and treated with **1**-MNPs or vehicle at the concentrations described above. Finally, glioblastoma A172 cells were seeded in 24-well plates ($15x10^4$ cells/well) and grown for 24 hours. Afterwards cells were washed with PBS twice and treated with the indicated concentrations of **1**-MNPs in DMEM-1% FBS. A172 and

hCMEC/D3 cells were also treated with Na[**1**] salt from 0 to 7.5 mM in each corresponding basal media.

All cells were incubated for 24 hours with corresponding medium containing **1**-MNPs or the Na[**1**] salt in duplicates. Afterwards, cells were used to assess cell viability or to determine the intracellular uptake of the **1**-MNPs.

Cell viability assays: MTT (3-[4,5-dimethylthiazol-2-yl]-2,5-diphenyltetrazolium bromide) is a yellow compound that turns into a purple formazan after its reduction by mitochondrial enzymes, which are only present in metabolically active live cells, but not in dead cells. Formazan can be photometrically quantified at 590 nm.

After incubation either with **1**-MNPs, Na[**1**] or vehicle solution, cells were washed with PBS and incubated with 50 μL of MTT in 300 μL of each treatment media (final concentration of MTT at 0.5 mg/mL). After 90 minutes, in which the MTT reduction took place, the cell medium was discarded and 200 μL of dimethylsulfoxide was added to each well plate. Absorbance by the isolated supernatant was measured at 590 nm in duplicate. Final data is expressed as percentage of viable cells *vs* the control media condition. Differences versus the control condition were subjected to analyses of variance followed by Dunnett post hoc tests (statistical significance was considered when $p < 0.05$).

Cell count: This assay uses a proprietary mix of two DNA intercalating fluorescent dyes in a single reagent (the Count & Viability Assay Kit, Millipore). One of the dyes permeates the membrane and stains all cell nuclei. The second dye only stains cells with compromised membranes of dying or dead cells. This combination allows for determining the number of total and viable cells in a given sample using a Muse™ Cell Analyzer (Millipore). Briefly, hCMEC/D3 and A172 cells were seeded in flasks/dishes of similar surface, grown until sub-confluence and the number of viable cells after 24 h treatment with **1**-MNPs was quantified using the above-mentioned method in a small portion of the cell suspension (100 μL). Data expressed as percentage of viable cells was used to calculate the amount of iron/cell.

Dried cells preparation for magnetization measurements, XPS, HRSTEM, EELS and EFTEM studies: Total cells collected from the cell count cultures were centrifuged at 1500 rpm for 5 minutes, then the cell pellet was resuspended in 50 μL of each cell culture media, and transferred into a polycarbonate capsule to be dried at 60 °C using a speed vacuum centrifuge (1500 rpm for 1 hour).

*Cytoplasmatic **1**-MNPs detection by Prussian blue and **1**-MNPs visualization by Transmission Electron Microscopy*: Growing hCMEC/D3 and A172 cells were treated with increasing doses of **1**-MNPs as described above. Afterwards, Prussian blue stain was performed to prove the iron uptake by the cells as described.

For verifying the presence of cytoplasmatic MNPs core by TEM, cells were prepared as follows: cells were seeded in 25 cm^2 flasks, grown, treated with **1**-MNPs for 24 h (for the hCMEC/D3 cells, [Fe] = 25 μg/mL; for the A172 cells, [Fe] = 50 μg/mL), trypsinized, and collected by standard centrifugation. Then 1.5 mL of 2% glutaraldehyde in cacodylate buffer was added to the remaining pellet and cells were quickly incubated in the fixation solution at 4 ºC for 1 h, post-fixed in 1 % OsO_4, dehydrated in 12 steps by using 50-100 % acetone[20] and embedded in Epon resin. Finally, ultrathin sections (70 nm) were transferred onto copper grids and analyzed by TEM at 120 kV.

In parallel, to assess the presence of the *m*-carboranyl cluster surrounding the observed MNPs core present in the cytoplasm, Electron Energy Loss Spectroscopy (EELS) was performed using the same cells' samples as used for subcellular **1**-NMPs localization.

*In vivo **1**-MNPs administration*: To explore potential "*in vivo"* toxicity of the new **1**-MNP nanohybrids, adult C57BL/6 mice (males, 11-12 weeks-old) received one intravenous administration of 80 μL of **1**-MNPs at218 μg/mL iron concentration or corresponding vehicle solution. Briefly mice were anesthetized with 5 % isoflurane in Medicinal Air (from Air Liquide), weighted and treated with **1**-MNPs or vehicle solution by retro-orbital injection as described.[21] After recovery from anesthesia, mice were returned to their housing boxes and supervised daily looking for sudden death, seizures, dystonia, dehydratation or restrictions in mobility. Additionally, body weight was registered before administration (baseline), at day 1, 2, 3 and 10 in treated and naïve mice. Importantly, the amount of iron administered with the **1**-MNPs was close to the approved dose for Feridex® in humans (0.56 mg/Kg of body weight). Differences in weight between groups were subjected to analyses of variance and statistical significance was considered when $p < 0.05$.

RESULTS AND DISCUSSION.

It has been recently reported[18] that pH produces an effect on hydrodynamic radius of the aqueous **1**-MNPs suspensions. In addition, there are many studies revealing that MNPs behave differently in biological media than in water at physiological pH (7.45)[22] because of the presence of inorganic salts, proteins, amino acids or polysaccharides in biological media.[23] This is why studies of colloidal stability of the **1**-MNPs suspension at different culture media and temperatures (room temperature (r.t) and 37 °C) have been run in this paper.

Prior to testing the *in vitro* toxicity of **1**-MNPs, it was important to perform colloidal stability assays of **1**-MNPs in commonly used biological media for cell culturing (DMEM-F12-1% FBS, DMEM-1% FBS, EGM2-2%FBS and RPMI) as well as with the well-known phosphate buffered saline (PBS) solution that contains inorganic salts (NaCl, Na_2HPO_4, KH_2PO_4, KCl). So, the stability of colloidal dispersions of **1**-MNPs (50 μg **1**-MNPs/mL) in PBS and culture media was studied at different times (10 min. and 24 h.), and temperatures (r.t. and 37 °C). The results are on display in Table 1.

In all culture media no precipitation was observed neither after 10 min nor after incubating 24 h at r.t. or at 37 ºC while in PBS **1**-MNPs sedimented within 24 h. In the case of DMEM F12–1% FBS, 1% non-essential amino acids and 1% antibiotics, and in RPMI the size of detected particles was close to the mean particle diameters determined by TEM, $Ø_{TEM} = 7.6 \pm 0.6$ nm. In EGM-2 medium with 2%FBS and in DMEM-1%FBS **1**-MNPs rapidly formed aggregates with hydrodynamic diameters in the range of 50-140 nm and 60-170 nm respectively, maintaining the invariable size was for 24 h. Comparing results at r.t. and 37 ^{o}C, a slight increase in hydrodynamic diameters was observed in all culture media as displayed in Table 1.

Table 1. Hydrodynamic diameter and diffusion coefficients values of **1**-MNPs suspensions at different culture media and temperatures (r.t. and 37 °C) measured by DLS

Media	T, °C °C	$Ø_{HYD}$, (nm)	Diffusion Coefficient, (μ^2/s)
10 min			
PBS	r.t	76.1 ± 31.1	4.90
RPMI	r.t	9.0 ± 2.3	4.16
	37	8.4 ± 2.0	4.19
DMEM F12–1%	r.t	9.8 ± 2.5	3.40
FBS	37	8.2 ± 2.6	3.63
EGM-2 medium	r.t	90.3 ± 40.7	4.43
with 2%FBS	37	98.7 ± 41.6	5.69
DMEM-1% FBS	r.t	103.4 ± 40.7	4.14
	37	106.6 ± 42.9	5.13
24 hours			
PBS	1276 ± 435 (precipitated)		
RPMI	r.t	10.8 ± 4.4	3.92
	37	11.0 ± 12.9	4.09
DMEM F12–1%	r.t	9.5 ± 2.2	3.50
FBS	37	8.5 ± 2.3	4.03
EGM-2 medium	r.t	99.5 ± 41.9	4.31
with 2%FBS	37	101.0 ± 42.6	5.54
DMEM-1% FBS	r.t	123.6 ± 40.8	3.42
	37	133.3 ± 43.4	4.24

*Determination of **1**-MNPs uptake by the cells*: The hybrid nature of the MNPs is conceptually divided into the inorganic core, the engineered surface coating comprising the ligand shell and the corona of adsorbed biological molecules. Empirical evidence shows that all these three components may degrade individually *in vivo* and can drastically modify the life cycle and biodistribution of the whole heterostructure. Thus, the MNPs may be decomposed into different parts, whose biodistribution and fate would need to be analyzed individually. The first step of the biological studies was to confirm the uptake of as sterilized **1**-MNPs by the cultured cells (hCMEC/D3 and A172). As shown in the right panels of Figure 1. The Prussian blue stain enables us to identify the presence of intracellular iron after 24 h treatment with **1**-MNPs. These experiments suggest that there has been cytoplasmatic endocitosis of the iron core of the **1**-MNPs.[24] Cell viability assay shows that brain endothelial (hCMEC/D3) cells were more sensitive to **1**-MNP toxicity than glioblastoma A172 cells (Figure 1A and 1B) since doses of 25 µg $Fe^{2+/3+}$/mL significantly reduced endothelial cell viability. In this regard, previous investigations have reported safety of other iron oxide compounds at similar concentrations in both endothelial and other cancer cells.[24] The reduction in hCMEC/D3 viability could be only partially explained by the vehicle solution, but certainly the **1**-MNPs nanohybrid induced cell toxicity starting at 25 ug/mL. At the same administration doses of **1**-MNPs, glioblatoma A172 cells presented full viability as observed in Figure 1. However higher doses already induced cell toxicity to this cancer cells, maybe due to the acidity of *m*-carboranylphosphinic acid present in the vehicle solution.

*Quantification of **1**-MNPs uptake by cells*: To confirm the uptake of MNPs core by the A172 and hCMEC/D3 cells after 6 or

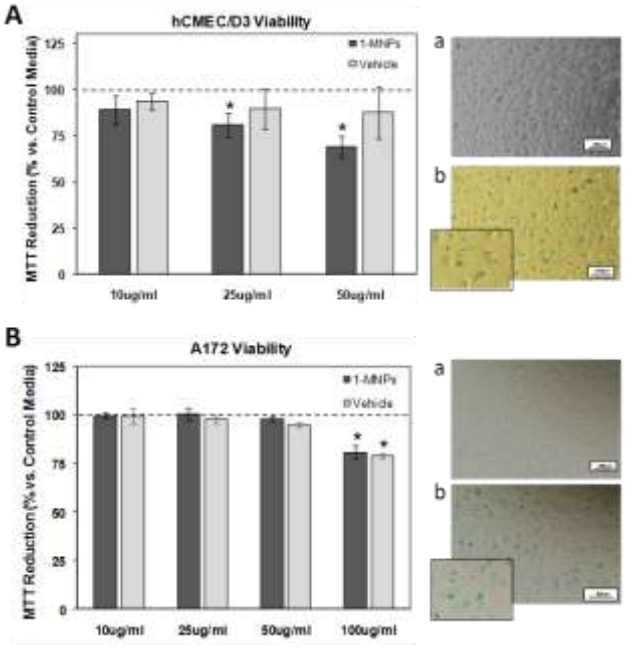

Figure 1. Cell viability was tested after exposing brain endothelial cells (A), and Glioblastoma cells (B) to increasing doses of **1**-MNPs and corresponding vehicle solutions for 24 hours. Data is expressed as mean ±SD of n=3/4 per condition; * $p<0.05$ indicates differences vs. control media (dashed line). Right panels correspond to images of each cell line (a) and to iron deposits observed after Prussian Blue Stain (b, treatment dose 10 µg/mL).

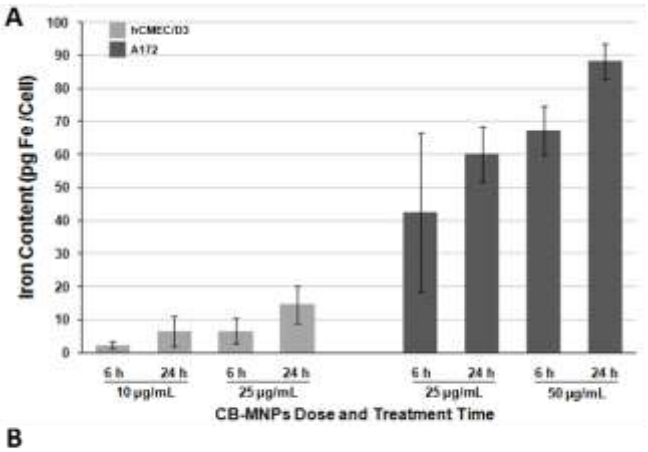

B

	hCMEC/D3				A172			
	10µg/mL		25µg/mL		25µg/mL		50µg/mL	
	6h	24h	6h	24h	6h	24h	6h	24h
MEAN	2.32	6.56	6.61	14.66	42.49	60.07	67.38	88.26
SD	1.16	4.52	3.73	5.69	24.14	8.27	7.33	5.37

Figure 2. The amount of $Fe^{2+/3+}$ per viable cell was determined after treating cells with increasing doses of 1-MNPs for 6 or 24 hours. Bar graph (A) shows that the amount of Fe/cell was time- and dose-dependent in both brain endothelial and glioblastoma cell lines. The tested glioblastoma cells (A172) were capable to uptake the largest amounts of iron at all sub-toxic tested doses (B). Data is expressed as mean ±SD pg $Fe^{2+/3+}$/Cell of n=3 independent experiments per condition.

24 h of incubation in the presence of **1**-MNPs, the cells were dried, as described at the experimental section and magnetism measurements were run (see S. I.). The uptake of **1**-MNPs was measured through the MNPs core and calculated as follows: first, dividing the MR value of the treated cells by the total number of cells which provides the magnetization per cell (emu/cell), then further dividing this value by the remanent magnetization of the **1**-MNPs (emu/g **1**-MNPs) at 5 K to give the amount of iron per cell.[25] The results determine the amount of iron per cell and show a clear time- and dose-dependent relationship with both endothelial and glioblastoma cell lines as shown in Figure 2A. Moreover at the same tested dose of **1**-MNPs (25 ug/ml) A172 cells presented larger higher cellular iron content than endothelial cells (a 6-fold and 4-fold increase

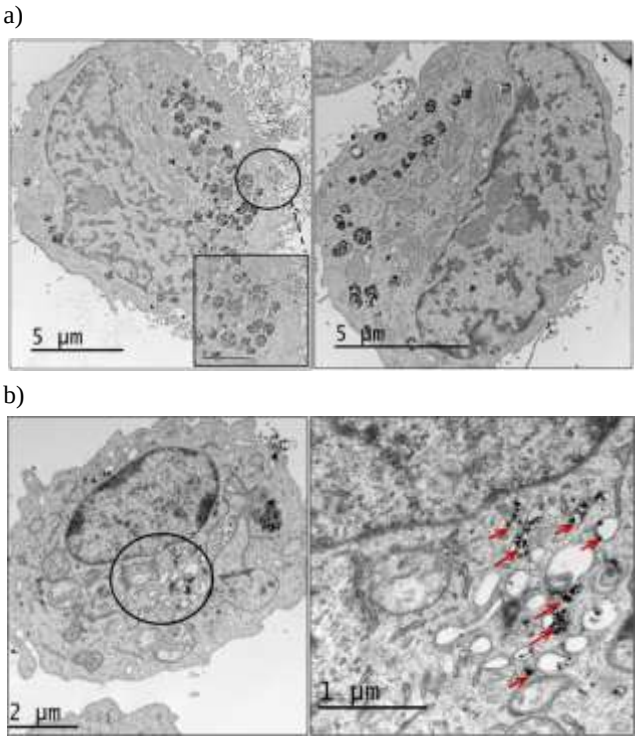

Figure 3. Transmission electron microscope (TEM) image of a) glioblastoma cells (A172) and b) endothelial hCMEC/D3 cells showing the presence of **1**-MNPs into the cytoplasm.

after 6 and 24 hours, respectively) as shown in Figure 2B, indicating a higher capacity for cell labeling with iron oxides without toxic effects (Figure 2). These are interesting results suggesting that by using low doses of MNPs, glioblastoma cancer cells might be largely labelled with the **1**-MNPs compound compared to other neighbouring cells in the tissue.

*Visualization of **1**-MNPs uptake by cells*: The presence of cytoplasmatic MNPs core and its intracellular localization into hCMEC/D3 and A172 cells were visualized by TEM analysis in membrane-bound compartments matching with endosomal or lysosomal organelles (Figure 3) at least 24 hours after labeling, as described for other iron oxide compounds.[24a,26] However, the presence of the *m*-carboranyl cluster surrounding the observed MNPs core present in the glioblastoma A172 cytoplasma could not be confirmed by means of EELS and EFTEM elemental maps, probably because of the low levels of boron, thus only Fe was clearly detected (see S. I.).

To overcome this drawback and unambiguously prove the presence of the *m*-carboranyl cluster coordinated at the MNPs core, high resolution XPS and EELS spectra on the A172 dried-cells sample were run. Peaks at 189 and 133 eV in the XPS analysis, which are characteristic of B-B[27] and P-O bonding, were observed that, clearly confirmed the presence of *m*-carboranyl phosphinate coordinated to the MNP core (Figure 4). EELS analysis on the A172 dried-cells sample also shows the B-K and PL2,3 edges present in the sample proving that carboranylphosphinate coordinates to MNPs surface.

Finally, the toxicity of the ligand shell coating the MNPs core (Na[**1**] salt) was determined in both A172 and hCMEC/D3 cells in a dose-response cell viability assay. As observed for the whole **1**-MNPs compound endothelial cells were more sentitive to the Na[**1**] salt than the glioblastoma cells since Letal Dose 50 was around 1 mM compared to the 7.5 mM observed in A172 cells; see Figure 5A and 5B. Those doses correspond to 230 $\mu g_{Na[1]}$/mL and 1725 $\mu g_{Na[1]}$/mL of Na[**1**], respectively.

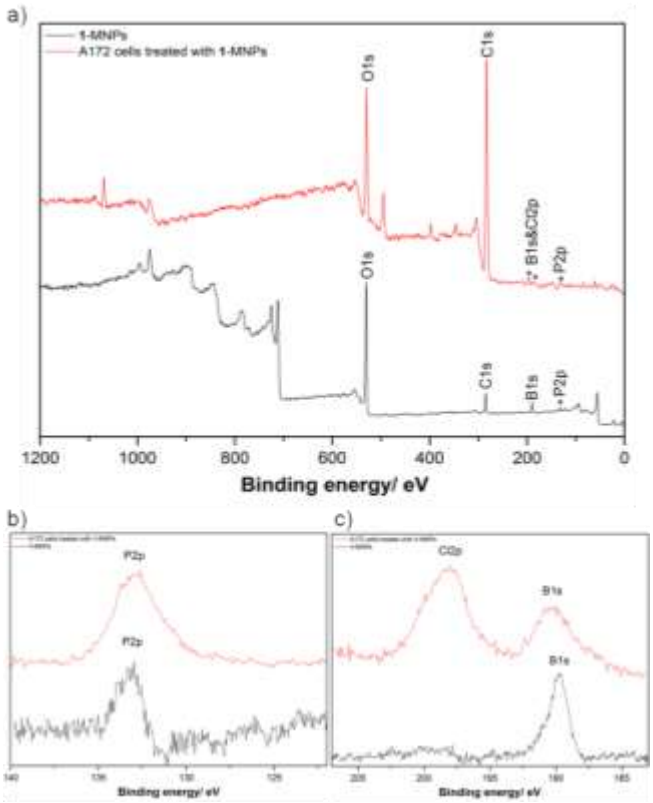

Figure 4. a) High resolution spectra XPS of **1**-MNPs and A172 cells treated with 1-MNPs. High resolution spectra XPS of **1**-MNPs and A172 cells treated with **1**-MNPs in the B 1s and P 2p regions, (b) and (c) respectively.

Evaluation of in vivo toxicity of the 1-MNP compound in mice: Before testing a drug or compound in a person we must find out their potential harmful effects in experimental models, and rodents have been widely used for this purpose. We aimed at proving for the first time that the **1**-MNPs were well tolerated and did not induce major acute toxicity signs such as death, seizures or convulsions but also acute pain, distress, decreased/increased motor activity or dehydratation by monitoring body weight before and after treatment. Briefly, mice received 80 µL of **1**-MNPs intravenously which corresponds to 0.58±0.03 mg/kg of body weight, very close to the approved dose for Feridex® in humans (0.56 mg/Kg of body weight) and previously tested in other "*in vivo*" studies.[28] Importantly, all mice survived the study-period (10 days) with no major signs of

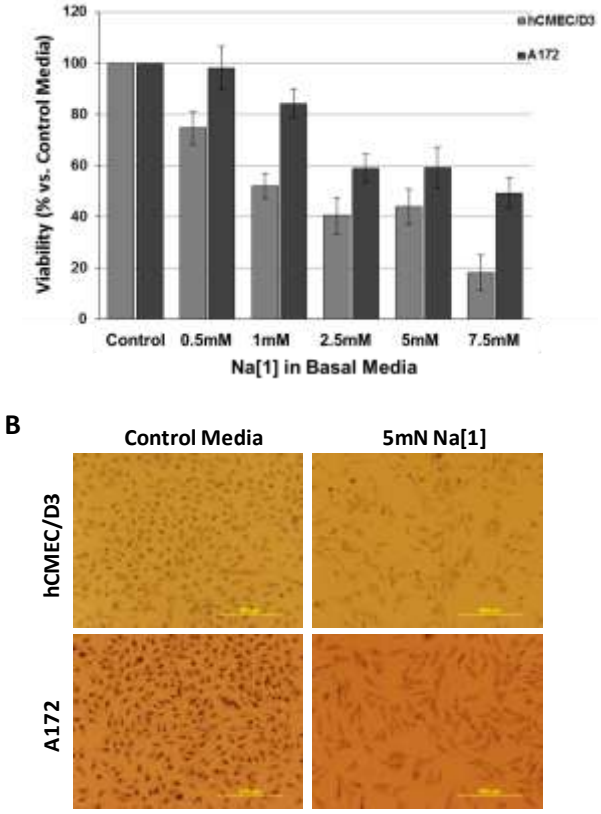

Figure 5. Cell viability was tested after exposing brain endothelial cells (hCMEC/D3 cells) and glioblastoma cells (A172) to increasing concentrations of the Na[**1**] salt and compared to control treatment (vehicle). A) bar graph representing cell viability after 24 h treatment (mean ±SD). B) Representative images of cells after MTT reduction.

toxicity. In particular we found that the individual body weight of the 2 treated groups were comparable with the control group (naïve mice) by fluctuating from day to day without a clear trend of increasing or decreasing (Figure 6A).

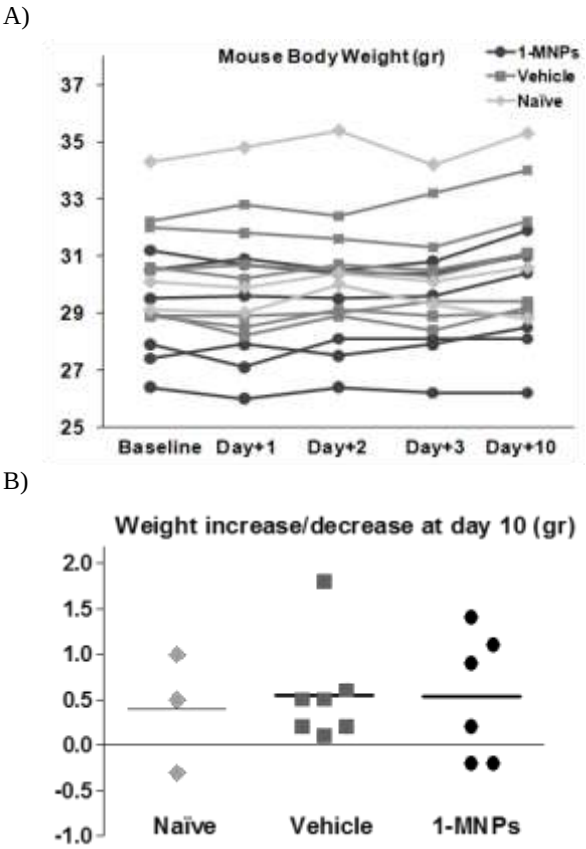

Figure 6. Mouse weight after *in vivo* administration of **1**-MNPs or vehicle in mice. (A) Mice were weighted before **1**-MNPs (n=6) or Vehicle (n=7) intravenous administration, and followed-up at 1, 2, 3 and 10 days of injection. A group of naïve mice who did not receive any treatment were also weighted at the same days (n=3). (B) The Individual weight increase or decrease at day 10 was calculated for each mouse and represented, showing no differences between treatment groups.

CONCLUSIONS.

The newly synthesized boron nanohybrids 1-MNPs showed colloidal stability at different culture media and temperatures (room temperature and 37°C). Biological studies confirmed the uptake of **1**-MNPs by the cultured cells (hCMEC/D3 and A172) that was visualized via Prussian blue staining identifying the presence of intracellular iron after 24 h treatment with **1**-MNPs. These experiments suggested that there has been cytoplasmatic endocitosis of the iron core of the 1-MNPs that was further confirmed by TEM of both types of studied cells treated with 1-MNPs. High resolution XPS and EELS spectra on the A172 dried-cells sample unambiguously proved the presence of the m-carboranylphosphinate; peaks at 189 and 133 eV, which are characteristic of B-B and P-O bonding were observed clearly confirming the presence of boron cluster ligands. Quantification of 1-MNPs uptake by cells displayed that glioblastoma A172 cells presented larger cellular iron contents than brain endothelial (hCMEC/D3) cells, suggesting that by using low doses of MNPs, glioblastoma cancer cells might be largely labeled with the **1**-MNPs compound compared to other neighboring cells in the tissue. This newly synthesized boron nanohybrids have significant biocompatible properties at certain administration

doses allowing cell labeling with potential applications to penetrate into malignant tumoral cells as drug carriers or for Boron Neutron Capture Therapy. Importantly, in terms of drug safety we have shown that the systemic administration of the **1**-MNPs nanohybrids does not show major signs of toxicity in mice, supporting its potential translation into the biomedical setting. We believe that these new boron cluster-MNPs nanohybrids **1**-MNPs might offer a broad scope for exciting research and future biomedical applications.

ASSOCIATED CONTENT

Supporting Information. Prussian Blue Iron Stain Protocol in hCMEC/D3 cells, STEM images and EELS analysis spectra on the square area of A172 cells; HAADF STEM images and EDX spectra on the square area of A172 cells; EFTEM elemental maps of A172 cells; HAADF STEM image and EELS spectra on the square area of A172 cells. Energy loss peaks with onsets at 188 eV and at 133 eV corresponding respectively to B and $PL_{2,3}$ containing in the sample; DLS studies of **1**-MNPs in different biological media. "This material is available free of charge via the Internet at http://pubs.acs.org."

AUTHOR INFORMATION

Corresponding Author

clara@icmab.es
anna.rosell@gmail.com.

Author Contributions

The manuscript was written through contributions of all authors. / All authors have given approval to the final version of the manuscript.

Funding Sources

This work has been supported by the Spanish Ministerio de Economía y Competitividad (CTQ2013-44670-R, SAF2016-80236-R, CIBERNED CB06/05/1104), the Generalitat de Catalunya (2014/SGR/149),; Miguel Servet program (CPII15/00003) and the RETICS program (RD12/0014/0005 and RD16/0019/0021), both from the Fondo de Investigaciones Sanitarias- Instituto de Salud Carlos III and co-financed by the European Regional Development Fund (ERDF). C. V. thanks COST CM1302 project. E. O. thanks MICINN for FPU predoctoral grant.

ACKNOWLEDGMENT

E. O. is enrolled in the PhD program of the UAB.

REFERENCES

[1] a) Faivre, D.; Bennet, M. *Nature* **2016**, *535*, 235–236. b) Kaittanis, C.; Santra, S.; Santiesteban, O. J.; Henderson, T. J.; Perez, J. M. *J. Am. Chem. Soc.* **2011**, *133*, 3668−3676. c) Haun, J. B.; Yoon, T.-J.; Lee, H.; Weissleder, R. *Wiley Interdiscip. Rev.: Nanomed. Nanobiotechnol.* **2010**, *2*, 291−304.

[2] a) Pankhurst, Q. A.; Thanh, N. T. K.; Jones, S. K.; Dobson, J. *J. Phys. D: Appl. Phys.* **2009**, *42*, 224001.b) Lee, N.; Yoo, D.; Ling, D; Cho, M. H.; Hyeon, T; Cheon, J. *Chem. Rev.* **2015**, *115*, 10637−10689.

[3] a) Lee, N.; Hyeon, T. *Chem. Soc. Rev.* **2012**, *41*, 2575−2589. b) Casula, M. F.; Floris, P.; Innocenti, C.; Lascialfari, A.; Marinone, M.; Corti, M.; Sperling, R. A.; Parak, W. J.; Sangregorio, C. *Chem. Mater.* **2010**, *22*, 1739−1748.

[4] a) Jun, Y.-W.; Lee, J.-H.; Cheon, J. *Angew. Chem., Int. Ed.* **2008**, *47*, 5122−5135. b) Yoo, D.; Lee, J.-H.; Shin, T.-H.; Cheon, J. *Acc. Chem. Res.* **2011**, *44*, 863−874. c) Ling, D.; Hyeon, T. *Small* **2012**, *9*, 1450-1466.

[5] Feliu, N.; Docter, D.; Heine, M.; del Pino, P.; Ashraf, S.; Kolosnjaj-Tabi, J.; Macchiarini, P.; Nielsen, P.; Alloyeau, D.; Gazeau, F.; Stauber, R. H.; Parak, W. J. *Chem. Soc. Rev*. **2016**, *45*, 2440-2457.

[6] a) Berry, C. C. J. Phys. D: Appl. Phys. 2009, 42, 224003 (9 pp). b) Majewski, P.; Thierry, B. *Crit. Rev. Solid State Mater. Sci.* **2007**, *32*, 203-215.

[7] Poater, J.; Solà, M.; Viñas, C.; Teixidor, F. *Angew. Chem. Int. Ed.* **2014**, *53*, 12191 –12195.

[8] a) Teixidor, F.; Viñas, C.; Demonceau, A.; Nuñez, R. *Pure App. Chem.* **2003**, *75*, 1305–1313. b) Scholz, M.; Hey-Hawkins, E. *Chem. Rev*. **2011**, *111*, 7035–7062.

[9] a) Grimes, R.N.; *Carboranes Third Edition:* Elsevier Inc., New York/Oxford, 2016. b) Hawthorne, M.F. *Advances in Boron Chemistry*; The Royal Society of Chemistry: Cornwall, U.K., 1997, 261-272. c) Plesek, *J. Chem. Rev.* **1992**, *92*, 269-278.

[10] a) Lesnikowski, Z. J. *J. Med. Chem.* **2016**, *59*, 7738-7758. b) Lesnikowski, Z. J. *Exp. Op. Drug Disc*. **2016**, *11*, 569-578. c) Hosmane, N. S. Boron Science: New Technologies and Applications, CRC Press Ed., Boca Raton, 2012. d) Hawthorne, M. F. *Angew. Chem. Int. Ed.*, **1993**, *32*, 950-984. e) Soloway, A. H.; Tjarks, W.; Barnum, B. A.; Rong, F-G.; Barth, R.F.; Codogni, I. M.; Wilson, J. G. *Chem. Rev.* **1998**, *98*, 1515-1562. f) Valliant, J. F.; Guenther, K. J.; King, A. S.; Morel, P.; Schaffer, P.; Sogbein, O. O.; Stephenson, K. A. *Coord. Chem. Rev.* **2002**, *232*, 173-230. g) Sivaev, I. B.; Bregadze, V.; Sjöberg, S. in Research and Development in Neutron Capture Therapy, ed. W. Sauerwein, R. Moss and A. Wittig, Monduzzi Editore S.p.A., Bologna, 2002, pp. 19–23.A. h) Julius, R.; Farha, O.; Chiang, J.; Perry, L.; Hawthorne, M. F. *Proc. Natl. Acad. Sci. U.S.A.* **2007**, *104*, 4808-4813.

[11]) a) Bregadze, V. I. *Chem. Rev*. **1992**, *92*, 209-223. b) Olid, D. Núñez, R.; Viñas, C.; Teixidor, F. *Chem. Soc. Rev*., **2013**, *42*, 3318-3336.

[12] a) Dash, B. P.; Satapathy, R.; Maguire, J. A.; Hosmane, N. S. *New J. Chem.* **2011**, *35*, 1955–1972 b) Schwartz, L.; Eriksson, L.; Lomoth, R.; Teixidor, F.; Viñas, C.; Ott, S. *Dalton Trans.* **2008**, *18*, 2379-2381. c) Peterson, J. J.; Werre, M.; Simon, Y. C.; Coughlin, E. B.; Carter, K. R. *Macromolecules*, **2009**, *42*, 8594-8598. d) Kokado, K.; Chujo, Y. *J. Org. Chem.* **2011**, *76*, 316-319. e) Bae, Y.-S.; Spokoyny, A. M.; Farha, O. K.; Snurr, R. Q.; Hupp, J. T.; Mirkin, C. A. *Chem. Commun.* **2010**, *46*, 3478-3480. f) Vives, G.; Tours, J. M. *Acc. Chem. Res.* **2009**, *43*, 473-487. g) Morin, J. F.; Shirai, Y.; Tour, J. M. *Org. Lett.* **2006**, *8*, 1713-1716. h) Kahlert, J. U.; Rawal, A.; Hook, J. M.; Rendina, L. M.; Choucair, M. *Chem. Commun*. **2014**, *50*, 11332-11334. i) Núñez, R.; Romero, I.; Teixidor, F.; Viñas, C. *Chem. Soc. Rev*. **2016**, *45*, 5147-5173. j) Lamrani, M.; Hamasaki, R.; Mitsuishi, M.; Miyashita, T.; Yamamoto, Y. *Chem. Commun.* **2000**, *17*, 1595-1596.

[13] a) Fox, M.A.; Hughes, A.K. *Coord. Chem. Rev*. **2004**, *248*, 457-476. b) Jude, H.; Disteldorf, H.; Fischer, S.; Wedge, T.; Hawkridge, A.M.; Arif, A.M.; Hawthorne, M.F.; Muddiman, D.C.; Stang, P.J. *J. Am. Chem. Soc.* **2005**, *127*, 12131-12139. c) Puga, A.V.; Teixidor, F.; Kivekäs, R.; Sillanpää, R.; Viñas, C. *Chem. Eur. J.* **2009**, *15*, 9764-9772. d) Hardie, M. J.; Raston, C. L., *Chem. Commun*. **2001**, *10*, 905-906. e) Yao, Z.-J.; Jin, G.X. *Coord. Chem. Rev*. **2013**, *257*, 2522-2535. F) Scheer, M.; Schindler, A.; Groger, C.; Virovets, A. V.; Peresypkina, E. V. *Angew. Chem. Int. Ed*. **2009**, *48*, 5046-5049.

[14] a) Teixidor, F.; Núñez, R.; Viñas, C.; Sillanpää, R.; Kivekäs, R. *Angew. Chem., Int. Ed.* **2000**, *39*, 4290-4292. b) Núñez, R.; Farrás, P.; Teixidor, F.; Viñas, C.; Sillanpää, R.; Kivekäs, R. *Angew. Chem.,Int. Ed*. **2006**, *45*, 1270-1272. c) Teixidor, F.; Barbera, G.; Vaca, A.;

Kivekäs, R.; Sillanpää, R.; *J. Am. Chem. Soc*. **2005**, *127*, 10158-10159. d) Spokoyny, A. M.; Machan, C. W.; Clingerman, D. J.; Rosen, M. S.; Wiester, M. J.; Kennedy, R. D.; Stern, C. L.; Sarjeant, A. A.; Mirkin, C. A. *Nat. Chem*. **2011**, *3*, 590-596.

[15] a) Luderer, M. J.; Puente, P.; Azab, A. K. *Pharm. Res.* **2015**, *32*, 2824–2836. b) Sun, T; Li, Y. Y.; Huang, Y. L.; Zhang, Z. Z.; Yang, W. L.; Du, Z. W.; Zhou, Y. X. *Oncotarget* **2016**, *7*, 43095-43108. c) Gao, Z. Y.; Horiguchi, Y.; Nakai, K.; Matsumura, A.; Suzuki, M.; Ono, K.; Nagasaki, Y. *Biomaterials*, **2016**, *104*, 201-212. d) Heber, E. M.; Hawthorne, M. F.; Kueffer, P. J.; Garabalino, M. A.; Thorp, S. I.; Pozzi, E. C. C.; Hughes, A. M.; Maitz, C. A.; Jalisatgi, S. S.; Nigg, D. W.; Curotto, P. ; Trivillin, V. A.; Schwint, A. E. *Proc. Natl. Acad. Sci. U.S.A.* **2014**, *111*, 16077-16081. e) Otero, R.; Seoane, S.; Sigueiro, R.; Belorusova, A. Y.; Maestro, M. A.; Perez-Fernandez, R.; Rochel, N.; Mourino, A. *Chem. Sci*, **2016**, *7*, 1033-1037. f) Zhu, Y.; Lin, Y.; Zhu, Y. Z.; Lu, J.; Maguire, J. A.; Hosmane, N. S. *J. Nanomater*. **2010**, 409320-409327. g) Xuan, S.; Zhao, N.; Zhou, Z. H.; Fronczek, F. R.; Vincente, M. G. H. *J. Med. Chem*. **2016**, *59*, 2109-2117. h) Cioran, A. M.; Musteti, A. D.; Teixidor, F.; Krpetić, Ž.; Prior, I. A.; He, Q.; Kiely, C. J.; Brust, M.; Viñas, C. *J. Am. Chem.Soc*. **2012**, *134*, 212-221. i) Sauerwein, W. A. G.; Wittig, A.; Moss, R.; Nakagawa, Y. (Eds.) *Neutron Capture Therapy. Principles and Applications.* Springer Science & Business Media **2012**. j) Bialek-Pietras, M.; Olejniczak, A. B.; Tachikawa, S.; Nakamura, H.; Lesnikowski, Z. J. *Bioorg. Med. Chem*. **2013**, *21(5)*, 1136-1142.

[16] a) Luderer, M. J.; Puente, P.; A. K. Azab, A. K. *Pharm Res*. **2015**, *32*, 2824–2836. b) Sun, T; Li, Y. Y.; Huang, Y. L.; Zhang, Z. Z.; Yang, W. L.; Du, Z. W.; Zhou, Y. X. *Oncotarget* **2016**, *7*, 43095-43108. c) Gao, Z. Y.; Horiguchi, Y.; Nakai, K.; Matsumura, A.; Suzuki, M.; Ono, K.; Nagasaki, Y. *Biomaterials* **2016**, *104*, 201-212. d) Calabrese, G., Daou, A.; Rova, A.; Tseligka, E.; Vizirianakis, I.S.; Fatouros, D.G.; Tsibouklis, J. *Med.Chem.Commun*. **2017**, *8*, 67-72.

[17] Oleshkevich, E.; Teixidor, F.; Choquesillo-Lazarte, D.; Sillanpää, R.; Viñas, C. *Chem. Eur. J.* **2016**, *11*, 3665–3670.

[18] Oleshkevich, E.; Teixidor, F.; Rosell, A.; Viñas, C. submitted.

[19] Weksler, B. B.; Subileau, E. A.; Perrière, N.; Charneau, P.; Holloway, K.; Leveque, M.; Tricoire-Leignel, H.; Nicotra, A.; Bourdoulous, S.; Turowski, P.; Male, D. K.; Roux, F.; Greenwood, J.; Romero, I. A.; Couraud, P. O. *FASEB J*. **2005**, *19*, 1872-1874.

[20] Dehydration with acetone in 12 steps: 50% acetone, 5 min, x1; 70% acetone, 5 min, x2; 90% acetone, 5 min, x3; 95% acetone, 5 min, x3; 100% acetone, 15 min, x3.

[21] Yardeni, T.; Eckhaus, M.; Morris, H.D.; Huizing, M.; Hoogstraten-Miller, S. Lab Anim (NY). **2011**, *40*, 155-160.

[22] Aires, A.; Ocampo, S.M.; Cabrera, D.; de la Cueva, L.; Salas, G.; Teran, F.J.; Cortajaren, A.L. *J. Mater. Chem. B* **2015**, *3*, 6239-6247.

[23] Salvati, A.; Pitek, A.S.; Monopoli, M.P.; Prapainop, K.; Bombelli, F.B.; Hristov, D.R.; Kelly, P.M.; Aberg, C.; Mahon E.; Dawson, K. A. *Nat. Nanotechnol*. **2013**, *8*, 137–143.

[24] a) Carenza, E.; Barceló, V.; Morancho, A.; Levander, L.; Boada, C.; Laromaine, A.; Roig, A.; Montaner, J.; Rosell, A. *Nanomedicine* NBM **2014**, *10*, 225-234. b) Matuszak, J.; Zaloga, J.; Friedrich, R.P.; Lyer, S.; Nowak, J.; Odenbach, S.; Alexiou, Ch.; Cicha, I. *J. Magn. Magn. Mater*. 2015, *380*, 20-26. c) Sundstrøm, T., Daphu, I., Wendelbo, I., Hodneland, E., Lundervold, A., Immervoll, H., Skaftnesmo, K.O.; Babic, M.; Jendelova, P.; Sykova, E.; Lund-Johansen, M.; Bjerkvig, R.; Thorsen, F. *Cancer Res*. **2013**, *73*, 2445-2456.

[25] Uptake quantification of **1**-MNPs content /cell = $MR_{capsule}$/(Ntotal cells - $MR_{\mathbf{1}\text{-MNPs}}$).

[26] a) Angelopoulos, I.; Southern, P.; Pankhurst, Q.A.; Day, R.M. *J Biomed Mater Res A*. **2016**, 104, 2412-2419. b) Wilhelm, C.; Gazeau, F. *Biomaterials* **2008**, 29, 3161-3174.

[27] Lu, X.; Liu, W.; Ouyang, J.; Tian, Y. *Applied Surface Science* **2014,** *311*, 749-752.

[28] Wang, Y.-X. J. *Quant Imaging Med Surg*. **2011**, 1, 35–40.

Synopsis TOC:

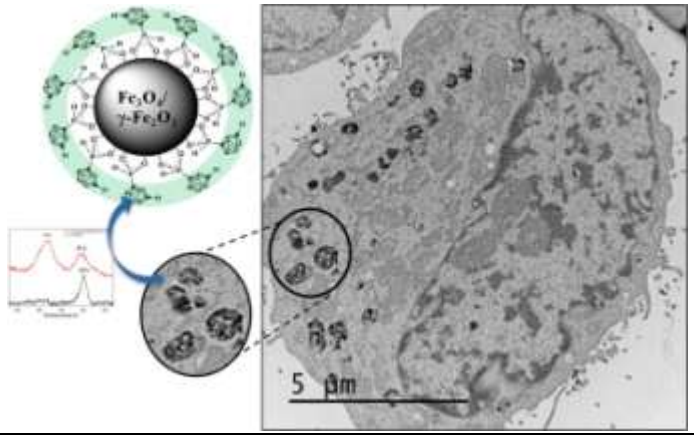

SUPPORTING INFORMATION

Biocompatible Fully Inorganic Nanohybrids for Biomedical Applications: Combining Magnetic Nanoparticles and Icosahedral Boron Clusters.

Elena Oleshkevich,[a] Anna Morancho,[b] Koen M. O. Galenkamp,[c,d,e] Alba Grayston,[b] Joan X. Comella,[c,d,e] Francesc Teixidor,[a] Anna Rosell,[b,*] Clara Viñas[a,*].

[a] Institut de Ciència de Materials de Barcelona (ICMAB-CSIC),Campus UAB, 08193 Bellaterra, Spain.

[b] Neurovascular Research Laboratory, Vall d'Hebron Research Institute, Universitat Autònoma de Barcelona, Passeig Vall d'Hebron 119-129, 08035 Barcelona, Spain.

[c] Cell Signaling and Apoptosis Group, Institut de Recerca de l'Hospital Universitari de la Vall d'Hebron (VHIR), Barcelona, Spain

[d] Institut de Neurociències, Departament de Bioquímica i Biologia Molecular, Facultat de Medicina, Universitat Autònoma de Barcelona, Bellaterra, Spain

[e] Centro de Investigación Biomédica en Red sobre Enfermedades Neurodegenerativas (CIBERNED), Madrid, Spain

Figure S1.- Prussian Blue Iron Stain Protocol in hCMEC/D3 cells after 24h treatment in EGM-2 2% FBS medium with different concentration of nanoparticles.

Figure S2. a) STEM images of glioblastoma cells (A172) with different magnification. b) EELS analysis spectra on the square area showing the characteristic peaks for Fe.

Figure S3.- EFTEM elemental maps of glioblastoma cells (A172); Fe can be observed on the cells samples.

Figure S4.- a) High-angle annular dark-field scanning transmission electron microscopy (HAADF-STEM) image of A172 cells and b) EDX spectra on the square area showing the characteristic peaks for Fe and P.

Figure S5.- a) HAADF STEM image of A172 cells and b) EELS spectra on the square area. Energy loss peaks with onsets at 188 eV correspond to B containing in the sample.

Figure S6.- HAADF STEM image of A172 cells and EELS spectra on the square area. Energy loss peaks with onsets at 133 eV correspond to $P_{L2,3}$ containing in the sample.

Figure S7. **-** a) The image of the polycarbonate capsules with dried cell pellets used for the SQUID measurements. b) STEM images of dried cells extracted from polycarbonate capsules and dispersed in water.

Figure S8. **-** DLS studies of **1**-MNPs in different biological media (DMEM-F12-1% FBS, 1% non-essential amino acids and 1% antibiotics; EGM2 medium with 2%FBS, DMEM-1%FBS, RPMI, and PBS solution), at different times (10 min. and 24 h.) and different temperatures (r.t., 37ºC). Concentration of 50μg **1**-MNPs/ml.

Figure S1.- Prussian Blue Iron Stain Protocol in hCMEC/D3 cells after 24h treatment in EGM-2 2% FBS medium with different concentration of nanoparticles.

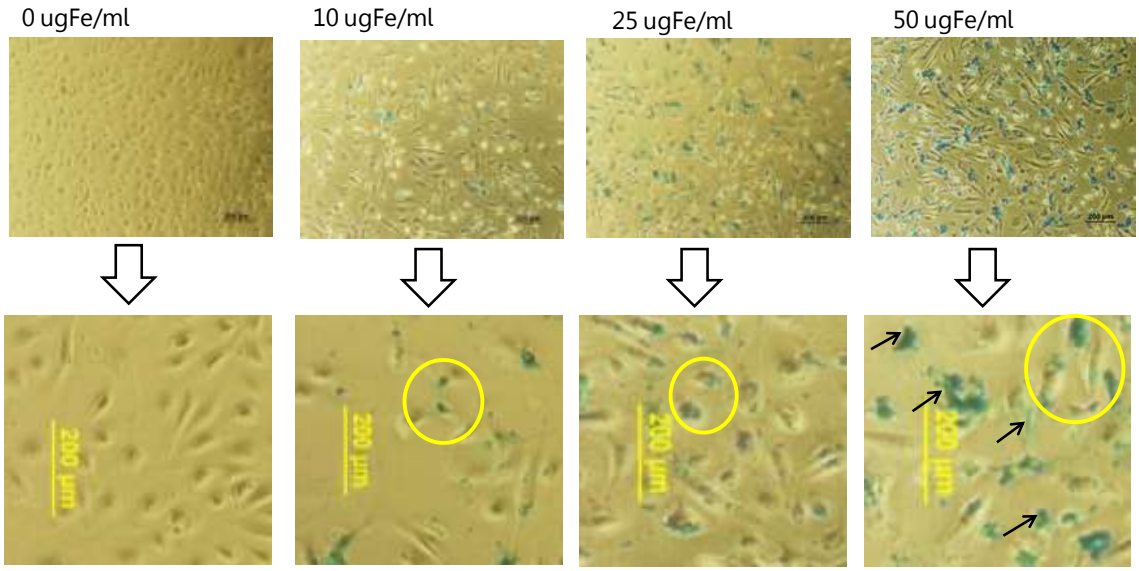

Figure S2. a) STEM images of glioblastoma cells (A172) with different magnification.

b) EELS analysis spectra on the square area showing the characteristic peaks for Fe.

a)

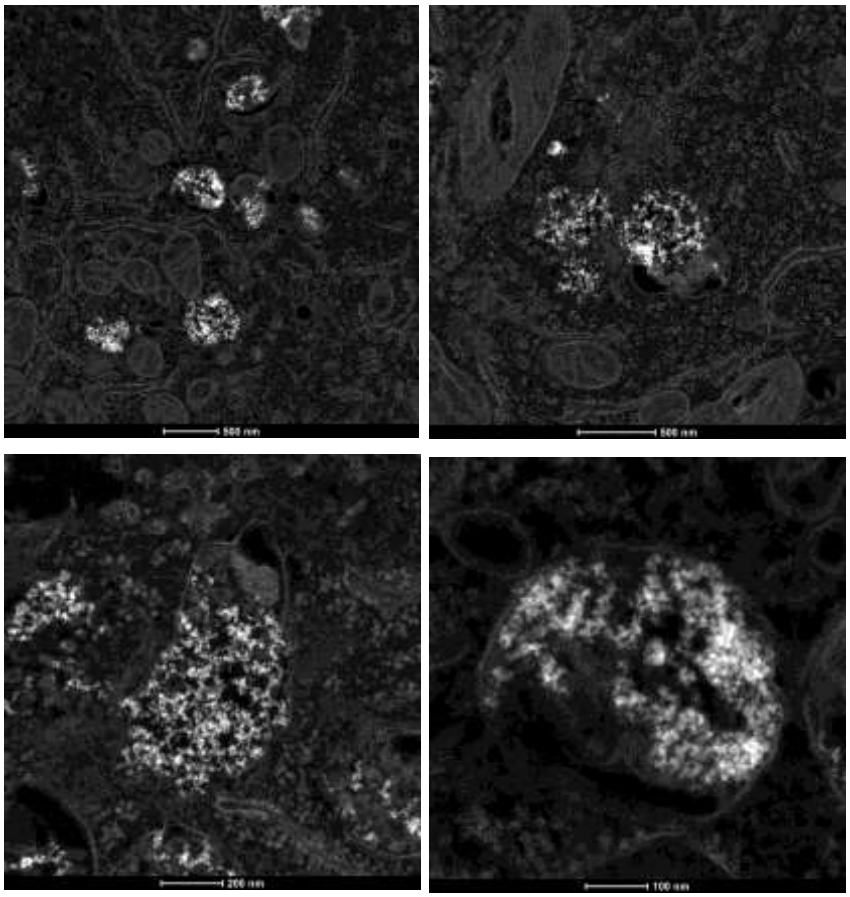

b)

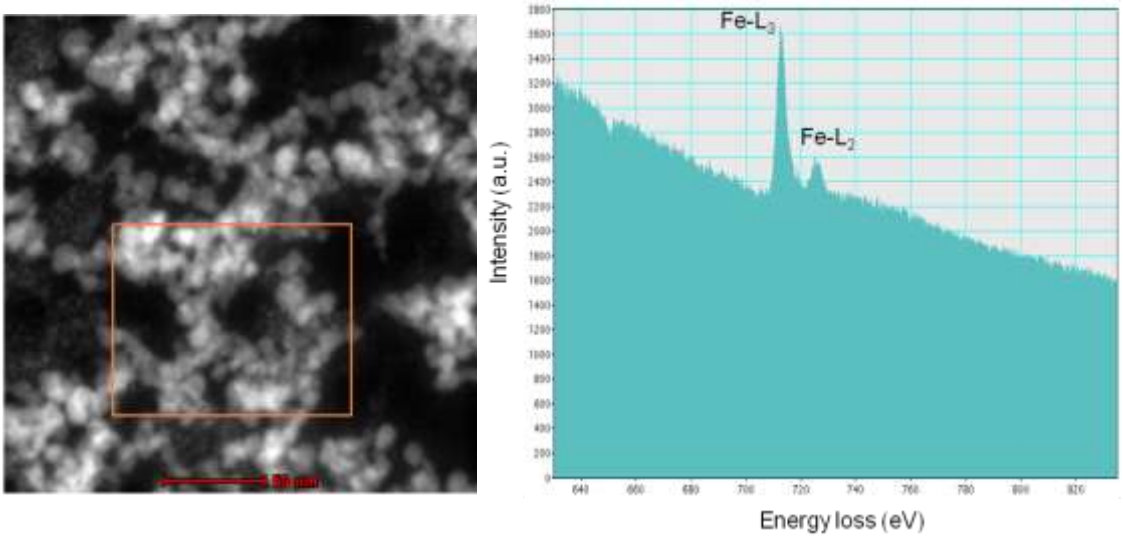

Figure S3.- EFTEM elemental maps of glioblastoma cells (A172). Fe can be observed on the cells samples.

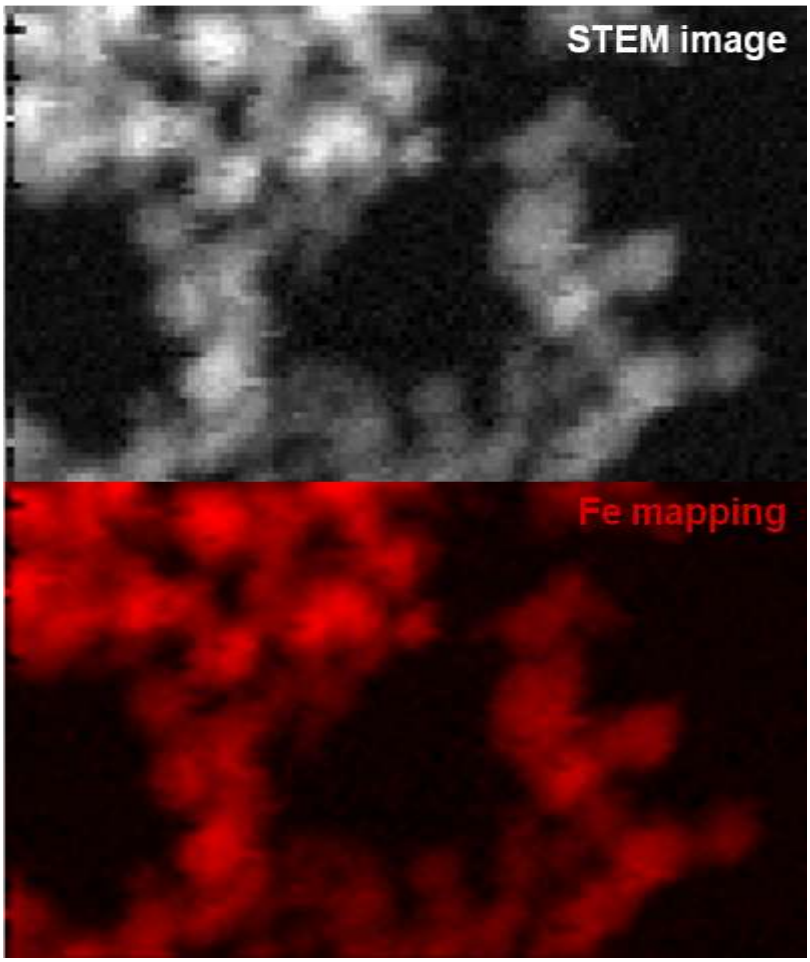

Figure S4.- a) High-angle annular dark-field scanning transmission electron microscopy (HAADF-STEM) image of A172 cells and b) EDX spectra on the square area showing the characteristic peaks for Fe and P.

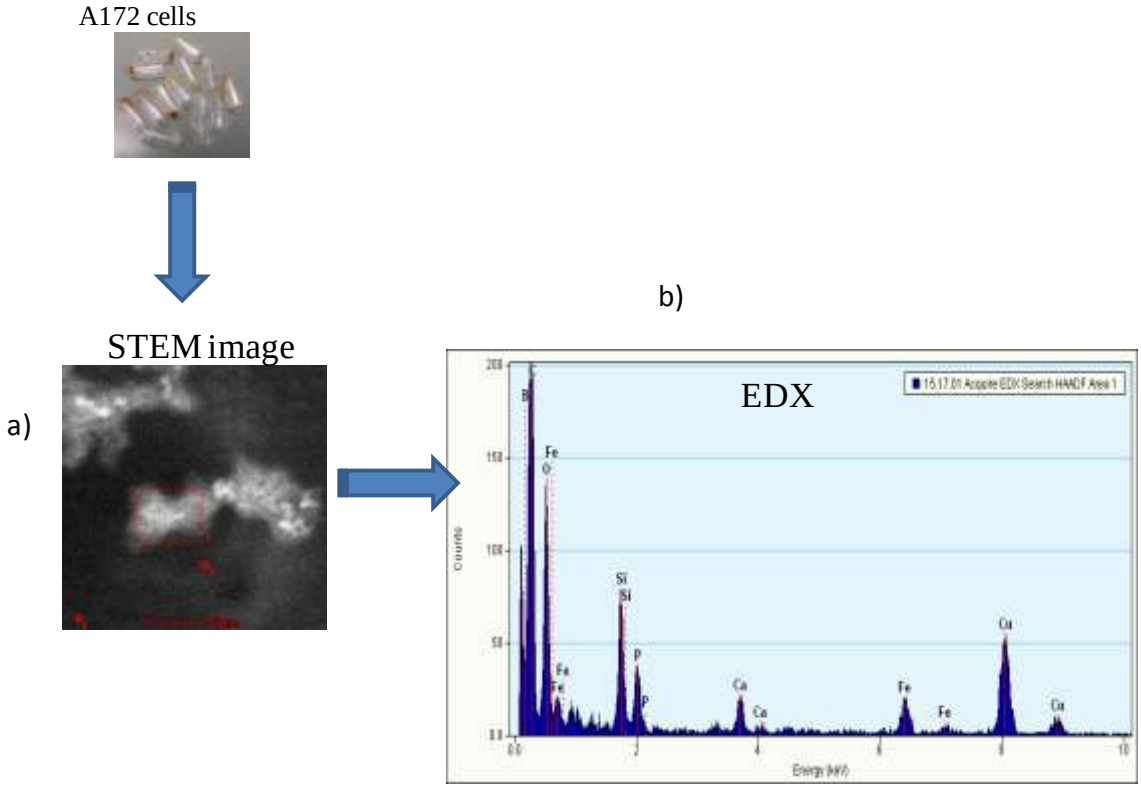

Figure S5.- a) HAADF STEM image of A172 cells and b) EELS spectra on the square area. Energy loss peaks with onsets at 188 eV correspond to B containing in the sample.

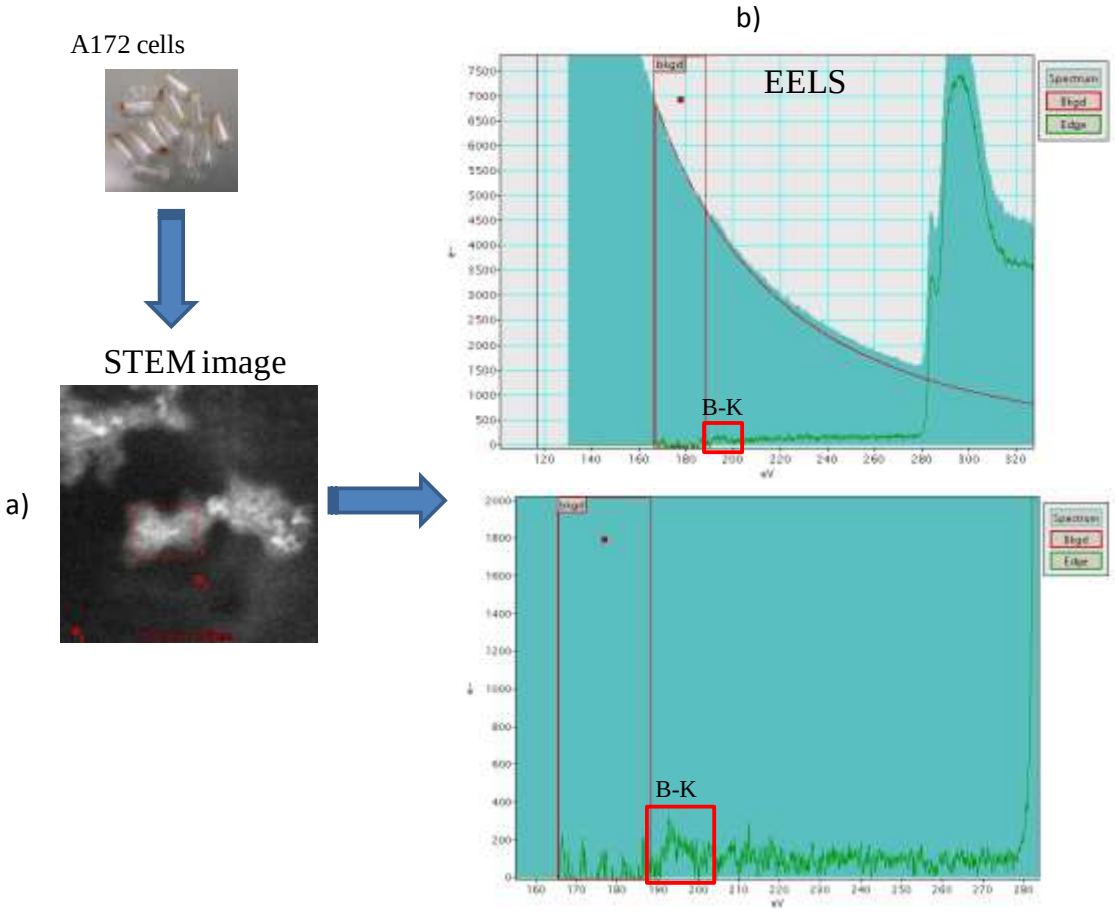

Figure S6.- HAADF STEM image of A172 cells and EELS spectra on the square area. Energy loss peaks with onsets at 133 eV correspond to $P_{L2,3}$ containing in the sample.

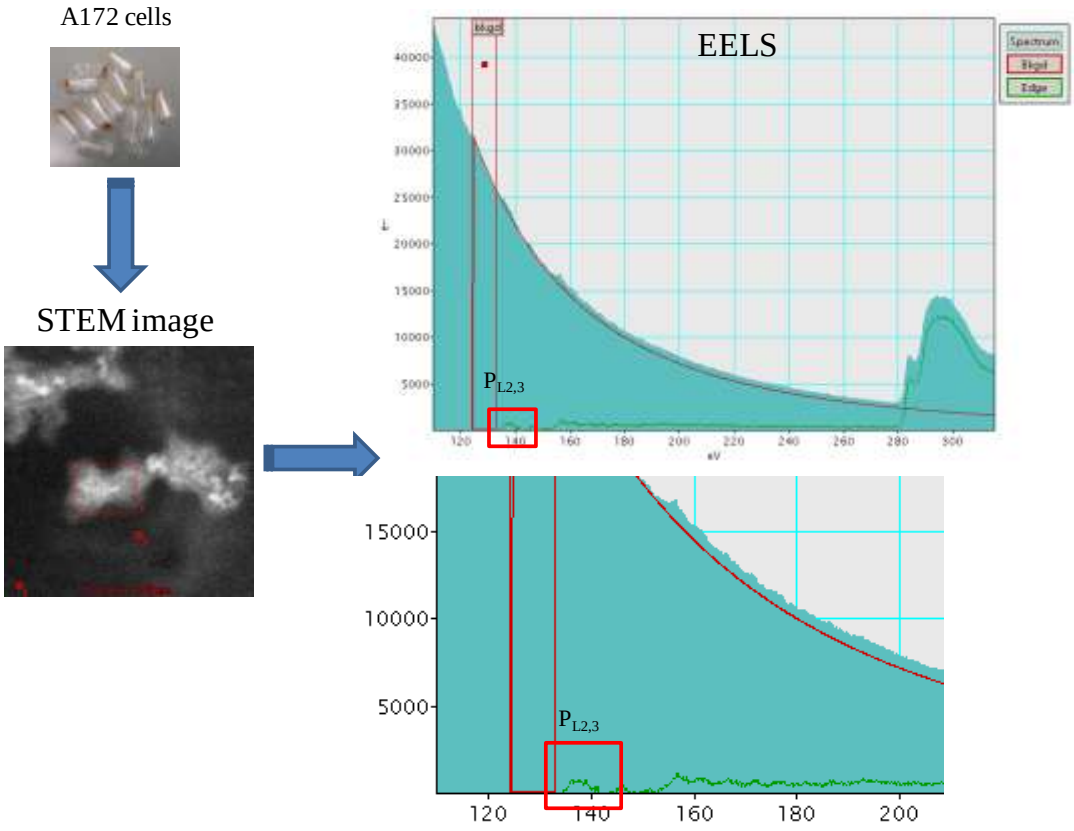

Figure S7. a) The image of the polycarbonate capsules with dried cell pellets used for the SQUID measurements. b) STEM images of dried cells extracted from polycarbonate capsules and dispersed in water.

a)

b)

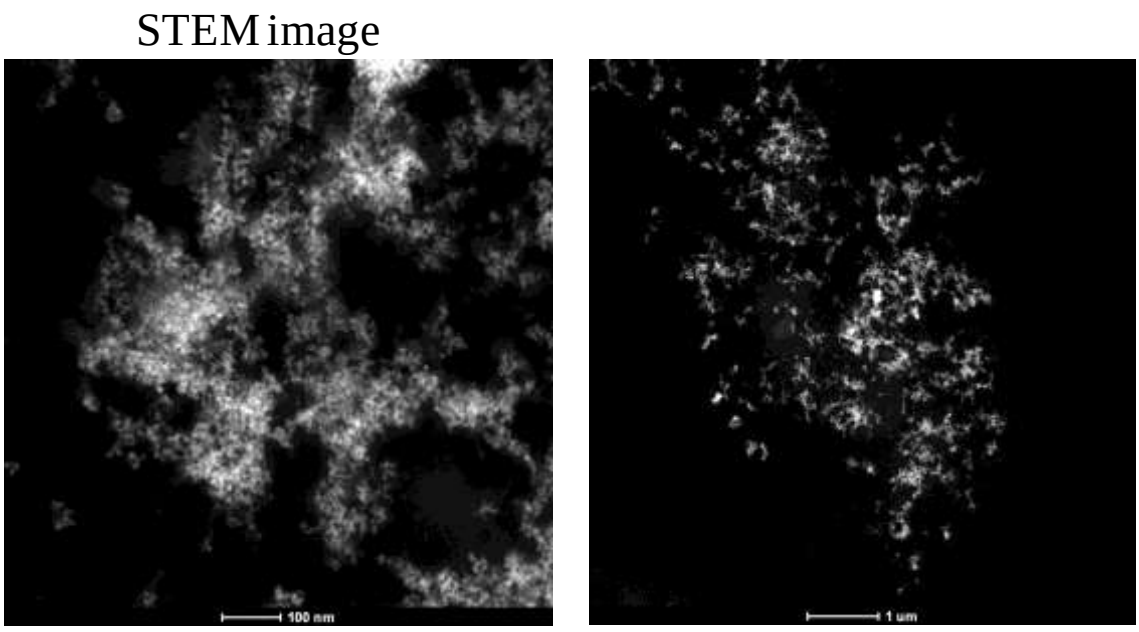

Figure S8. - DLS studies of **1**-MNPs in different biological media (DMEM-F12-1% FBS, 1% non-essential amino acids and 1% antibiotics; EGM2 medium with 2%FBS, DMEM-1%FBS, RPMI, and PBS solution), at different times (10 min. and 24 h.) and different temperatures (r.t., 37ºC). Concentration of 50μg **1**-MNPs/ml.